Differential and numerical models of hysteretic systems with stochastic and deterministic inputs

Stephen McCarthy

NATIONAL UNIVERSITY OF IRELAND, CORK

Department of Applied Mathematics

Thesis submitted for the degree of Doctor of Philosophy

May 2013

Supervisor: Dr. Dmitrii Rachinskii

Head of Department/School: Dr. James Grannell

Contents

I, Stephen McCarthy, certify that this thesis is my own work and I have not obtained a degree in this university or elsewhere on the basis of the work submitted in this thesis.

Stephen McCarthy

List of Figures

Abstract

Many deterministic models with hysteresis have been developed in the areas of economics, finance, terrestrial hydrology and biology. These models lack any stochastic element which can often have a strong effect in these areas. In this work stochastically driven closed loop systems with hysteresis type memory are studied. This type of system is presented as a possible stochastic counterpart to deterministic models in the areas of economics, finance, terrestrial hydrology and biology. Some price dynamics models are presented as a motivation for the development of this type of model. Numerical schemes for solving this class of stochastic differential equation are developed in order to examine the prototype models presented. As a means of further testing the developed numerical schemes, numerical examination is made of the behaviour near equilibrium of coupled ordinary differential equations where the time derivative of the Preisach operator is included in one of the equations. A model of two phenotype bacteria is also presented. This model is examined to explore memory effects and related hysteresis effects in the area of biology. The memory effects found in this model are similar to that found in the non-ideal relay. This non-ideal relay type behaviour is used to model a colony of bacteria with multiple switching thresholds. This model contains a Preisach type memory with a variable Preisach weight function. Shown numerically for this multi-threshold model is a pattern formation for the distribution of the phenotypes among the available thresholds.

Acknowledgements

There are many people that I must thank, for without their support this thesis would not have to come to fruition. Firstly I wish to thank my supervisor Dr. Dmitrii Rachinskii whose constant support and guidance were invaluable to me when working on this thesis over the last few years.

I would also like to thank my parents Pat & Liz for their encouragement and support, both emotional and financial, without which I would not have been able to even get started on this road.

I should also thank all of friends who were always there when I needed a distraction and my mind taken off the work. There are too many people to name everyone, but I must make special mention of a few people, Eoin, Mark, Stephen, James, Killian, Noirin, Baz, Sarah and Saorlaith. To the members of WARPS who made every Thursday evening nice and relaxing and a high point of the week.

I would also like to thank anyone who has passed through the postgraduate room down in the Western Gateway, they were always friendly and encouraging either talking shop or just having a bit of friendly banter. I would like to thank some of the old hysteresis people who went through the department before me for their advice and guidance through the world of hysteresis, Denis, Hugh and Sasha.

Most importantly I wish to thank my fiancée Karen who was always encouraging and supportive especially during periods of doubt and uncertainty. This thesis would not be here today without her.

Chapter 1

Introduction

Many models of hysteretic systems have been proposed and studied since the idea of hysteresis was first introduced towards the end of the 19th century. Many of the properties (both deterministic and stochastic) of these models are well established in the literature. Differential models which contain the time derivative of the output of a hysteresis element occur naturally in physical areas and have been the subject of much study, see for example [1, 2]. In the last ten or more years there has been an increasing amount of work done in moving the development of models of this type from application to problems in physics to applications in the areas of economics, terrestrial hydrology, biology and finance as well, for example [3, 4]. While deterministic models in these areas are interesting and give some insights into how the real systems behave, these areas have a significant stochastic element which is not considered in the deterministic models, for example due to the uncertainty in the occurrence of rainfall or in the unpredictability of the behaviour of people in an economic setting.

Therefore a question of interest is, how to model the stochastic element present in these areas. This thesis aims to construct some simple prototype models that could possibly be used as stochastic counterparts to the deterministic differential hysteretic models in the areas of economics, finance, terrestrial hydrology and biology. An example model from the area of economics is developed in order to present a basis for the proposed prototype model. A means of numerically implementing this prototype model will also be developed. Some of the numerical techniques developed here will be used for the examination of the behaviour near equilibrium of models based on coupled deterministic differential equations which contain the Preisach operator in one of the equations. In addition some study will

be given to the development of models for two phenotype bacteria growth which will hope to show how the implementation of hysteretic behaviour by the bacteria can be beneficial to the overall growth of the bacteria when the environment varies stochastically. This hysteretic type behaviour will be used as the basis for a model of a colony of bacteria with multiple different switching threshold values.

There exist many well established results regarding hysteresis operators with stochastic inputs. In this area, theory has been developed for the Preisach operator with stochastic input and many of the properties are known, for example see [5,6]. Open loop systems with hysteresis have been the main topic of study in this area, this thesis will examine closed loop stochastic systems with hysteresis which have been the subject of less study.

The thesis is laid out as follows: Chapter 2 defines and discusses the hysteresis operators that are used in the work presented in the remainder of the thesis. In Chapter 3 two numerical schemes for solving stochastic differential equations which contain the time derivative of the output of the Preisach operator are developed. These schemes are developed in order to solve a price dynamics model with negative feedback which is presented in Chapter 3. Comparison between the solution returned by both schemes for the same realisation of the Wiener process is made in order to determine which of the schemes is more accurate. The stronger scheme is then validated in a more rigorous way. A second price dynamics model is also presented in Chapter 3, this model contains a positive feedback element instead of the negative feedback of the first model.

Chapter 4 examines models where an equation involving the derivative of the output of the Preisach operator is coupled with an ordinary differential equation as a method of further validating the numerical schemes presented in Chapter 3. The aim of Chapter 4 is to compare the results from the implementation of the numerical scheme for the system with theoretical results for the behaviour of the system near equilibrium for several variations on the configuration of the system. The similarity between systems of this type and certain singularly perturbed systems is explored. Chapter 5 presents and examines a model for two phenotype bacteria in a continuously varying environment. Environments that vary stochastically and periodically will both be considered. The introduction of a cost for the bacteria to undergo switching between the two phenotypes allows for a hysteretic switching routine to give the bacteria a greater fitness. This shows for the first time that hysteresis behaviour allows the bacteria in the model to increase their growth rate thus gaining an evolutionary advantage over memoryless bacteria.

This hysteretic switching routine is then used to develop a model for a bacteria colony which has many different switching thresholds. Chapter 6 presents some conclusions on the work carried out.

Chapter 2

Hysteresis

Hysteresis is a naturally occurring phenomenon which has been the subject of much study for many years. A small amount of information regarding the history of hysteresis is given in [7, 8]. The idea of hysteresis was first introduced in the field of magnetism by James Ewing in [9]. Following its introduction as a phenomenological idea in magnetism it was also found to be present in many more varied fields, including plastics and soil mechanics. The phenomenon of hysteresis has been found to naturally exist anywhere there is a delay between the application of a force and the removal of that force and its subsequent effect.

However it took until the 1970's before any formal rigorous mathematical framework for hysteresis existed. This was work carried out by the group of mathematicians led by M.A. Krasnosel'skii, their formalisation of the mathematics of hysteresis was presented in [10]. This text forms the bedrock of current mathematical hysteresis research and has led to many more publications on the topic of mathematical hysteresis including [1, 2, 11] to name a small few.

Now let us consider what hysteresis is more carefully. In [12] the idea of hysteresis was explained by James Ewing as "When there are two quantities M and N, such that cyclic variations of N cause cyclic variation of M, then if the changes of M lag behind those of N, we may say that there is a hysteresis in the relation of M and N". An alternative representation was given by Krasnosel'skii and Pokrovskii in their text [10]. In this text they consider a transducer based approach to understanding the concept. The transducer based approach is also used in [11] to explain the concept of hysteresis and I will use the explanation given there for my definition of hysteresis.

For clarity I reproduce this explanation here. One can consider a dynamical

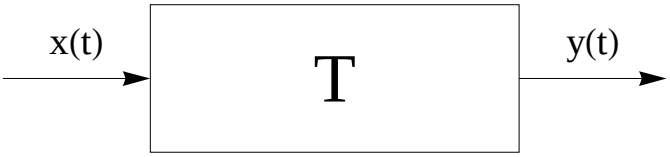

Figure 2.1: Transducer representation of a dynamical system. Where $x(t)$ is the input to the system T giving the output y(t).

system as an input $x(t)$ to a transducer giving an output $y(t)$, this is visually represented in Figure 2.1. In the terminology of [11] the transducer T is a hysteresis transducer "if its input-output relationship is a multibranch nonlinearity for which branch-to-branch transitions occur after input extrema". The idea of this kind of multibranch nonlinearity is shown in Figure 2.2. This definition of a hysteresis operator means that in addition to being a naturally occurring phenomenon these operators could also be considered to be a way of encapsulating memory in the system. This notion that hysteresis is a form of memory also means that the output from a hysteresis transducer can not be simply gotten from the input, in addition something about the current state of the transducer must also be know. In simple terms the previous history of the input also needs to be given, this property is known as path dependence.

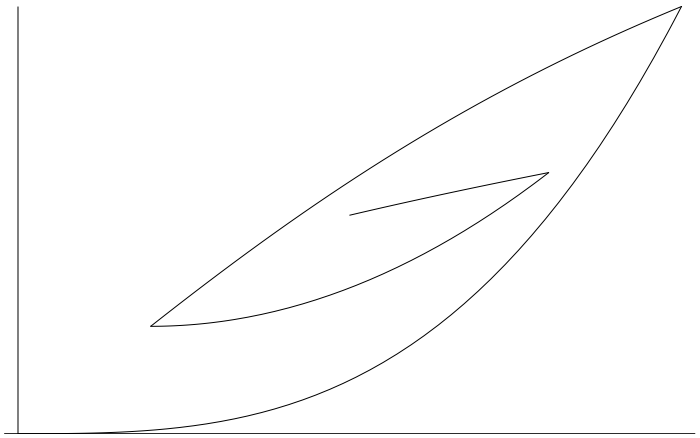

Figure 2.2: Input-output relationship of a hysteresis transducer.

Given the hysteresis operators considered in this body of work I must also define one other property known as rate independence. The monograph of Mayergoyz gives a definition of rate independence, from [11] a hysteresis transducer is rate independent if "branches of such hysteresis nonlinearities are determined only by the past extremum values of input, while the speed (or particular manner) of input variations between extremum points has no influence on branching". I highlight this concept in Figure 2.3 where the two different inputs which achieve

the same sequence of maxima and minima but follow different paths to achieve them have the same plot for the input-output relationship.

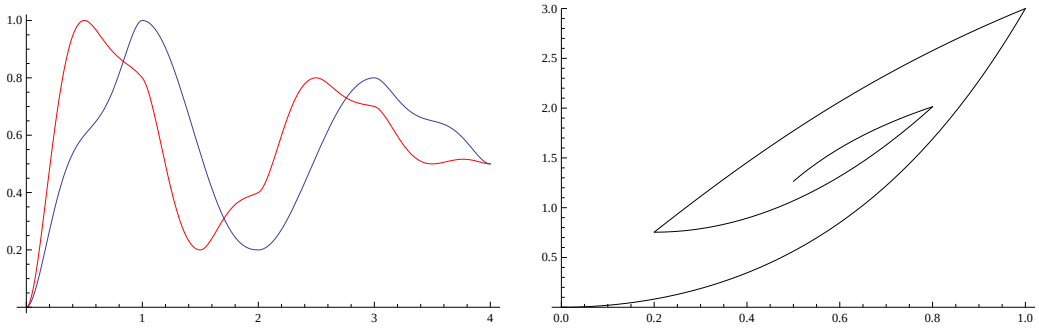

(a) Input plots (b) Input-Output Relationship

Figure 2.3: Plots showing the rate independence property of hysteresis transducers. (a) Shows two different inputs which achieve the same extrema but approach them differently. (b) Shows the input-output relationship common to each input.

This property means that only the value of the input extrema and the order they are obtained are revelent to the path dependence determination of the current state of the transducer.

2.1 Non-ideal relay

In [10] a mathematical approach for dealing with hysteresis was proposed. This approach was to use elementary hysteresis carriers which were called hysterons. One of the hysterons introduced was the non-ideal relay. The dynamics of the non-ideal relay are illustrated in Figure 2.4. There is a threshold value of input β at which the relay turns on and a different lower threshold α at which the relay switches off. If the input only varies between the two threshold values then the output remains the same as when it last crossed one of the threshold values. That is no switching takes place in the region $\alpha < x < \beta$.

The relay is in one of two possible states 0 (the relay is switched off) or 1 (the relay is switched on) at any moment in time (in the literature it is sometimes found that the states are presented as ± 1, take for example [11], this is obtained by a simple change in the definitions).

Define the state of the relay at any time moment t such that $t \geq t_0$, where t_0 is

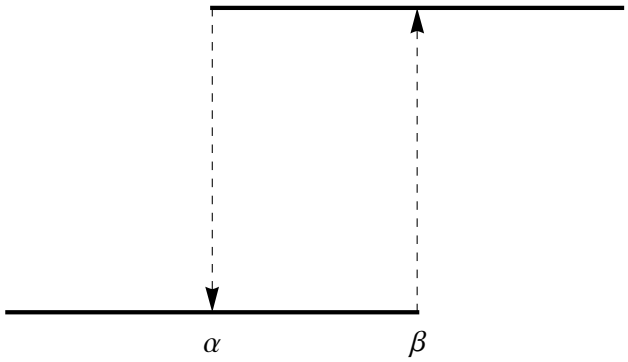

Figure 2.4: Dynamics of the non-ideal relay operator with thresholds α and β with $\beta > \alpha$.

the initial time moment, by the equation

$$\begin{aligned} y(t) &= R_{\alpha,\beta}[\eta_0]x(t) \\ &= \begin{cases} 1 & \text{if } \exists\ t_1 \in [t_0, t] \text{ s.t. } x(t_1) \geq \beta,\ x(\tau) > \alpha\ \forall \tau \in [t_1, t] \\ 0 & \text{if } \exists\ t_1 \in [t_0, t] \text{ s.t. } x(t_1) \leq \alpha,\ x(\tau) < \beta\ \forall \tau \in [t_1, t] \\ \eta_0 & \text{if } \alpha < x(\tau) < \beta\ \forall \tau \in [t_0, t] \end{cases} \end{aligned} \tag{2.1}$$

where $\eta_0 = y(t_0)$ is the initial state of the relay at the moment t_0. Thus if the initial state η_0 is known then the state of the relay is uniquely determined after a moment t_0 for a given input $x(t)$, $t \geq t_0$.

2.2 Play operator

2.2.1 Ordinary play operator

Another hysteron introduced in [10] is the ordinary play operator. The dynamics of this operator can be understood by examining a simple physical system. Consider a system consisting of a cylinder C of length h, contained within the cylinder is a piston P. Both the piston and cylinder are free to move along the z-axis, see Figure 2.5.

Let the function $x(t)$ describe the position of the piston given by the point A in Figure 2.5 and the function $y(t)$ describe the position of the cylinder given by the point B. In the case of only the piston being driven by a force then the position

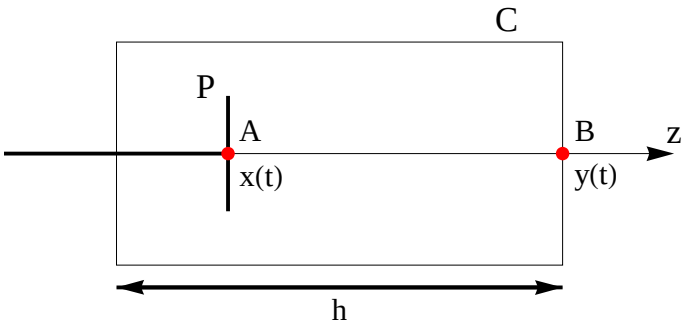

Figure 2.5: Simple physical system representing the dynamics of the ordinary play operator. The system consists of a piston P contained with in a cylinder C of length h. The piston and the cylinder are free to move along the z-axis indicated by the arrow. The position of point A is given by the function $x(t)$ and the position of the point B is given by the function $y(t)$.

of the cylinder will only be altered by interactions with the piston, therefore

$$y(t) = L[t_0, y(t_0)]x(t) \quad (t \geq t_0) \tag{2.2}$$

where the operator $L[t_0, y(t_0)]$ is defined for arbitrary $y_0 = y(t_0)$ for valid inputs $x(t)$ such that $y_0 - h \leq x(t_0) \leq y_0$. This condition on valid inputs in terms of the physical system means that the piston lies within the cylinder at the initial time moment t_0. Consider now a monotone increasing input applied to the piston. In this situation the piston is driven to the right hand side of Figure 2.5, while the cylinder remains in the same place until a moment t_1 when the piston makes contact with the wall of the cylinder. After the moment t_1 the cylinder and the piston move together. A graphical representation of this dynamics in the input-output plane is shown in Figure 2.6a.

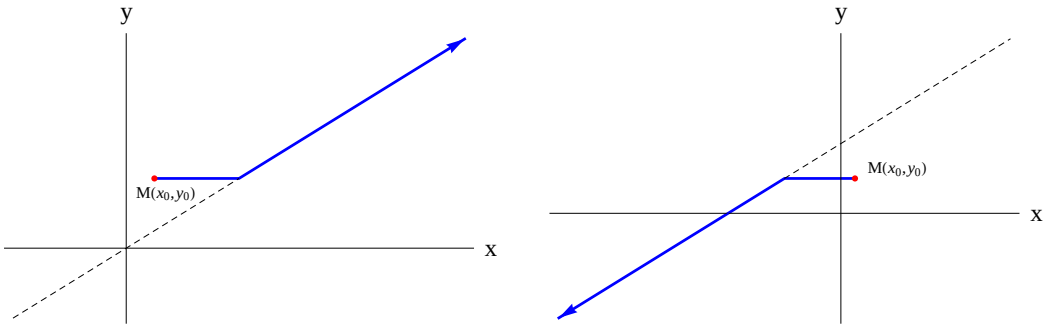

(a) Monotone increasing input (b) Monotone decreasing input

Figure 2.6: Dynamics of the ordinary play operator in the $x-y$ plane for monotone inputs. The point $M(x_0, y_0)$ is the initial position of the system.

Figure 2.6b shows the dynamics for the case of monotone decreasing inputs. In

this situation the piston is pulled to the left in Figure 2.5 and the cylinder remains fixed until the piston encounters the back wall of the cylinder and they continue on together. The output the ordinary play operator at any given moment $t \geq t_0$ can then be defined for monotone inputs as

$$y(t) = \begin{cases} y_0 & y_0 - h \leq x(t) \leq y_0 \\ x(t) & x(t) \geq y_0 \\ x(t) + h & x(t) \leq y_0 - h \end{cases} \tag{2.3}$$

How to alter this from monotone inputs to complex continuous inputs can be understood if the behaviour of the system for a simple periodic input is considered graphically. From Figure 2.6 and equation (2.3) it is clear that the lines $y = x$ and $y = x+h$ on the input-output plane are important to the dynamics of the ordinary play operator, they act as bounding lines for any trajectory of the ordinary play operator projected onto this plane. For a graphical examination of the play operator consider first these two lines as in Figure 2.7a. The point $M(x_0, y_0)$ shown in Figure 2.7a is a valid initial condition for the ordinary play operator if it lies between the two lines. Consider now the system subjected to a simple periodic input, which first increases to a maximum value and then decreases to its minimum value. In the initial increasing period the system behaves like for a monotone increasing input, until the moment t_M when the input reaches its maximum value, x_M. The trajectory of the system up until this moment is shown in Figure 2.7b.

In order to understand what happens when the input starts to decrease after the moment t_M, consider again the representative physical system shown in Figure 2.5. In this system the piston would have moved to the right as the input increased, catching the edge of the cylinder so that they move together until the moment t_M when the piston achieves its maximum displacement. At this moment the piston will stop pushing the cylinder and start to pull back away from the wall of the cylinder, as a result the cylinder will remain stationary until the piston reaches the back wall of the cylinder at which point they will again move together. Graphically this means that the trajectory move horizontally away from the maximum point. The trajectory will remain horizontal until it intersects the line $y = x + h$, at which point it will decrease along this line until the moment t_m when the input reaches its minimum value. The trajectory up until the moment t_m is shown in Figure 2.7c. After this moment the piston will separate from the cylinder, and the trajectory will move horizontally away from this minimum

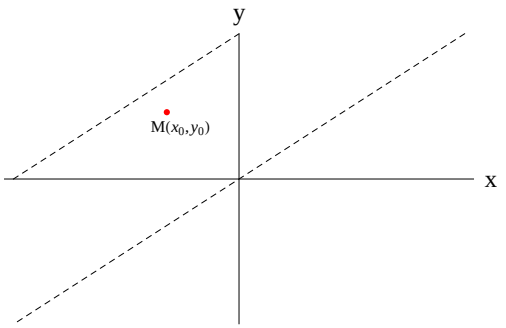

(a) The bounding lines $y = x$ and $y = x + h$ and starting position $M(x_0, y_0)$.

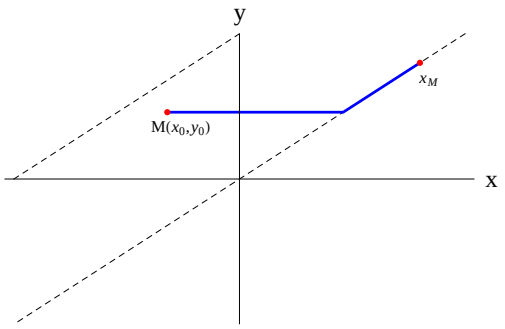

(b) Trajectory of the system from t_0 until t_M the time when the input reaches its maximum

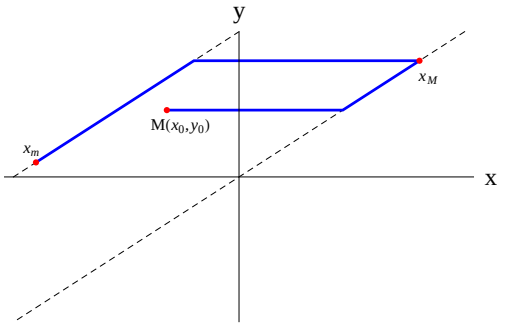

(c) Trajectory of the system up until the moment t_m when the input achieves its minimum value

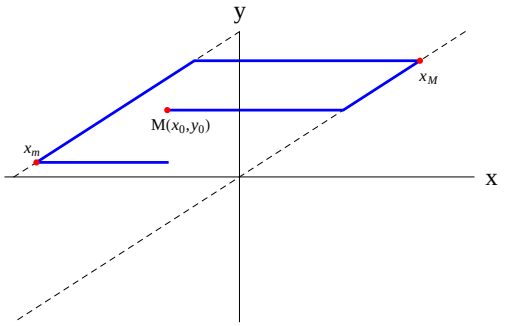

(d) Trajectory of the system at the end of the period.

Figure 2.7: Dynamics of the ordinary play operator for periodic inputs.

point. The trajectory at the end of the period is shown in Figure 2.7d.

Thus redefine the operator equation (2.2) as

$$y(t) = L[h, y_c]x(t) \tag{2.4}$$

where h is the distance between the two bounding lines on the input-output plane and y_c is a memory term. Initially $y_c = y_0$ however the value of y_c is changed to the current $y(t)$ value after every extremum in the input. This way the output of the ordinary play operator for any continuous input is given by

$$y(t) = \begin{cases} y_c & y_c - h \leq x(t) \leq y_c \\ x(t) & x(t) \geq y_c \\ x(t) + h & x(t) \leq y_c - h \end{cases} \tag{2.5}$$

as long as the value of y_c is updated to the current value of $y(t)$ whenever there is an extremum in the input.

2.2.2 Generalised play operator

From the graphical explanation of the ordinary play operator in Subsection 2.2.1, it is clear that the dynamics of the ordinary play operator could be defined in simple terms as horizontal motion while the input remains between two straight boundary lines and that the system increases along the right most boundary line and decreases along the left most boundary line. Under this concept it clear how the ordinary play operator can be made into a generalised play operator, if the two straight boundary lines are instead replaced by two curves Γ_r and Γ_l, see Figure 2.8.

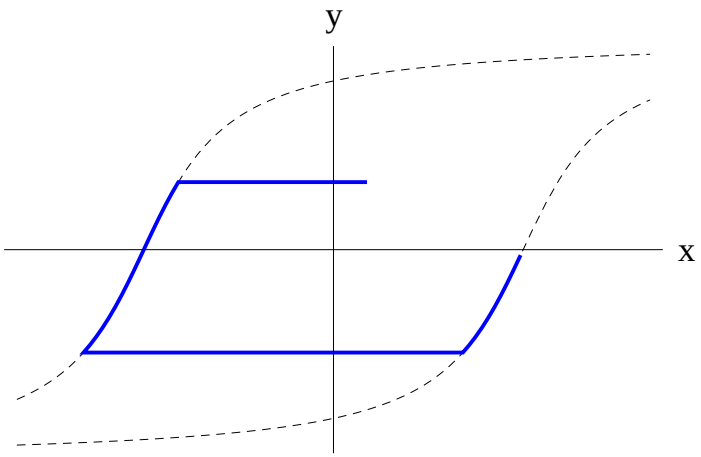

Figure 2.8: Sample dynamics of the generalised play operator.

In the generalised play operator the trajectory remains horizontal while varying between the curves Γ_r and Γ_l, the system increases along the curve Γ_r and decreases along the curve Γ_l. The output of the generalised play operator can be defined as

$$y(t) = \hat{L}[\Gamma_r(x), \Gamma_l(x), y_c]x(t) \tag{2.6}$$

where y_c is as before, $\Gamma_r(x)$ is the function whose graph is Γ_r and $\Gamma_l(x)$ is the function with the graph equal to Γ_l. This output is then given by

$$y(t) = \begin{cases} \max[y_c, \Gamma_r(x(t))] & x \text{ increasing} \\ \min[y_c, \Gamma_l(x(t))] & x \text{ decreasing} \end{cases} \tag{2.7}$$

as long as y_c is updated after every extremum of the input as before.

2.3 Preisach model

The Preisach model of hysteresis was first suggested by F Preisach in his paper [13] as a model of ferromagnetism. It has been widely applied to model magnetism see for example [14–16]. The model has also been used to model a broader range of areas for example elastoplasticity [17–19], terrestrial hydrology [20–22], economics [23–25], shape memory alloys [26–28] and more.

Using the mathematical formalism of [10] one can consider the Preisach operator as a continuum of non-ideal relays connected in parallel. The threshold values of the constituent relays can be represented as points on the plane $\Pi = \{(\alpha, \beta) : \beta \geq \alpha\}$ this plane is known as the Preisach half-plane. The output of a parallel connection of hysterons was defined in [10] as the weighted sum of the outputs of the individual hysterons with each given the same input. In determining the output of the Preisach operator exchange the sum for an integral, due to the continuum of relays used, where the integral is taken over the Preisach half-plane. Thus the Preisach operator maps the continuous input $x(t)$ for $t \geq t_0$ to the continuous output $y(t)$ according to equation (2.8).

$$\begin{aligned} y(t) &= P[\eta_0(\alpha, \beta)]x(t) \\ &= \iint_{\Pi} \mu(\alpha, \beta) R_{\alpha,\beta}[\eta_0(\alpha, \beta)]x(t)\, \mathrm{d}\alpha \mathrm{d}\beta \qquad t \geq t_0 \end{aligned} \tag{2.8}$$

In this equation $\mu(\alpha, \beta)$ is an integrable nonnegative function called the Preisach weight function which describes the weighting of the non-ideal relay with thresholds α, β (it can often be referred to as the Preisach density function in the literature). The function $\eta_0(\alpha, \beta)$ is a binary function called the initial state of the Preisach operator and is an infinite-dimensional parameter describing the state of all the constituent relays at the initial time moment t_0. For convenience later I will shorten the notation by omitting any reference to the initial state wherever it will not lead to confusion thus the output of the operator will be referenced as $y(t) = (Px)(t)$.

It should be noted that it is also possible to construct a discrete version of the Preisach operator by using a finite set of non-ideal relays and where the integral is replaced by a summation and the Preisach weight function is replaced by a finite set of nonnegative weights μ_i.

2.3.1 Geometrical interpretation

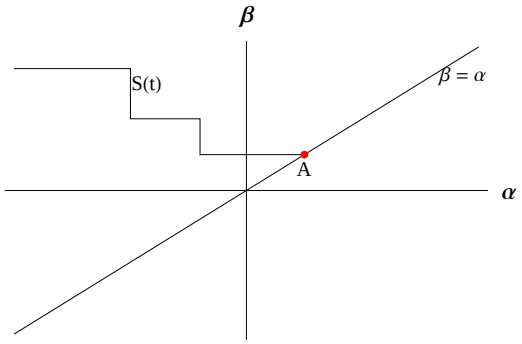

Figure 2.9: The Preisach half-plane. The boundary line $S(t)$ separates the domain where the points (α, β) correspond to the relays which are switched on (below the line $S(t)$) from the domain where the relays are switched off (above the line $S(t)$) at a given moment t. The coordinates of the point A equal the input value $x(t)$.

Calculation of the integral in equation (2.8) for the output of the Preisach operator is simplified by the geometric interpretation of the states of the Preisach operator, see for example [11]. At a given moment t, some of the relays that make up the Preisach operator are switched on and the remainder are switched off, this corresponds to two regions on the Preisach half-plane divided by a boundary line $S(t)$ see Figure 2.9.

In Figure 2.9 the region to the left of the boundary line $S(t)$ and above the bisector line $\beta = \alpha$ is the region where the relays are switched on, denote this as region S_1, and to the right of the line $S(t)$ and above the bisector the region where the relays are switched off, denote this as region S_2. So the output of the Preisach operator can be thought of as

$$y(t) = \iint_{S_1} \mu(\alpha, \beta) R_{\alpha,\beta} x(t) \, \mathrm{d}\alpha \mathrm{d}\beta + \iint_{S_2} \mu(\alpha, \beta) R_{\alpha,\beta} x(t) \, \mathrm{d}\alpha \mathrm{d}\beta.$$

However in the region S_2 all the relays are switched off so $R_{\alpha,\beta} x(t) = 0$ for all inputs $x(t)$ and in region S_1 the relays are switched on so $R_{\alpha,\beta} x(t) = 1$ for all inputs $x(t)$. This means that the output of the Preisach operator is reduced to

$$y(t) = \iint_{S_1} \mu(\alpha, \beta) \, \mathrm{d}\alpha \mathrm{d}\beta. \tag{2.9}$$

That is the output value $y(t)$ equals the integral of the Preisach weight function $\mu(\alpha, \beta)$ over the region S_1. The evolution of the input results in the evolution

of the boundary line $S(t)$ and subsequently to the region S_1 and as a result the output of the operator. The changes to the boundary line $S(t)$ over time can be defined in the geometric interpretation by a few basic rules.

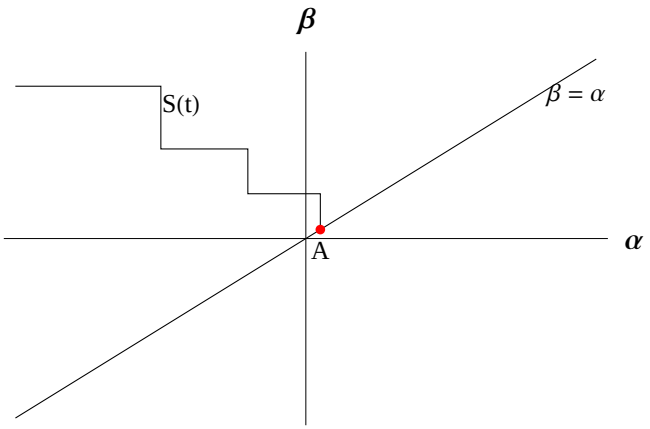

Figure 2.10: An example of creating a new corner in the line $S(t)$ at an extremum (turning) point of the input $x(t)$.

The coordinates of the point of intersection between the lines $S(t)$ and $\beta = \alpha$, marked A in Figure 2.9, equals the current value of the input $x(t)$. Changes in the input value can be converted to changes in the position of A along the line $\beta = \alpha$ as follows, when $x(t)$ increases the point A moves from left to right, similarly when $x(t)$ decreases the point A moves from right to left. Movement of the point A alters the shape of the line $S(t)$. If A moves from left to right, that is for increasing input, then the initial link of the line $S(t)$ is horizontal and moves up the β axis. If A moves from right to left, that is for decreasing input, then the initial link of the line $S(t)$ is vertical and moves along the α axis.

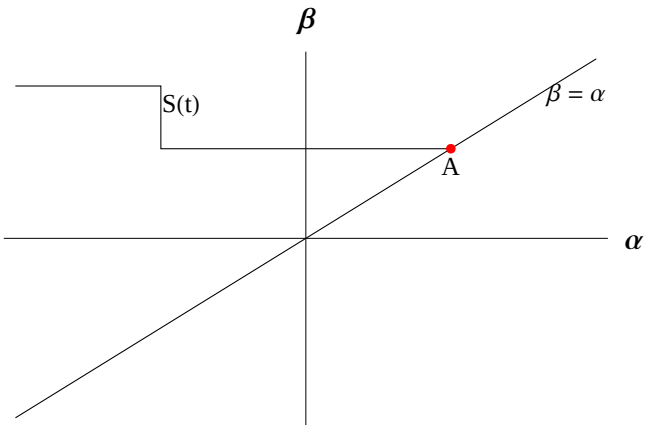

Figure 2.11: An example of erasing (wiping out) corners in the line $S(t)$.

If for example Figure 2.9 represents a moment $t = t_1$ when the input $x(t)$ reaches a local maximum value and then $x(t)$ decreases until a later moment $t = t_2$, then

Figure 2.10 shows the line $S(t_2)$. Note that a new corner has been added to the line $S(t)$.

Assuming further that $x(t_2)$ is a local minimum of the input and $x(t)$ increases after the moment $t = t_2$, Figure 2.11 shows the line $S(t)$ at the later moment $t = t_3 > t_2$, when the value of the input has become equal to the ordinate of one of the corners of the line $S(t_2)$ shown in Figure 2.10. Of note is that $S(t)$ has been changed by the removal of any corners that have a lower ordinate than the current value $x(t_3)$ of the input. For a complete discussion on all the rules for the movement of the boundary line please see [11].

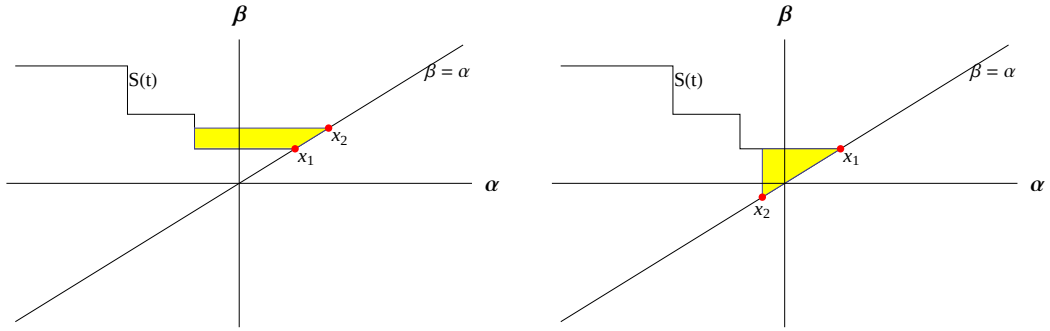

(a) The input increases from the value x_1 to x_2. As a result the relays in the shaded area are switched on; other relays do not change their state. The output (2.9) increases by the integral of the Preisach weight function $\mu(\alpha, \beta)$ over the shaded area

(b) The input decreases from the value x_1 to x_2. As a result the relays in the shaded area are switched off; other relays do not change their state. The output (2.9) decreases by the integral of the Preisach weight function $\mu(\alpha, \beta)$ over the shaded area

Figure 2.12: Changes in the output of the Preisach operator.

In Figure 2.12 the effect that the change on the boundary line $S(t)$ has on the output of the operator is shown. Figure 2.12a shows that an increase of the input from x_1 to x_2 adds the shaded area to the region S_1 so as a result the value of the output increases by the integral of the Preisach weight function $\mu(\alpha, \beta)$ over the shaded area. Similarly for the decreasing case shown in Figure 2.12b if the input decreases from x_1 to x_2 the shaded area is removed from the region S_1 so the output is decreased by the integral of $\mu(\alpha, \beta)$ over the shaded area.

2.3.2 Preisach memory state

The boundary line $S(t)$ is known as the state of the Preisach operator. Its position on the Preisach half-plane is defined by the location of its corners described by the coordinate pairs (m_k, M_k). Figure 2.13 shows the projection of these corners onto the bisector $\beta = \alpha$. The dynamics of the input results in the deletion of certain

corners and the creation of new ones and is thereby translated to the dynamics of the state and the output of the Preisach operator as described in Subsection 2.3.1. At a given moment t, the abscissas $m_0, m_1, \ldots, m_k$ of the corners of $S(t)$ form a subset of the set of all local minima of the input $x(t)$ which have been achieved prior to the moment t. They are called the dominant minima of the input, see [11] for the definition and discussion. Likewise the ordinates $M_0, M_1, \ldots, M_{k'}$ of the corners of $S(t)$ are a specific selection of the local maxima of the input which $x(t)$ has achieved prior to the moment t; they are called the dominant maxima. The dominant extrema (also known as the past shock values of the input) at every instant are ordered as

$$\ldots < m_k < \ldots < m_1 < m_0 < x(t) < M_0 < M_1 < \ldots < M_{k'} < \ldots$$

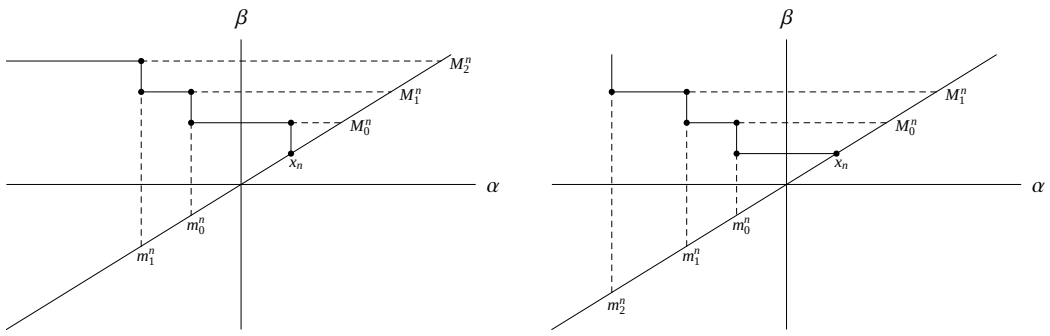

(a) The configuration of the Preisach memory state when the length of the array ω_M, that is the number of elements in the array ω_M, is greater than the length of ω_m.

(b) The configuration of the Preisach memory state when the length of the array ω_m, that is the number of elements in the array ω_m, is greater than the length of ω_M.

Figure 2.13: Two possible configurations of the Preisach memory state.

The set of dominant minima form an array of numbers that will be referred to as ω_m, the set of dominant maxima form an array that will be referred to as ω_M. There are four possible configurations of the Preisach memory state $S(t)$. The particular arrangement for a given sequence of main extrema is determined in part by the length of the arrays ω_M and ω_m (that is the number of elements in each array). Figure 2.13 shows the two configurations possible when the length of the arrays are not equal. In the case that the lengths of the arrays are equal then the state can be arranged in two possible ways, one where the initial link of $S(t)$ connecting the point $(x(t), x(t))$ on the bisector $\beta = \alpha$ to the first corner of the Preisach state is horizontal and the other where the initial link is vertical.

In order to uniquely describe the state, I use an additional variable ζ which can have either the value 1 or -1. The value 1 corresponds to the arrangement of the

state where the initial link is horizontal and the -1 value means that the initial link is vertical. Thus, given an input value $x(t)$ at the moment t, the value of the variable ζ and the two arrays $\omega_m = \{m_0, m_1, \ldots\}$, $\omega_M = \{M_0, M_1, \ldots\}$ containing the values of the dominant main extrema at this moment completely defines the state S(t) (and thus the memory of the system at the moment t).

2.3.3 Properties of the operator

2.3.3.1 Wipeout property

In Subsection 2.3.1 it was mentioned that when an increasing input reached the ordinate of one of the corners of the line $S(t)$ then any corners with a lower ordinate are removed from the boundary line. Similarly for a decreasing input whenever the input reaches the abscissa of a corner then any corners with a higher abscissa are removed. This property of the Preisach operator is called the wipeout property. This means that only certain extrema, known as the dominant extrema see [11] for definition and discussion, form the memory of the Preisach operator. From [11] the wipeout property is defined as "Only the alternating series of dominant input extrema are stored by the Preisach model. All other input extrema are wiped out."

2.3.3.2 Congruency property

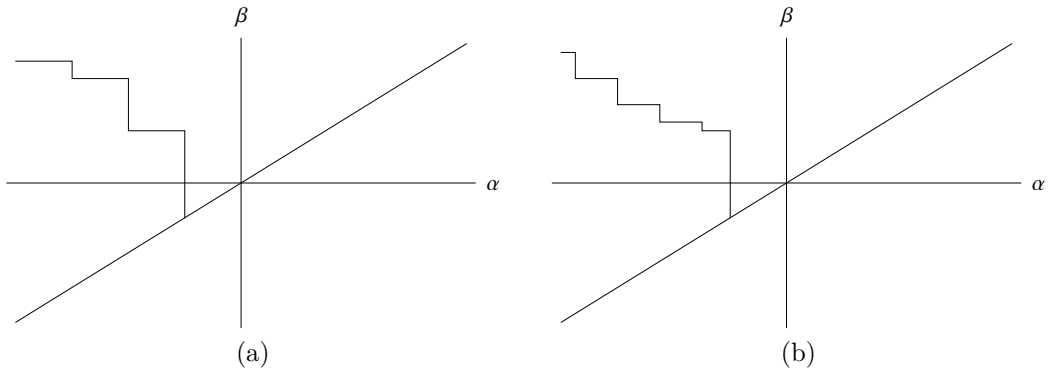

Figure 2.14: Example of the states of two Preisach hysteresis operators with different past inputs.

Consider two Preisach operators P_1 and P_2 with different past histories, see Figure 2.14, which at some moment t_0 are subjected to the same periodic input that varies between the two consecutive extremum values, x^+ and x_-.

The minor hysteresis loops formed by the oscillation of this input in the input-output plane are at different points on the plane due to the different past histories of each operator, see Figure 2.15. However these loops are congruent, these two loops can be overlayed on each other by a translation along the y-axis.

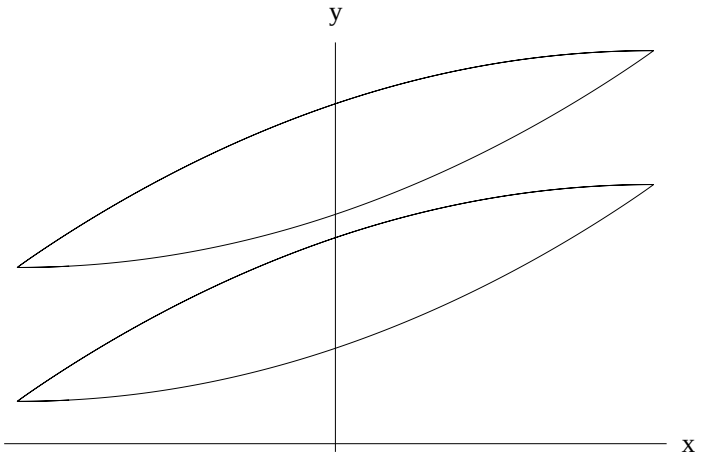

Figure 2.15: Plot of the congruent minor hysteresis loops formed by periodic input to two Preisach operators with different initial states, like those in Figure 2.14.

This property is known as the congruency property. From [11] the congruency property is defined as "All minor hysteresis loops corresponding to back-and-forth variations of inputs between the same two consecutive extremum values are congruent."

It should be noted that the wipeout and congruency properties form the necessary and sufficient conditions for a nonlinearity of hysteresis type to be represented by the Preisach model, for proof of this I direct the reader to [11] where it is referred to as the "Representation Theorem".

2.4 Prandtl-Ishlinskii operator

A classical model of elastic-plastic behaviour is the Prandtl-Ishlinskii model of hysteresis. This model is generally presented as a parallel connection of stop operators (this operator can often be referred to as a basic elastic-plastic element, see for example [1]), however the model can also be developed in terms of the play operator introduced earlier in this chapter due to the close relationship between the play and stop operators. In terms of the play operator the Prandtl-Ishlinskii

model is then

$$w(t) = \int_0^\infty p(r)\mathrm{d}r v(t) - \int_0^\infty p(r)L[2r, y_c(r)]v(t)\mathrm{d}r \tag{2.10}$$

where $p(r)$ is a density function describing the weights of all the play operators and $L[2r, y_c(r)]$ is the ordinary play operator with width $2r$ between the two bounding lines in the input-output plane and memory element $y_c(r)$ which is updated after each extremum in the input $v(t)$. Of note regarding the Prandtl-Ishlinskii operator when it is constructed from the ordinary play operator is that it is only capable of mapping symmetric hysteresis loops and it does not exhibit saturation (when formulated from the stop operator it does exhibit saturation effects).

The Prandtl-Ishlinskii operator can be modified in order to allow for the representation of both saturation and asymmetric hysteresis loops. This modified operator is referred to as the generalised Prandtl-Ishlinskii operator and is obtained by forming the Prandtl-Ishlinskii operator using generalised play operators instead of the ordinary play operator, see for example [29, 30].

Note it is possible to form a discrete version of the Prandtl-Ishlinskii operator in a similar manner to the discrete Preisach operator, where a finite number of play operators are used.

2.4.1 Relation to the Preisach operator

An important result, first established by Krejčí in [31] and widely used in the modelling of systems with the Preisach operator see for example [32], is that the Preisach operator can be represented as

$$(Px)(t) = \int_0^\infty g(r, L[2r, y_c(r)]x(t))\mathrm{d}r \tag{2.11}$$

where $g(r, L[2r, y_c(r)]x(t))$ is a generalised play operator where all the horizontal segments have the same length and the graph of g defines the boundary lines Γ_l and Γ_r, $g(r, L[2r, y_c(r)]x(t))$ is a specific case of the Krasnosel'skii-Pokrovskii Canonical Representation Theorem, see [10]. That is it is a generalised Prandtl-Ishlinskii operator composed of generalised plays. A geometrical representation of the construction of the Preisach operator in this way is shown in [33].

Chapter 3

Numerical solution of stochastic differential equations with the Preisach operator

A significant amount of work has been done on developing, studying and solving deterministic differential models which contain the Preisach operator. Of these models the simplest models consist of a single scalar differential equation coupled with the Preisach operator input-output relationship.

These types of models have been used in the context of terrestrial hydrology of homogenous soil water systems where the Preisach operator introduces a hysteretic constitutive relationship between the moisture content in the soil and the pressure (matric potential) to the ordinary differential equation obtained by averaging out any spatial variation from the Philip-Richards balance equation [21, 22, 34].

Another example is provided by models of macroeconomic systems and multiagent market models where the Preisach operator is used to incorporate shock type memory into the system [23, 24]. Each of these areas contain a stochastic nature which is not fully encapsulated by deterministic models.

Stochastic aspects of the Preisach operator input-output relationship have been fairly well understood in the case of open loop systems where the properties of the stochastic input are known or measurable *a priori* [5]. The formalism of the phenomenological Preisach model is rather general in modelling rate-independent systems exhibiting hysteresis and shock type memory.

The theory of a stochastically driven Preisach operator has been motivated by,

and successfully applied to a variety of problems such as modelling thermal relaxation and viscosity (aftereffect) in ferromagnetic materials [35, 36], creep in superconductors [37], signal processing and passage of noise through hysteretic systems [38], effect of noise on data storage technologies and data collapse [39] and others.

Differential models of closed loop systems involving the Preisach operator have received less attention. The existing body of results refers mainly to systems with piecewise smooth trajectories such as models of stochastically driven mechanical systems, shape memory alloys and hysteretic oscillators [40]; estimation of damage and fatigue [41] and models of terrestrial hydrology [4].

As a stochastic extension to the deterministic equations with the Preisach operator considered in [22–24] in the context of modelling hydrological systems and economic systems, the following formal stochastic differential equation is proposed

$$\xi \mathrm{d}x_t + \mathrm{d}(Px)_t = a(x_t, t)\mathrm{d}t + b(x_t, t)\mathrm{d}W_t \tag{3.1}$$

where P denotes the Preisach operator, *i.e.*, $(Px)_t = (Px)(t)$ denotes output of the Preisach model with continuous input $x_t = x(t)$; ξ is a positive parameter; W_t is the Wiener process and $a(\cdot, \cdot)$, $b(\cdot, \cdot)$ are continuous functions.

This extension may be of interest in the areas of hydrology, economics and finance where stochastic effects are prevalent. As a prototype example considered below is a simple price dynamics model leading to a discrete time counterpart of equation (3.1) with constant a and b. This price dynamics model adopts, in a simplified form, the philosophy of the modelling approach proposed in [42–46] which leads to a hierarchy of powerful multiagent models of economic systems.

Equation (3.1) can also be used for examining the effect of feedback on various open loop systems modelled by the Preisach operator and by the inverse Preisach operator with a stochastic input, as well as for testing the effect of noise on deterministic differential models involving the shock type memory.

The simplest example of the shock type memory is the running maximum (running minimum) of the input which is one of the standard market indicators in the financial setting. Stochastic differential equations involving running extrema have been studied, for instance, in [47]. From this perspective, equation (3.1) can be viewed as a similar model that incorporates a more complex memory of the past shock type events. The role of such shocks in economic systems is discussed in [23]. Equation (3.1) is thus the simplest model incorporating both the Preisach

memory operator and a stochastic component.

The mathematical formalism of the continuous time system (3.1) is not the subject of this study. The aim of this study is to develop and implement an Euler type formal discretisation of (3.1).

3.1 A motivating example

Consider a simple model of a market which consists of many traders. Each trader is modelled by a non-ideal relay with thresholds α, β where $\alpha \leq \beta$ and the thresholds are different for each different trader. Hence, a single trader is in one of two possible states $s = \pm 1$.

Let $s = -1$ be the 'long' state, that is the trader has purchased an asset at a price lower than the value of his β threshold and waits until the price goes up to the value of his β threshold before selling it with profit, which switches the trader to the state $s = 1$ which is the 'short' state, that is the trader has not purchased an asset and waits for the price to fall to the level of his α threshold at which he wants to buy the asset at this price, causing the trader to switch to the state $s = -1$.

In this context consider a market with M traders, with the i-th trader having thresholds α_i, β_i, and using the concepts presented in Chapter 2 construct a discrete version of the Preisach model of them. If the input to the system is taken to be the price, p, of the asset, then following [45] gives the output

$$\sigma = \frac{1}{M} \sum_{i=1}^{M} \mu_i s_i \tag{3.2}$$

which measures the sentiment of the market. Here s_i is the state of the i-th trader and $\mu_i \geq 0$ is his weight in forming public opinion about the value of the asset (possibly related to the amount of money or asset he has, etc.).

The dynamics of the price of the asset are assumed to follow the equation from [45]. That is, the price evolves in discrete time as

$$p_{t+h} = p_t \exp\left[\eta_t \sqrt{h} + \left(a - \frac{1}{2}\right) h - \kappa \Delta \sigma_t\right] \tag{3.3}$$

where h is the time step; the sequence of independent Gaussian random quantities $\eta_t \sim N(0, 1)$ models the external random information stream; a is the trend term;

$-\frac{1}{2}$ correction term is the same as in the classical setting where it comes from Ito's formula; $\kappa > 0$ is a parameter measuring the effect of the sentiment on the market and $\Delta\sigma_t = \sigma_{t+h} - \sigma_t$ is the change in sentiment which creates a pressure on price. The minus sign in front of the hysteresis term $\kappa\Delta\sigma_t$ accounts for the fact that as more traders switch to the 'long' state a positive pressure pushing the price up is created. Similarly, when more traders switch to the 'short' state this causes a pressure on the price to move down. That is there is a negative feedback loop. Note that setting $\kappa = 0$ transforms (3.3) to the discrete form of the standard geometric Brownian motion.

If the variable

$$r = \ln \frac{p}{p_0}$$

is introduced instead of p to perform a logarithmic scaling of the price, then equation (3.3) can be rewritten as

$$\Delta r_t = \eta_t \sqrt{h} + \left(a - \frac{1}{2}\right) h - \kappa \Delta\sigma_t \tag{3.4}$$

with $\Delta r_t = r_{t+h} - r_t$. It should be noted that according to (3.2), σ_t is the output of the discrete Preisach model with the input p_t. However r_t can be used as the input instead of p_t if the thresholds of the relays are also rescaled (or, equivalently, the Preisach weight function). This is achieved by scaling the threshold values α_i, β_i of the i-th relay to be instead $\ln(\alpha_i/p_0)$, $\ln(\beta_i/p_0)$. Denote by P the discrete Preisach operator obtained with the scaling. Then equation (3.4) becomes

$$\Delta r_t + \kappa \Delta(Pr)_t = \eta_t \sqrt{h} + \left(a - \frac{1}{2}\right) h \tag{3.5}$$

where $\Delta(Pr)_t = (Pr)_{t+h} - (Pr)_t$. Thus the formal continuous time counterpart of equation (3.5) is

$$\mathrm{d}r_t + \kappa \mathrm{d}(Pr)_t = \left(a - \frac{1}{2}\right) \mathrm{d}t + \mathrm{d}W_t \tag{3.6}$$

which has the form of equation (3.1) with constant coefficients for a and b.

A couple of remarks about the model are presented here. First, equation (3.6) can be integrated explicitly in terms of the inverse Preisach operator, that is equation (3.6) is the same as

$$r_t - r_0 = (I + \kappa P)^{-1} \left[\left(a - \frac{1}{2}\right)(t - t_0) + W_t - W_0\right] \tag{3.7}$$

where I is the identity operator and t_0, r_0 and W_0 are the initial conditions (for the details regarding the properties of the inverse operator $(I + \kappa P)^{-1}$ see [1]). This formula provides a rigorous interpretation of solutions to the continuous time equation (3.6) and can also be used to prove the convergence of the discretisation (3.5) to the continuous limit (3.6) as $h \to 0$. A similar formula and the same approach can be used if the trend term $a = a(t)$ is a function of time (for example, when accounting for seasonality in the trend). However, if a depends on the price of the asset $r(t)$, then (3.6) is a closed loop system not amenable to explicit integration. In this case, a mathematical formalism for the continuous time equation (3.6) is an open problem as it is for the more general equation (3.1).

Secondly, equation (3.6), when rearranged into the form of equation (3.1), has a parameter $\xi = 1/\kappa$. This parameter can be assumed to be of order 1. However, in models of economic systems proposed in [24] (as well as in the hydrological context, see [34]) the cases of interest are $\xi \ll 1$ and $\xi = 0$. The case $\xi = 0$ can be singular and requires special treatment. For example, in the deterministic setting, it has been shown that solutions of equation (3.1) with $b = 0$ have better regularity for $\xi > 0$ than $\xi = 0$. Moreover, non-uniqueness of solutions to the initial value problem is possible for $\xi = 0$, see [34]. Nevertheless, natural generic conditions ensures the uniqueness property and the convergence of the solution of the deterministic equation $\xi > 0$ to the solution of the equation with $\xi = 0$ as $\xi \to 0$. Numerical schemes for solving deterministic equations with $\xi = 0$ have been developed in [48–50]; the limit $\xi \to 0$ has been used in [4] to solve equations with a stochastic component that have piecewise smooth trajectories.

3.2 Numerical schemes

In this section two Euler type time discretisations of equation (3.1) are outlined. The difference between the two schemes is in the method that is used to evaluate the change in the output of the Preisach operator on a time step.

In the first scheme the increment Δy_n of the output is evaluated in the same way as proposed in the deterministic setting in [48–50]. It is assumed that the time step taken is sufficiently small so that; (i) the shaded area $S(t_{n+1})\backslash S(t_n)$ shown in Figure 2.12a is well approximated by the rectangular area which has width equal to the increment Δx_n of the input and the length equal to the initial link of the staircase line $S(t_n)$; (ii) a typical Δx_n is much smaller than ξ and therefore the

increment of Δy_n of the output at the turning points of x_n is close to $\xi \Delta x_n$; and, (iii) for most other (non-turning) points of x_n the set $S(t_{n+1}) \backslash S(t_n)$ is trapezoid as in Figure 2.12. This scheme will be referred to as the rectangular method.

Alternatively, Δy_n can be calculated using the exact expression for the shaded area show in Figure 2.12 and the corresponding numerical scheme is called the triangular method.

To simplify the notation the Preisach operator that has the weight function which is non-zero only inside the triangle T formed by the lines $\beta = \alpha$, $\alpha = \beta_0$ and $\beta = \alpha_0$, see for example Figure 3.1, is considered. This triangle will be referred to as the bounding triangle on the Preisach half-plane. Where α_0 and β_0 are constant values that are chosen so that all variations of x_n are contained within the triangle T. Inside the triangle T the function $\mu(\alpha, \beta) \equiv \mu(t)$, that is there is no variation of μ in either α or β. Let $\mu_n = \mu(t_0 + nh)$. The triangle T is implemented by including the values α_0 and β_0 in the arrays ω_m and ω_M respectively. Since variation outside of the triangle T is not allowed these elements always remain in the arrays as the element with the largest magnitude.

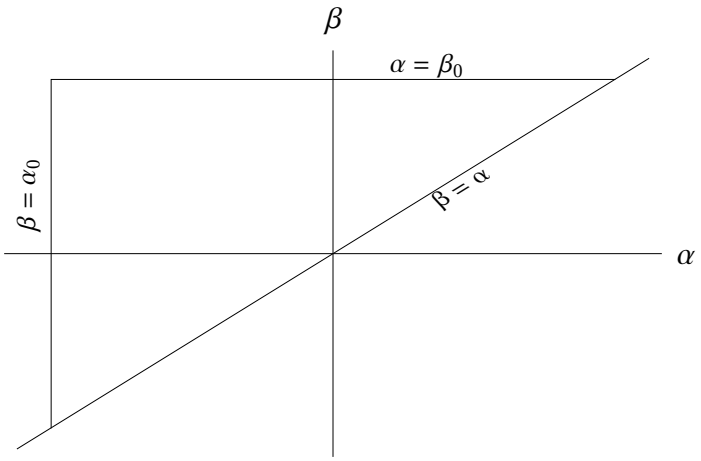

Figure 3.1: An example of the bounding triangle on the Preisach plane.

3.2.1 Rectangular method

Define the following finite difference for the right hand side of equation (3.1)

$$d_n = a(x_n, t_0 + nh)h + b(x_n, t_0 + nh)\sqrt{h}\Delta W_n$$

where h is the time step; $n = 0, 1, \ldots$ and ΔW_n are independent Gaussian random variables

$$\Delta W_n \sim N(0, 1).$$

In the rectangular method, the increment of the output of the Preisach operator on the n-th time step is approximated by the product of the increment $\Delta x_n = x_{n+1} - x_n$ of the input and the length l_n of the initial link of the state of the Preisach operator at the moment n and the value of the Preisach weight function μ_n at the moment n. This leads to the discretisation of equation (3.1) in the form

$$(\xi + \mu_n l_n)\Delta x_n = d_n \tag{3.8}$$

where

$$l_n = \begin{cases} x_n - m_0^n & \text{if } d_n > 0,\ d_{n-1} > 0 \\ 0 & \text{if } d_n d_{n-1} < 0 \\ M_0^n - x_n & \text{if } d_n < 0,\ d_{n-1} < 0 \end{cases} \tag{3.9}$$

Here m_0^n and M_0^n are the first elements of the arrays ω_M and ω_M of the main minima and maxima at the moment n; d_{-1} equals the value ζ_0 of the variable ζ at the initial moment. Note the sign of the increment Δx_n coincides with the sign of d_n; l_n is zero at the turning points of x_n, that is $l_n = 0$ whenever $\Delta x_n \Delta x_{n-1} < 0$ (equivalently, $d_n d_{n-1} < 0$), while $l_n > 0$ whenever $\Delta x_n \Delta x_{n-1} > 0$ (equivalently, $d_n d_{n-1} > 0$).

The numerical scheme has been implemented in the following steps to account for updating the memory arrays ω_m and ω_M, the variable ζ_n and the value of x_n. For $t = t_0 + nh$:

(i) Calculate the value of d_n;

(ii) Evaluate the turning points as follows:

- If $d_n d_{n-1} < 0$ (i.e., x_n is a turning point), then:
  - (a) If $d_n > 0$ add the element x_n to the memory array ω_m and set $\zeta_{n+1} = 1$;
  - (b) If $d_n < 0$ add the element x_n to the memory array ω_M and set $\zeta_{n+1} = -1$;
- If $d_n d_{n+1} > 0$ the memory arrays ω_m, ω_M remain the same and $\zeta_{n+1} = \zeta_n$;

(iii) Calculate the new x value as

$$x_{n+1} = x_n + \frac{d_n}{\xi + \mu_n l_n};$$

(iv) Update the memory arrays for the new position of x by performing deletions of their elements if either of the following conditions are met:

(a) For $d_n > 0$ remove the elements $M_0^n, \ldots, M_k^n$ satisfying $M_i^n \leq x_{n+1}$ from the array ω_M; remove the same number of elements $m_0^n, \ldots, m_k^n$ from the array ω_m;

(b) For $d_n < 0$ remove the elements $m_0^n, \ldots, m_k^n$ satisfying $m_i^n \geq x_{n+1}$ from the array ω_m and the same number of elements $M_0^n, \ldots, M_k^n$ from ω_M.

3.2.2 Triangular method

This alternative method, utilises the exact expression for the increment Δy_n of the output of the Preisach operator corresponding to the increment Δx_n of the input, i.e.,

$$\Delta y_n = (Px)(t_0 + (n+1)h) - (Px)(t_0 + nh)$$

where $x(t)$ is a monotone interpolation of the input between the discrete values $x_n = x(t_0 + nh)$ and $x_{n+1} = x(t_0 + (n+1)h)$. This leads to the discretisation

$$\xi \Delta x_n + \Delta y_n = d_n \tag{3.10}$$

of equation (3.1) with d_n the same as in the Subsection 3.2.1. This formula defines x_{n+1} implicitly given the value x_n and the state of the Preisach operator (i.e., the arrays ω_m and ω_M and the variable ζ) at the moment n; again, the sign of the increment Δx_n equals the sign of d_n and Δy_n has the same sign. Solving equation (3.10) for x_{n+1} is equivalent to explicit inversion of the operator $\xi I + P$ and leads to eight cases depending on the signs of d_n and ζ_n and the lengths of the arrays ω_m and ω_M (that is the number of elements in the arrays ω_m and ω_M). The geometrical interpretation considered in Chapter 2 makes this inversion straightforward (see Figure 2.12). An iterative procedure is used to find x_{n+1} with the number of iterations depending on how many corners should be erased from the state of the Preisach operator when the input increases from x_n to x_{n+1}.

In Chapter 2 it was stated that there are four possible configurations of the Preisach state $S(t)$. An example for each possible arrangement within the confines of the triangle T is shown in Figure 3.2. Which arrangement the current state corresponds to is determined by the arrays ω_m and ω_M as well as the variable ζ. I define two new variables $\bar{\omega}_m^n$ and $\bar{\omega}_M^n$. The variable $\bar{\omega}_m^n$ is the length of the array ω_m at the moment $t_0 + nh$ (that is $\bar{\omega}_m^n$ is the number of elements in the array ω_m at the moment $t_0 + nh$) and $\bar{\omega}_M^n$ is the length of the array ω_M at the moment $t_0 + nh$.

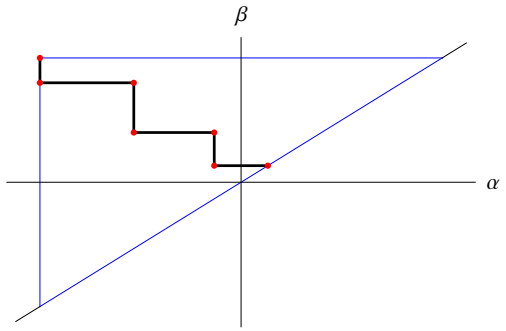

(a) Arrangement corresponding to the case $\bar{\omega}_M^n = \bar{\omega}_m^n$ and $\zeta = 1$.

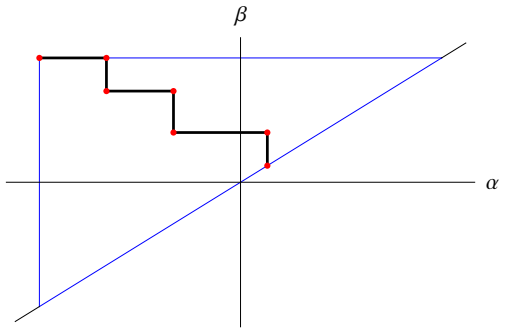

(b) Arrangement corresponding to the case $\bar{\omega}_M^n = \bar{\omega}_m^n$ and $\zeta = -1$.

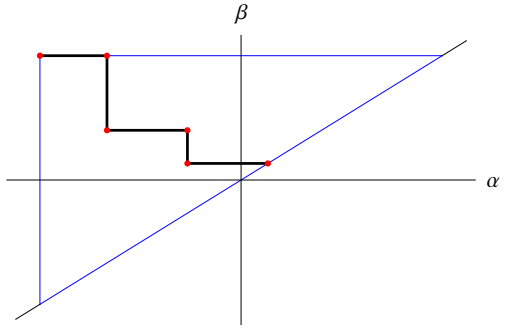

(c) Arrangement corresponding to the case $\bar{\omega}_M^n < \bar{\omega}_m^n$ and $\zeta = 1$.

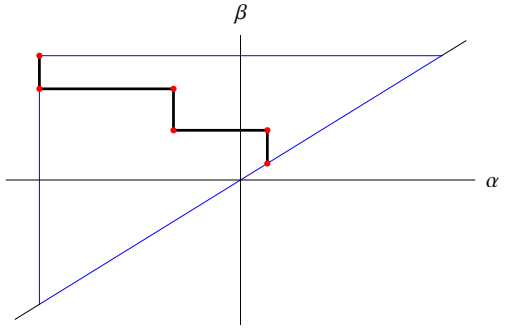

(d) Arrangement corresponding to the case $\bar{\omega}_m^n < \bar{\omega}_M^n$ and $\zeta = -1$.

Figure 3.2: Examples of all possible arrangements of the Preisach staircase line $S(t)$. The blue lines represent the bounding triangular domain on the Preisach plane Π for which the Preisach weight function μ is non-zero. The black line are the Preisach states $S(t)$.

Each arrangement must be considered separately when determining the change in the output of the Preisach operator. Consider first arrangements of the form shown in Figure 3.2a. This arrangement is characterised by $\bar{\omega}_m^n = \bar{\omega}_M^n$ and $\zeta = 1$. For the case of increasing input, that is $d_n > 0$. I introduce the value

$$\Sigma_0 = \xi(M_0^n - x_n) + \mu_n \left(\frac{(M_0^n - m_0^n)^2}{2} - \frac{(x_n - m_0^n)^2}{2} \right)$$

If $\Sigma_0 \geq d_n$ then $x_{n+1} \leq M_0^n$ (i.e., the value of x_{n+1} lies below the first corner of

the staircase state $S(t_0 + nh)$) and equation (3.10) is equivalent to

$$\xi(x_{n+1} - x_n) + \mu_n \left(\frac{(x_{n+1} - m_0^n)^2}{2} - \frac{(x_n - m_0^n)^2}{2} \right) = d_n$$

solving this quadratic equation for x_{n+1} gives

$$x_{n+1} = \frac{1}{\mu_n} \left((\mu_n m_0^n - \xi) + \sqrt{2\mu_n d_n + (\xi + \mu_n (x_n - m_0^n))^2} \right)$$

where the positive root is chosen to ensure that $x_{n+1} > x_n$. If however $\Sigma_0 < d_n$ then compare d_n consecutively with the elements $\Sigma_1, \Sigma_2, \ldots$ of the increasing sequence

$$\Sigma_k = \Sigma_{k-1} + \xi(M_k^n - M_{k-1}^n) + \mu_n \left(\frac{(M_k^n - m_k^n)^2}{2} - \frac{(M_{k-1}^n - m_k^n)^2}{2} \right)$$

where the index $k = 1, 2, \ldots, (\bar{\omega}_m^n - 1)$ until a Σ_k is found such that $\Sigma_k \geq d_n > \Sigma_{k+1}$. These relations ensure that $M_{k-1}^n < x_{n+1} \leq M_k^n$ and equation (3.10) is equivalent to

$$\Sigma_{k-1} + \xi(x_{n+1} - M_{k-1}^n) + \mu_n \left(\frac{(x_{n+1} - m_k^n)^2}{2} - \frac{(M_{k-1}^n - m_k^n)^2}{2} \right) = d_n$$

solution of this equation implies

$$x_{n+1} = \frac{1}{\mu_n} \left((\mu_n m_k^n - \xi) + \sqrt{2\mu_n (d_n - \Sigma_{k-1}) + (\xi + \mu_n (M_{k-1}^n - m_k^n))^2} \right).$$

For this arrangement of the staircase state in the case of decreasing input (that is $d_n < 0$) then the value Σ_0 is

$$\Sigma_0 = \xi(m_0^n - x_n) - \mu_n \left(\frac{(x_n - m_0^n)^2}{2} \right).$$

Then if $\Sigma_0 \leq d_n$ the value of x_{n+1} lies above the first corner that is $x_{n+1} \geq m_0^n$. This gives the quadratic equation for (3.10)

$$\xi(x_{n+1} - x_n) - \mu_n \left(\frac{(x_n - x_{n+1})^2}{2} \right) = d_n$$

Solution of this equation implies that x_{n+1} is

$$x_{n+1} = \frac{1}{\mu_n} \left(\mu_n x_n + \xi - \sqrt{\xi^2 - 2\mu_n d_n} \right)$$

where the negative root is chosen to ensure that $x_{n+1} < x_n$. If the value of Σ_0 is not sufficiently small (that is $\Sigma_0 > d_n$) then d_n is compared with the decreasing sequence

$$\Sigma_k = \Sigma_{k-1} + \xi(m_k^n - m_{k-1}^n) + \mu_n \left(\frac{(M_{k-1}^n - m_{k-1}^n)^2}{2} - \frac{(M_{k-1}^n - m_k^n)^2}{2} \right)$$

where the index $k = 1, 2, \ldots, (\bar{\omega}_m^n - 1)$ so that a value Σ_k is found so that $\Sigma_k \leq d_n \leq \Sigma_{k-1}$. This gives the following equation for (3.10)

$$\Sigma_{k-1} + \xi(x_{n+1} - m_{k-1}^n) + \mu_n \left(\frac{(M_{k-1}^n - m_{k-1}^n)^2}{2} - \frac{(M_{k-1}^n - x_{n+1})^2}{2} \right) = d_n$$

this equation implies that x_{n+1} is then

$$x_{n+1} = \frac{1}{\mu_n} \left(\mu_n M_{k-1}^n + \xi - \sqrt{2\mu_n(\Sigma_{k-1} - d_n) + (\xi + \mu_n(M_{k-1}^n - m_{k-1}^n))^2} \right).$$

A similar algorithm for solving equation (3.10) applies in the three other arrangements. Consider now arrangements of the Preisach state similar to the one shown in Figure 3.2b. This arrangement is characterised by the properties $\bar{\omega}_m^n = \bar{\omega}_M^n$ and $\zeta = -1$. For increasing input, $d_n > 0$, then the value Σ_0 is

$$\Sigma_0 = \xi(M_0^n - x_n) + \mu_n \left(\frac{(M_0^n - x_n)^2}{2} \right)$$

If this value is sufficient to exceed the value of d_n (that is $\Sigma_0 \geq d_n$ such that $x_{n+1} \leq M_0^n$) then (3.10) is equivalent to

$$\xi(x_{n+1} - x_n) + \mu_n \left(\frac{(x_{n+1} - x_n)^2}{2} \right) = d_n.$$

Solving this equation for x_{n+1} gives

$$x_{n+1} = \frac{1}{\mu_n} \left(\mu_n x_n - \xi + \sqrt{\xi^2 + 2\mu_n d_n} \right)$$

where the positive root is chosen for the same reason as before. If the value Σ_0 does not give an upper bound on the value x_{n+1} then compare the value d_n with the increasing sequence

$$\Sigma_k = \Sigma_{k-1} + \xi(M_k^n - M_{k-1}^n) + \mu_n \left(\frac{(M_k^n - m_{k-1}^n)^2}{2} - \frac{(M_{k-1}^n - m_{k-1}^n)^2}{2} \right)$$

where the index $k = 1, 2, \ldots, (\bar{\omega}_M^n - 1)$. Once an element Σ_k is found such that $\Sigma_k \geq d_n > \Sigma_{k-1}$ then equation (3.10) becomes

$$\Sigma_{k-1} + \xi(x_{n+1} - M_{k-1}^n) + \mu_n \left(\frac{(x_{n+1} - m_{k-1}^n)^2}{2} - \frac{(M_{k-1}^n - m_{k-1}^n)^2}{2} \right) = d_n$$

Which solution of gives for x_{n+1}

$$x_{n+1} = \frac{1}{\mu_n} \left(\mu_n m_{k-1}^n - \xi + \sqrt{2\mu_n(d_n - \Sigma_{k-1}) + (\xi + \mu_n(M_{k-1}^n - m_{k-1}^n))^2} \right)$$

For the case of decreasing input ($d_n < 0$) for this arrangement. Take the value

$$\Sigma_0 = \xi(m_0^n - x_n) + \mu_n \left(\frac{(M_0^n - x_n)^2}{2} - \frac{(M_0^n - m_0^n)^2}{2} \right)$$

If this value is a lower bound on the value of x_{n+1} (that is $\Sigma \leq d_n$ so that $x_{n+1} \geq m_0^n$) then equation (3.10) is the same as

$$\xi(x_{n+1} - x_n) + \mu_n \left(\frac{(M_0^n - x_n)^2}{2} - \frac{(M_0^n - x_{n+1})^2}{2} \right) = d_n$$

Thus the value of x_{n+1} is

$$x_{n+1} = \frac{1}{\mu_n} \left(\mu_n M_0^n + \xi - \sqrt{(\xi + \mu_n(M_0^n - x_n))^2 - 2\mu_n d_n} \right)$$

If however the value Σ_0 is not smaller or equal to d_n then compare the value d_n with the decreasing sequence

$$\Sigma_k = \Sigma_{k-1} + \xi(m_k^n - m_{k-1}^n) + \mu_n \left(\frac{(M_k^n - m_{k-1}^n)^2}{2} - \frac{(M_k^n - m_k^n)^2}{2} \right)$$

where the index $k = 1, 2, \ldots, (\bar{\omega}_m - 1)$. Once a Σ_k is found so that $\Sigma_k \leq d_n < \Sigma_{k-1}$ then equation (3.10) is

$$\Sigma_{k-1} + \xi(x_{n+1} - m_{k-1}^n) + \mu_n \left(\frac{(M_k^n - m_{k-1}^n)^2}{2} - \frac{(M_k^n - x_{n+1})^2}{2} \right) = d_n$$

The solution of this equation for x_{n+1} is

$$x_{n+1} = \frac{1}{\mu_n} \left(\mu_n M_k^n + \xi - \sqrt{(\xi + \mu_n(M_k^n - m_{k-1}^n))^2 + 2\mu_n(\Sigma_{k-1} - d_n)} \right)$$

The remaining two arrangements of the Preisach staircase shown in Figures 3.2c

and 3.2d have similar implementation as those already presented for Figures 3.2a and 3.2b, respectively. However special consideration needs to be given to the indexing through the Σ sequences so as to not to reference elements of the arrays ω_m and ω_M which do not exist.

The arrangements of the type shown in Figure 3.2c are characterised by $\bar{\omega}_M^n < \bar{\omega}_m^n$ and $\zeta = 1$. If the state is in this arrangement then the increment from x_n to x_{n+1} is calculated in the same manner as that presented earlier for arrangements of the form shown in Figure 3.2a. The range of the index k is chosen as follows

(a) If the input is increasing ($d_n > 0$) then the index $k = 1, 2, \ldots, (\bar{\omega}_M^n - 1)$;

(b) If the input is decreasing ($d_n < 0$) then the index $k = 1, 2, \ldots, (\bar{\omega}_m^n - 1)$;

choosing the index in this manner ensures that the calculations are carried out over the whole domain of non-zero weight function μ and that no elements of the arrays ω_m and ω_M that do not exist are called.

The style of arrangement similar to that shown in Figure 3.2d is characterised by $\bar{\omega}_m^n < \bar{\omega}_M^n$ and $\zeta = -1$. The increment from x_n to x_{n+1} is calculated in the same way as that presented above for arrangements of the type shown in Figure 3.2b. The index k is chosen as

(a) If the input is increasing ($d_n > 0$) then the index $k = 1, 2, \ldots, (\bar{\omega}_M^n - 1)$;

(b) If the input is decreasing ($d_n < 0$) then the index $k = 1, 2, \ldots, (\bar{\omega}_m^n - 1)$;

this indexing ensures complete calculation and that only elements that exist are called.

The implementation of the triangular method has the same steps (i), (ii) and (iv) as described in Subsection 3.2.1 for the rectangular method. Step (iii) is modified and x_n is updated to obtain the next iteration x_{n+1} according to the algorithm presented in this subsection.

3.3 Results

As the first model example, consider discretisations of the formal equation

$$\xi \mathrm{d}x_t + \mathrm{d}(Px)_t = -x_t \mathrm{d}t + \mathrm{d}W_t \tag{3.11}$$

obtained by the rectangular and triangular methods using different time step size h. Comparisons are made of the trajectories obtained by the two methods for the same realisation of the discretised Wiener process (random walk) W_t. Also the trajectories of equation (3.11) with the trajectories of the Ornstein-Uhlenbeck equation

$$\xi \mathrm{d}x_t = -x_t \mathrm{d}t + \mathrm{d}W_t \tag{3.12}$$

obtained by the Euler method are compared. As the second example, the rectangular and triangular discretisations of the price dynamics model (3.6) are considered.

In all the examples, the Preisach weight function is set to $\mu(\alpha, \beta) \equiv 1$ within the triangle T. The boundary values α_0 and β_0 were taken to be $\alpha_0 = -50$ and $\beta_0 = 50$. The initial state of the Preisach operator is the staircase shown in Figure 3.3.

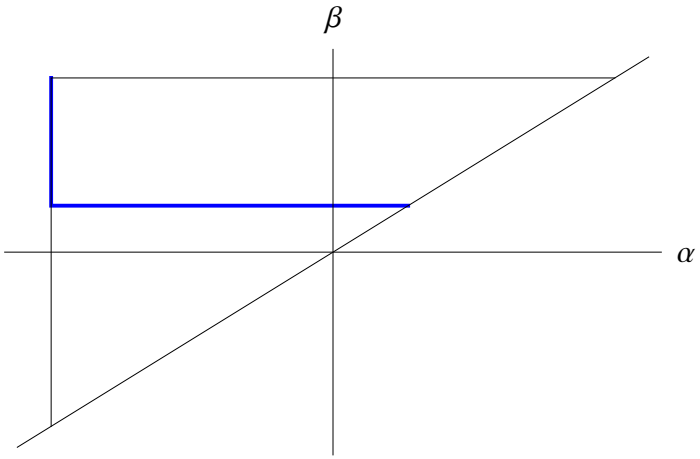

Figure 3.3: Initial state of the Preisach operator used in simulations. The blue line is the initial state of the Preisach operator used in the simulations in this chapter.

3.3.1 Rectangular method

The values of parameters used in the simulations shown in this subsection are $\xi = 0.1$; $h = 0.01$ and $x_0 = 2.0$. A numerical realisation of the rectangular method for equation (3.11) and the Euler method for equation (3.12) using these parameters is shown in Figure 3.4; x_0 is the initial value of the solution.

A look at Figure 3.4b which presents a zoomed in part of the full trajectory, shows that while solutions of discretisations of equations (3.11) and (3.12) experience

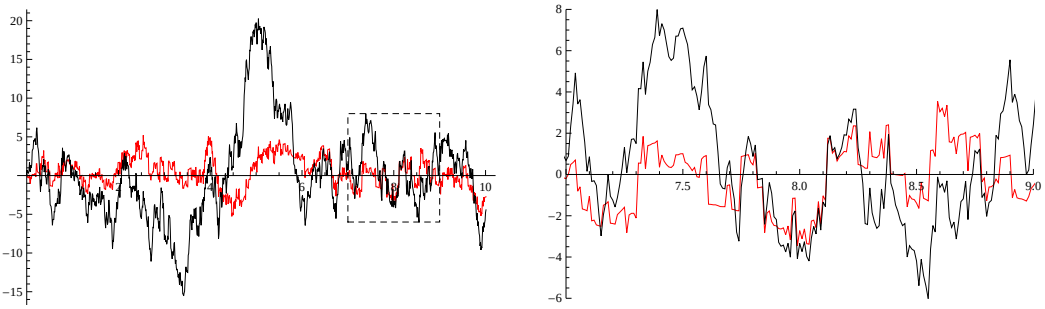

(a) The red line is the trace of solution x_t to equation (3.11) including the Preisach operator. The black line denotes the solution of equation (3.12) without the Preisach operator for the same realisation of W_t

(b) A zoom of the region indicated in (a).

Figure 3.4: Data generated from the implementation of the rectangular method.

ups and downs at roughly the same time moments for the same realisation of the random walk, the inclusion of the Preisach operator has limited the effect of jumps. It appears that the introduction of the Preisach operator in the stochastic equation (3.12) acts as a damping factor to the trajectory. It is characteristic of the damping that it is stronger on the parts of the trajectory demonstrating a stronger upwards or downwards trend. This feature can be explained by formulas (3.8) and (3.9).

If the solution satisfies $x_n \geq x_{n_0}$ on some time interval $n_0 \leq n \leq N$, then at every moment n from this interval such that $x_n > x_k$ for all $n_0 \leq k \leq n$, the quantity l_n also satisfies $l_n > l_k$ for all $n_0 \leq k \leq n$. In this sense, the upward trend of the solutions leads to the upward trend of l_n (and, similarly, the downward trend of x_n leads to the upward trend of l_n). At the same time, relation (3.8) implies stronger damping of the increment $\Delta x_n = x_{n+1} - x_n$ for larger l_n.

3.3.2 Triangular method

The parameters taken for the implementation of the triangular method for equation (3.11) and the Euler method for equation (3.12) are $\xi = 0.1$; $h = 0.1$ and $x_0 = 2.0$.

Figure 3.5 presents solutions obtained with these parameters for the same realisation of W_t. The Preisach operator term seems to be a limiting factor on the size of jumps, as is the case with implementation of the rectangular method. Figure 3.5b shows that while the two trajectories undergo up and down movements at the same time the inclusion of the Preisach operator has caused the changes to

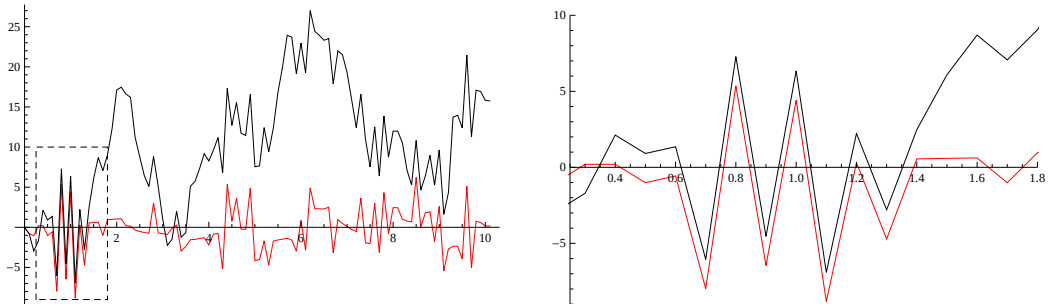

(a) The red line is the trace of solution x_t to equation (3.11) including the Preisach operator. The black line denotes the solution of equation (3.12) without the Preisach operator for the same realisation of W_t

(b) A zoom of the region indicated in (a).

Figure 3.5: Data generated from the implementation of the triangular method.

be less severe.

3.3.3 Comparison of the triangular and rectangular methods

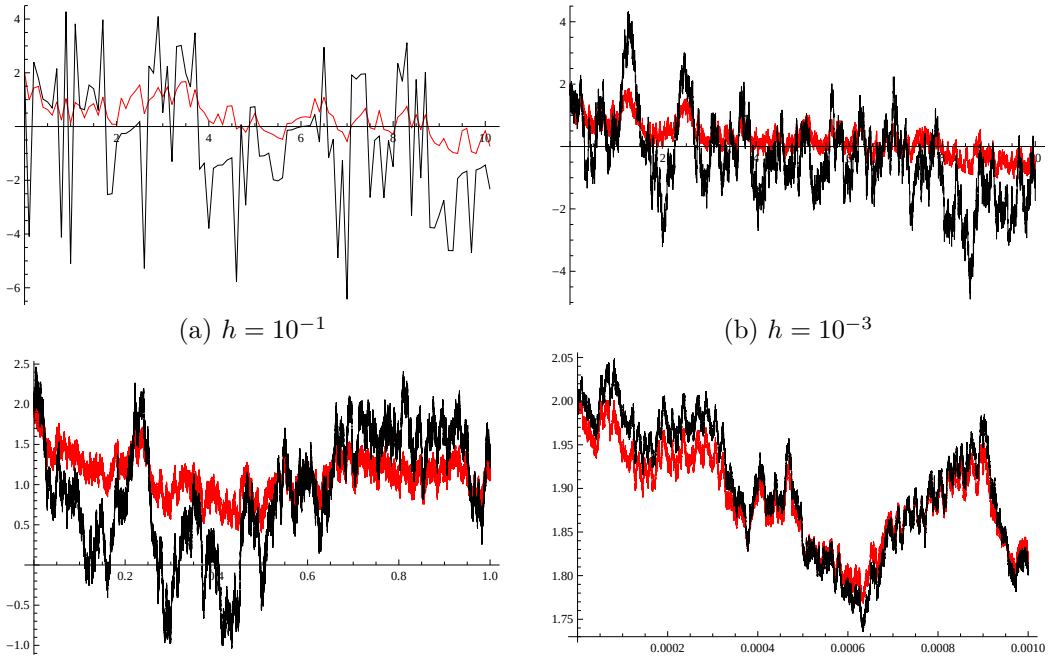

(a) $h = 10^{-1}$

(b) $h = 10^{-3}$

(c) $h = 10^{-5}$

(d) $h = 10^{-8}$

Figure 3.6: Solution of the discretisations of equation (3.11) as generated from the implementation of both the rectangular method (black) and the triangular method (red) for different time step sizes.

Figure 3.6 show realisations of the rectangular and triangular methods for equation (3.11) using different time step sizes and same realisation of the Wiener

process W_t. The parameters used in the generation of these results are $\xi = 0.1$ and $x_0 = 2$; the value of h for each plot is stated in the caption. The Figures show that the agreement between the two methods improves the smaller time step h becomes. In particular, for the given parameters, a good agreement between the two methods is achieved at $h = 10^{-8}$, see Figure 3.6d. Here the trajectories are close apart from a few discrepancies at some turning points where the rectangular method tends to produce larger jumps for the chosen small value of the parameter ξ.

3.3.4 Price dynamics model

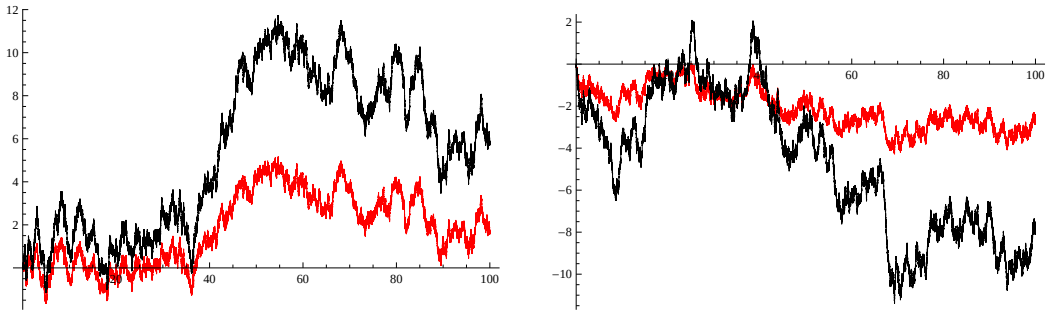

(a) The rectangular method (b) The triangular method

Figure 3.7: The red line show the plot of a solution $r(t)$ of equation (3.6) as generated from the implementation of the rectangular or triangular numerical methods. Parameter used in the simulations are $\kappa = 1$, $h = 0.001$, $r_0 = 0$ and $a = 0.5$. The black line in each panel is the solution of equation (3.6) with $\kappa = 0$, which coincides with the realisation of the random walk W_t used in the red plot for the given parameter values.

Considered in this subsection is the price dynamics model (3.6) presented in Section 3.1. Figure 3.7 compares the results of implementation of each the rectangular and triangular numerical methods in solving equation (3.6) with positive κ with the solution of the same equation for $\kappa = 0$ (i.e., equation $\mathrm{d}r_t = (a - 1/2)\mathrm{d}t + \mathrm{d}W_t$ without the Preisach operator term) obtained by the Euler method.

The values of parameters used for these plots were $\kappa = 1$; $h = 0.0001$; $x_0 = 2$ and $a = 0.5$. The plots demonstrate the same features as that were observed in the other examples above. Solutions of the model including the Preisach operator ($\kappa = 1$) and the model without the Preisach operator ($\kappa = 0$) have similar shape, however the inclusion of the Preisach operator leads to a damping effect. In the model including the Preisach operator the price does not go as high, as well this

falls in the price are limited and less severe, as opposed to in the model with $\kappa = 0$.

3.4 Validation of the numerical scheme

In Section 3.3 it was shown that the rectangular method on occasion produced higher jumps in response to turning points than the triangular method. Thus I believe the triangular method to be the more stable and better accuracy method to implement for the solution of equations of the form of (3.1).

As a result I consider a more rigorous validation of the triangular method. There currently exist many numerical schemes for solving equations of the form

$$\frac{\mathrm{d}(Px)(t)}{\mathrm{d}t} = f(x,t) \tag{3.13}$$

comparison of the result of the implementation of the triangular method to a model system of the form of (3.13) and that obtained for the implementation of the numerical scheme used in [51] for the same system will be made.

The model system is chosen to be the Preisach reservoir presented in [22]

$$\frac{\mathrm{d}(Px)(t)}{\mathrm{d}t} = k(g(t) - x) \tag{3.14}$$

where the function $g(t)$ is taken to be $g(t) = \sin(t)$. The initial state of the Preisach operator is taken to be a single horizontal segment connecting the point (x_0, x_0) on the bisector $\beta = \alpha$ to the boundary of the domain of non-zero weight function $\mu(\alpha, \beta)$, see for example Figure 3.3.

Figure 3.8 shows the comparison between the two numerical schemes. The figure shows that there is a good agreement between the two methods. This result implies that the triangular method can also be used for the solution of ordinary differential equations containing the Preisach operator under the derivative.

In [52] the authors presented an analytic expression for the probability density distribution for the first link of the Preisach staircase line $S(t)$ which has a length greater than ϵ after long time input by a Wiener process,

$$p(d_i) = \begin{cases} \dfrac{\epsilon}{(d_i)^2} & d_i > \epsilon \\ 0 & d_i \leq \epsilon \end{cases} \tag{3.15}$$

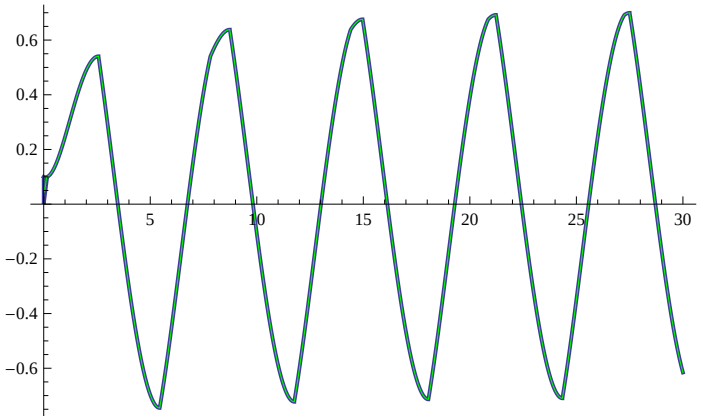

Figure 3.8: A comparison of the implementation of the triangular method (green) for the system (3.14) and the numerical scheme used in [51] (blue). The parameters used in the calculation were $k = 1$, $h = 0.01$, $\xi = 0$ and $x_0 = 0.1$.

where d_i is the length of the i-th link of the Preisach staircase line $S(t)$. The equation (3.1) can be integrated directly in the case of $a(x,t) = 0$, $b(x,t) = 1$ and $\xi = 0$ to be

$$x_t = P^{-1}W_t \tag{3.16}$$

where P^{-1} is the inverse Preisach operator. Using the methods presented in [52] a formula similar to 3.15 for the inverse Preisach operator can be developed. Solutions of the triangular method should satisfy this result since for the given parameters the triangular method gives the discretisation of equation (3.16).

In [52] they calculate the probability density distribution from the conditional probability density for the lengths of the Preisach staircase increasing in size as the element number is increased. This probability is determined by the length of the i-th link of the Preisach staircase d_i. In order to transform this result to the inverse Preisach operator replace the length d_i by the area of the Preisach plane incorporated by the i-th corner, denote this area as $\hat{d}_i$. The conditional probability density in terms of the areas is then

$$p(\hat{d}_i|\hat{d}_{i+1}) = \frac{\hat{d}_{i+1}}{(\hat{d}_i)^2} \tag{3.17}$$

The area $\hat{d}_i$ can be interpreted in terms of the lengths d_i as $\hat{d}_i = d_i^2/2$. This gives for equation (3.17)

$$p(d_i|d_{i+1}) = \frac{2(d_{i+1})^2}{(d_i)^4} \tag{3.18}$$

Integration of equation (3.18) gives the probability density distribution of the

length of the smallest link d_i such that $d_i \geq \epsilon$ for the inverse Preisach operator.

$$p(d_i) = \begin{cases} \dfrac{2\epsilon^2}{3(d_i)^3} & d_i > \epsilon \\ 0 & d_i \leq \epsilon \end{cases} \tag{3.19}$$

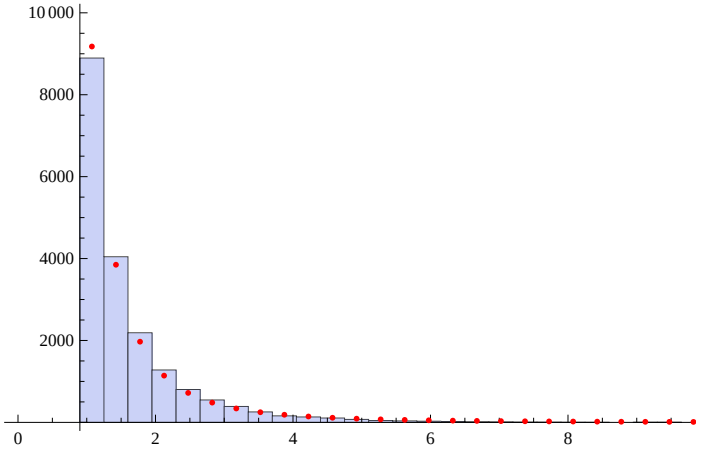

Figure 3.9: Distribution of the first link of the inverse Preisach operator memory state greater than $\epsilon = 1$ after long time input by the Wiener process W_t for 10000 simulations using the triangular method. The red dots correspond to the expected values calculated from the probability density distribution given by (3.19).

Confirmation of (3.19) for the triangular method is shown in Figure 3.9. This further validates the triangular method as a means of simulating stochastic differential equations of the form (3.1) (i.e., containing the Preisach operator).

3.5 A price dynamics model containing a positive feedback element

In this section a second price dynamics model will be developed. Consider a company manufacturing goods for the market, their level of production will be some form of function based on price the good will fetch on the market. If the assumption is made that the company currently produces the good at the maximum level of production which they can achieve based on the size of the factory or available equipment and staff, then if they wish to produce a greater volume of goods then there will be a cost associated with establishing this level, for example if a larger premises or additional staff or equipment are required for the increased production level. In this situation a small increase in the price may not cause the company to increase its production level due to the associated start

up costs of a greater production volume. However if the price of the good they produce increases to a certain level so that the generated profit will offset the associated start up cost, then the company will begin to produce the good in a larger volume. Assume that once this threshold level is crossed the company will keep investing in larger production volumes for as long as the price continues to rise.

If the price of the good begins to fall then the company may not wish to sell off any additional equipment or premises already bought, as this may only be a small temporary decrease in the price or due to associated difficulties in selling off any premises or equipment purchased or staff hired and the cost to get these back if the price once again rises. Assume then that the company waits until the price crosses a threshold level, which corresponds to the acceptable loss margin the company is willing to endure, at which point it reduces its own production level as the price falls. The production level of the company described here can be modelled by an ordinary play operator, as defined in Chapter 2. A model of this type was explained from an economic setting in [53].

If a market consisting of M companies similar to the one previously described then their aggregated opinion of the correct production level based on the current price p is given by

$$\sigma = \frac{1}{M}\sum_{i=1}^{M} \mu_i L[2r_i, y_c(r_i)]p(t) \tag{3.20}$$

where μ_i is the weight of the i-th company in determining the opinion on the market (possibly due to the company being a respected brand name for the good, etc.) and $L[2r_i, y_c(r_i)]$ is the ordinary play operator with width $2r_i$ between the two bounding lines on the input-output plane, that is $2r_i$ is the fall in price that a company requires to start reducing its production level when they are increasing production, and memory element $y_c(r_i)$. This represents a discrete form of the Prandtl-Ishlinskii operator. This model is unrealistic as it assumes that the companies have unlimited resources to invest in increased production, this can be accounted for if a composition function is applied to ordinary play operators so that they undergo saturation in a manner similar to that mentioned in Section 2.4.1, which gives for σ

$$\sigma = \frac{1}{M}\sum_{i=1}^{M} g(r_i, L[2r_i, y_c(r_i)]p(t)) \tag{3.21}$$

The price of the good is assumed to be similar to equation (3.3), that is the price

of the good in discrete time is

$$p_{t+h} = p_t \exp\left[\eta_t\sqrt{h} + \left(a - \frac{1}{2}\right)h + \kappa\Delta\sigma_t\right] \tag{3.22}$$

where all the terms are the same as they were for equation (3.3) and here $\Delta\sigma_t$ represents the change in the collective opinion (proportional to the total production level) of all the companies which creates a pressure on the price. The sign on the hysteresis term $\kappa\Delta\sigma_t$ is positive in this equation as it is assumed that as the companies invest more in the production of the good a pressure is applied to the price which tries to force it to increase, when the production levels falls it creates a pressure to lower the price. This means that there is a positive feedback loop on the price. The assumption of a positive feedback loop is made because as the price increases there is a also a growth in the production level of the good, this higher production level requires more investment by the companies in order for it to be achieved. The willingness of the companies to invest more results from a belief that there will be further price growth as time goes on, thus the price will be driven higher in order to recoup any additional costs associated with higher production which may lead to even more price increases.

As in the previous price dynamics model the price is rescaled to

$$s = \ln\frac{p}{p_0}$$

which gives for equation (3.22)

$$\Delta s_t = \eta_t\sqrt{h} + \left(a - \frac{1}{2}\right)h + \kappa\Delta\sigma_t \tag{3.23}$$

where $\Delta s_t = s_{t+h} - s_t$. Note that s_t can be taken as the input to Prandtl-Ishlinskii operator σ_t as long as the weight function is properly rescaled (alternatively the width of the constituent play operators could also be rescaled) in a manner similar to that done for the previous model (3.4). Thus equation (3.23) is

$$\Delta s_t - \kappa\Delta w_t = \eta_t\sqrt{h} + \left(a - \frac{1}{2}\right)h \tag{3.24}$$

where $\Delta w_t = w_{t+h} - w_t$ and w_t denotes the Prandtl-Ishlinskii operator. This equation has the formal continuous time counterpart

$$\mathrm{d}s_t - \kappa\mathrm{d}w_t = \left(a - \frac{1}{2}\right)\mathrm{d}t + \mathrm{d}W_t \tag{3.25}$$

As explained in Section 2.4.1 this generalised Prandtl-Ishlinskii operator is the same as the Preisach operator, see equation (2.11), which allows for the representation of the equation (3.25) as

$$\mathrm{d}s_t - \kappa \mathrm{d}(Ps)_t = \left(a - \frac{1}{2}\right)\mathrm{d}t + \mathrm{d}W_t \tag{3.26}$$

in this form (3.26) is similar to (3.6), however in (3.26) the Preisach term represents a positive feedback loop on the price of the good instead of the negative feedback of the previous model.

A couple of remarks about this model are in order. Firstly since the Preisach term in (3.26) represents a positive feedback loop on the price then strong upward or downward trends in trajectories which are solutions of this equation will be amplified as opposed to limited as was the case in the previous model, this amplification of upward or downward trend would be similar to "bubbles" and "crashes" seen in real world price time series. Secondly the positive feedback loop has the potential for avalanches in the output value, that is large jumps in the output caused by small changes in the input.

3.6 Conclusions

In this chapter two discrete time counterparts of the formal continuous time stochastic differential equation (3.1) involving the Preisach operator were developed. These two numerical schemes were applied to an Ornstein-Uhlenbeck type equation and to a simple price dynamics model involving the Preisach memory term.

Given a sufficiently small time step a good agreement between the two methods is seen. However the rectangular method at times has larger jumps in response to turning points than those shown by the triangular method. As a result the triangular method was examined in more detail as a means to validate the scheme. The triangular method showed a strong agreement with the numerical scheme used in [51] when used to model a deterministic system. The scheme also showed an agreement with the theoretical expectation for the distribution of the first link of the Preisach staircase line $S(t)$ greater than some value ϵ for the inverse Preisach operator. These results suggest that the triangular method is a valid means of solving equations of the form of (3.1)

The introduction of the Preisach operator acts as a limiting damping effect when compared with an equivalent form of a regular stochastic differential equation. This damping effect is more pronounced on the parts of the trajectory that demonstrate a stronger upwards or downwards trend. This effect can be explained by the fact that both upwards or downwards trends of trajectory result in an upwards trend of the quantity (3.9). This quantity causes the change in the function x_t to be smaller on a time step than in the matching regular stochastic differential equation.

The second model for price dynamics shown in Section 3.5 does not readily allow for implementation of the triangular method presented in this chapter. It is only a minor modification to alter the presented scheme to work for the positive feedback loop of this model instead of the negative feedback loop covered earlier in the chapter. However complex issues in implementing the scheme will arise in this model due to the possibility of avalanches (large jumps) of the output occurring for small changes in the input. The issue relates to the correct size of the jump in the output and currently is the subject of further study.

Chapter 4

Two dimensional deterministic models containing the Preisach operator

In Chapter 3 the triangular method was also implemented on a simple deterministic hysteretic model from the area of terrestrial hydrology, a good agreement was shown between the triangular method and the numerical scheme used in [51] which suggested that the scheme would also be useful in solving deterministic equations. As a way of further testing the accuracy of the triangular method consideration is given to the solution of systems of coupled deterministic equations where the derivative of the Preisach operator is contained in one of the equations. Some theoretical results relating to this type of system were presented in [54]. The aim of this chapter will be to modify the numerical scheme presented in Chapter 3 for solving coupled deterministic equations where the derivative of the Preisach operator is contained in one of the equations. This modified scheme will then be tested against the theoretical results presented in [54].

4.1 Motivation

Hysteresis effects underpin modern magnetic recording technologies and should be taken into account in microelectromechanical systems (MEMS) engineering. They can also manifest themselves through undesirable energy losses in electronic circuits, mechanical and other systems, where hysteresis can be a primary or significant source of energy dissipation. Mathematical models of systems with

hysteretic components help design power electronic systems [55]; implement real time hysteresis compensation in controllers and actuators [56–59]; design smart materials [60–62]; model and predict dynamics of earthquakes faults [63] and phase transitions [1, 64]; understand dynamics of complex networks [65, 66].

An illustrative example in the power electronics setting is an electrical circuit where an inductance element contains a ferromagnetic core (for example, a transformer). Kirchhoff's laws (or Maxwell's equations) lead to differential rate equations for voltages and currents; those are complemented by constitutive relationships, which, in case of a hysteretic ferromagnetic core, include an operator relationship between the fields H, magnetic field, and B, magnetic induction, in the core where H is proportional to the current and B is proportional to the rate of change of the voltage [31, 32, 55].

As a prototypical example consider the LCR circuit where the inductance element has a ferromagnetic core. If there is no hysteresis effect, or this effect can be neglected, then, in the simplest case B is proportional to H in the core and the emf in the inductor can be expressed as

$$E_{ind} = Lj' \tag{4.1}$$

where prime denotes the time derivative and j is the current through the inductor. Hence dynamics of the current j and the drop of the voltage u across the capacitor is described by the system

$$\begin{aligned} Lj' &= -Rj + u, \\ Cu' &= -j. \end{aligned} \tag{4.2}$$

However, if the hysteresis effect is substantial, then the constitutive relationship between B and H is not only nonlinear, but the instantaneous value of B depends both on the simultaneous value of H and some previous values of H. The Preisach operator is a widely used model of hysteretic constitutive relationship in ferromagnetic materials [67, 68]. Adopting this model of the relationship between the magnetization M and the magnetic field H results in the equation

$$B = \nu H + P(H) \tag{4.3}$$

with $\nu > 0$ where the Preisach input-output operator P maps the variable magnetic field $H(t)$ to the variable magnetization $M(t) = (P(H))(t)$ of the core, for definition and discussion of the Preisach operator see Chapter 2. This leads to a

similar expression for the emf induced in the inductor

$$E_{ind} = (Lj + P(j))' \tag{4.4}$$

where the Preisach density function is properly rescaled when passing from (4.3) to (4.4). When the linear functional relationship (4.1) is replaced with (4.4), system (4.2) changes accordingly to the system of differential equations

$$\begin{aligned} (Lj + P(j))' &= -Rj + u, \\ Cu' &= -j \end{aligned} \tag{4.5}$$

involving the Preisach hysteresis operator P.

System (4.5) is a functional differential equation with an infinite dimensional phase space as the rates of change of the variables depend both on the simultaneous values of the variables and, through the operator P, on their values in the past. Importantly, the rate-independence property of the operator P distinguishes the memory in this system from other types of memory such as in delay differential equations or convolution operators.

As oscillating contours and elements, including those with hysteretic components, are a common feature of various electrical circuits, mechanical systems and MEMS, several prototypical second order differential models of oscillators with the Preisach operator have been proposed and studied in engineering and mathematical literature. In particular, various aspects of the dynamics of forced oscillators have been studied in [69–78], including applications to accurate modelling and optimisation of parameters of power electronics systems in the presence of the ferroresonance phenomenon [55] and input-to-state stability of control systems. Cycles stemming from the Hopf bifurcation in a model of a Van der Pol type oscillator and a network of such oscillators were studied in [79–81]. In the electrical circuitry context, this model describes a circuit consisting of an LCR contour and a negative feedback loop (which can be implemented, for instance, by using tunnel diodes) and involving a ferromagnetic core in the inductor. The model equations

$$\begin{aligned} (Lj + P(j))' &= -Rj + u, \\ Cu' &= -j + \sigma_1 u - \sigma_2 u^3, \end{aligned} \tag{4.6}$$

when compared to (4.5), include additionally the current-voltage characteristic $j_d = -\sigma_1 u + \sigma_2 u^3$ of the negative feedback element with $\sigma_1 > 0$ and $\sigma_2 \geq 0$.

An alternative illustrative model is given from the area of terrestrial hydrology.

The following lumped model of a water flow through a slab of soil (used in Chapter 3 for testing the triangular method) has been derived in [82, 83] by combining Darcy's law with the hysteretic constitutive relationship between the moisture content and the water pressure in the soil, and averaging out the spatial variation of the variables:

$$\begin{aligned} u' &= k(a(t) - x), \\ u(t) &= (Px)(t). \end{aligned} \tag{4.7}$$

Here u is the amount of water in the soil column; x is the pressure (or, equivalently, the so-called matric potential) in the center of the soil column; a is the pressure on the surface of the soil controlled by the conditions in the atmosphere such as precipitation and humidity. The first equation is the balance equation stating that the rate of change of the water content equals the water flux from the surface into the soil slab, which is proportional to the difference of pressures on the surface and in the soil. The second equation is the constitutive hysteretic relationship between u and x defined by the properties of the porous media of the soil and modelled by the Preisach operator P. This model and its extensions with multiple flows from and to the soil slab have been studied in [4,22,50,84–88]. In particular, the Preisach operator density function has been identified for different types of soils on the basis of the measured constitutive relationship in [34]; the model has been fitted to experimental rainfall and soil water content data in [4, 22].

Consider now a similar model with two layers of two different soils. The upper layer is the same as above. In the lower layer, assume simply the linear constitutive relationship between the water content and the pressure. The resulting system

$$\begin{aligned} u' &= k_1(a - x) + k_2(y - x) \\ v' &= k_2(x - y) \\ u(t) &= (Px)(t) \\ v(t) &= Cy(t) \end{aligned}$$

where x, y are the pressures in the lower and upper soil layers, respectively; a is the pressure on the surface; u and v are the water contents in the upper and lower soil layers; k_1 and k_2 are hydraulic conductivities of those layers. If a is constant, then the equilibrium is achieved for $x = y = a$. Note that in hydrological applications it is natural to assume that the hydraulic conductivities depend on the pressure, $k_1 = k_1(x)$, $k_2 = k_2(y)$, and that the constitutive relationship is nonlinear, $v = C(y)$.

In this chapter, consideration is given to a general class of second order systems

of differential equations

$$\begin{aligned} (Px)' &= f(x,y), \\ y' &= g(x,y) \end{aligned} \tag{4.8}$$

with the Preisach operator P. Focus is on the dynamics of the system near an equilibrium point such as, for example, the zero equilibrium of system (4.5) or system (4.6). In the context of this local problem, it is important that systems (4.5) and (4.6) have the form (4.8) for $L = 0$. This corresponds to the physical approximation $Lj \ll P(j)$ which is typical of the inductors where almost all the magnetic flux is concentrated in the ferromagnetic core. Thus, one can consider system (4.8) as a natural approximation of electrical circuit models such as (4.5) and (4.6). Mathematically, the term Lj' with $L > 0$ in the left-hand side of equations (4.5), (4.6) has a smoothing effect, see [84, 85].

4.2 Differential system with Preisach memory

Consider solutions of system (4.8) with the Preisach operator $P = P[S_0]$ on time intervals $[t_0, t_1)$, $[t_0, t_1]$ and $[t_0, \infty)$. In the framework of dynamical systems theory, a solution has three components, $(x(t), y(t), S(t))$, where the last component describes the evolution of the state of the Preisach operator. That is, the phase space of system (4.8) is the space of triplets (x, y, S). In particular, the Cauchy problem for equation (4.8) consists in finding a solution satisfying a given initial condition $(x(t_0), y(t_0), S(t_0)) = (x_0, y_0, S_0)$. Due to the semigroup property of the Preisach operator [10], one can merge two solutions defined on consecutive time intervals $[t_0, t_1]$ and $[t_1, t_2]$ to form a solution on the time interval $[t_0, t_2]$ if the final point $(x(t_1), y(t_1), S(t_1))$ of the solution defined on the interval $[t_0, t_1]$ coincides with the initial point of the solution defined on the interval $[t_1, t_2]$. In this way, the usual continuation procedure works for system (4.8). Of note is that the rate-independence property of the Preisach operator implies that this operator commutes with the group of translations of time. Therefore, system (4.8) is autonomous; a translation of time maps a solution $(x(t), y(t), S(t))$ defined on an interval $[t_0, t_1]$ to the solution $(x(t+\tau), y(t+\tau), S(t+\tau))$ defined on the interval $[t_0 + \tau, t_1 + \tau]$.

In what follows, the term solution will be used in relation to a triplet $(x(t), y(t), S_0)$ or, whenever an initial state S_0 is either fixed or can be chosen arbitrarily from the set of all admissible initial states of the Preisach operator, to the pair $(x(t), y(t))$. Note that the evolution of the state $S(t)$ of the Preisach

operator is uniquely defined by the initial state S_0 and the input $x(t)$ of this operator according to the definition in Chapter 2, hence it is legitimate to consider triplets $(x(t), y(t), S_0)$ instead of $(x(t), y(t), S(t))$. In applications, S is typically not an observable variable.

The projection of solutions on the (x, y)-plane plays the main role for the results presented below.

For a given initial state S_0, a pair $(x(t), y(t))$, $t \in [t_0, t_1)$ is a solution of system (4.8) if the output $p(t) = (P[S_0]x)(t)$ of the Preisach operator and the component $y(t)$ are continuously differentiable, the component $x(t)$ is continuous, and equations (4.8) are satisfied at all points of the interval $[t_0, t_1)$.

A stationary solution of system (4.8) is a solution satisfying $(x(t), y(t)) \equiv (x_0, y_0)$. As the Preisach operator maps a constant input to a constant output, the component $S(t)$ of a stationary solution and the output $p(t) = (P[S_0]x)(t)$ of the Preisach operator are also constant, $S(t) \equiv S_0$, $p(t) \equiv p_0$. Therefore, as in the case of ordinary differential equations, for any stationary solution $(x(t), y(t)) \equiv (x_0, y_0)$,

$$f(x_0, y_0) = g(x_0, y_0) = 0. \tag{4.9}$$

Moreover, relations (4.9) imply that $(x(t), y(t)) \equiv (x_0, y_0)$ is a stationary solution of system (4.8) for any initial state S_0 of the Preisach operator. Hence, call a solution (x_0, y_0) of equations (4.9) an *equilibrium* of system (4.8).

The focus here will be on dynamics near an isolated equilibrium. Without loss of generality, the assumption is made that the equilibrium is placed at the origin. Results will be formulated in terms of the Jacobian matrix

$$Q = \begin{pmatrix} f_x(0,0) & f_y(0,0) \\ g_x(0,0) & g_y(0,0) \end{pmatrix} \tag{4.10}$$

evaluated at the zero equilibrium, where f_x, f_y, g_x, g_y are the partial derivatives of the functions f and g, which are assumed to be continuously differentiable and assume the non-degeneracy condition

$$j_0 = \det Q \neq 0, \tag{4.11}$$

which ensures that the zero equilibrium $(x_0, y_0) = (0, 0)$ is isolated.

For small changes in the input the integral of the Preisach weight function over the initial segment of the Preisach staircase can be used as a means of determining the

change in the Preisach operator, in a manner to similar to the rectangular method numerical scheme discussed in Chapter 3 or the numerical scheme presented in [48].

$$(Px)' = L(x)x' \tag{4.12}$$

where L is

$$L(\tilde{x}) = \begin{cases} \displaystyle\int_{\alpha_{S_0}(\tilde{x})}^{\tilde{x}} \mu(\alpha, \tilde{x}) \mathrm{d}\alpha, & \tilde{x} \geq x_0 \\ \\ \displaystyle\int_{\tilde{x}}^{\beta_{S_0}(\tilde{x})} \mu(\tilde{x}, \beta) \mathrm{d}\beta, & \tilde{x} \leq x_0 \end{cases} \tag{4.13}$$

in this equation $\alpha_{S_0}(\tilde{x})$ is the α coordinate where the initial segment ends if the segment is horizontal (that is the point where the line $\beta = \tilde{x}$ intersects the staircase line S_0) and $\beta_{S_0}(\tilde{x})$ is the β coordinate where the initial segment ends if the segment is vertical (that is the point where the line $\alpha = \tilde{x}$ intersects the staircase line S_0).

4.3 Modification of the numerical scheme

Numerical schemes for solving ordinary differential equations of the form of [48] (such as the one used in [51] which was used in Chapter 3 for comparison to the triangular method presented in that chapter) rely upon some of the time dependent properties of the right hand side of the equation for their implementation.

Since the system (4.8) has no time dependence then these schemes can not be implemented. The triangular method numerical scheme presented in Chapter 3 does not rely on time dependent properties so will not encounter the same difficulties as the other schemes. However the numerical scheme requires a slight modification in order to be implemented for solving systems like (4.8).

The value of d_n is taken to be

$$d_n = f(x_n, y_n)h$$

where h is the time step being taken in the simulation. The first step of the implementation of the triangular method is modified to be

(i) Calculate the value of d_n; if $d_n \approxeq 0$ then the time step is reduced by a factor of 100 and then the remaining steps are preformed as normal, else carry out the remaining steps with no modifications;

Where for simulations $d_n \cong 0$ is assumed $|d_n| \leq 10^{-12}$. This modification is made as numerical implementation of systems of the form (4.8) has a potential locus of difficulty in calculations on the line $f = 0$, as this line is a potential locus of non-uniqueness of the solution due to the non-differentiability of the Preisach operator along this line, thus the accuracy of the scheme needs to be improved near this line and to allow for this a smaller time step is taken. The theoretical results relating to systems like (4.8) presented in [54] state the dynamics of the trajectory are such that there are no sliding modes, so in a sense the dynamics are simpler than systems with noise considered in Chapter 3 as there will not be any constant repeated turning points as is possible in the case of noise or sliding modes. Thus there is no need to modify any of the memory updating steps present in the triangular method, which already makes a check on each time step for turning points of the input and deletions of Preisach memory elements. The equation for y is solved using a basic Euler numerical scheme, a higher order scheme is not implemented due to the coupling with the input of the Preisach operator which is calculated by the triangular method numerical scheme which is an Euler based scheme.

For the simulations here the bounding triangle T is given by $(\alpha_0, \beta_0) = (-5, 5)$ and the Preisach weight function $\mu = 1$ inside the triangle and $\mu = 0$ elsewhere. In the bounding triangle setting the point $\alpha_{S_0}\tilde{x}$ is the point which is smaller in magnitude of the pair, the point where the line $\beta = \tilde{x}$ intersects the staircase S_0 and α_0 the left boundary of the bounding triangle T. Similarly the point β_{S_0} is the point which is smaller in magnitude of the pair, the point where the line $\alpha = \tilde{x}$ intersects the staircase line S_0 and β_0 the upper boundary of the bounding triangle T.

4.4 Main results

In [54] three Theorems were proven (for completeness the proofs are presented in Appendix A) that could be used as a means of testing the modified numerical scheme presented in Section 4.3. These Theorems relate to the behaviour of a trajectory of the system near an equilibrium of the system 4.8. The system will respond in one of three ways depending upon the sign of f_x and on the sign of j_0. Presented in this section is the implementation of the triangular method for three model system each representing one of the three Theorems.

4.4.1 Behaviour of solutions near the curve $f = 0$

For any solution of system (4.8) defined for $t \geq t_0$, the state $S(t)$ at a moment $t > t_0$ has a nonzero initial horizontal segment whenever $f(x(t), y(t)) > 0$, and an initial nonzero vertical segment whenever $f(x(t), y(t)) < 0$. By this reason, and due to the special role of the line $f = 0$ mentioned in the previous Section, consider only initial data $(x(t_0), y(t_0), S(t_0)) = (x_0, y_0, S_0)$ satisfying $f(x_0, y_0) \neq 0$, where S_0 has a nonzero initial horizontal segment if $f(x_0, y_0) > 0$, and a nonzero initial vertical segment if $f(x_0, y_0) < 0$, any such data will be called admissible.

In what follows, assume the relations (4.9) at the origin $x_0 = y_0 = 0$ and the nondegeneracy condition (4.11).

4.4.2 Systems with $f_x(0, 0) > 0$

Theorem 4.1. *Let $f_x(0, 0) > 0$. There is a function $\varphi = \varphi(\delta)$ satisfying $0 < \varphi(\delta) < \delta$ such that if, at some moment τ, a trajectory of system (4.8) hits the line $f = 0$ at a point (x, y) with $0 < |x| < \varphi(\delta)$ for a sufficiently small δ, then the trajectory escapes the strip $|x| < \delta$. The x-component of the trajectory is strictly monotone between the moment τ and the moment $\tau_e > \tau$ when the trajectory first hits one of the lines $x = \pm\delta$ (hence, the trajectory does not intersect the line $f = 0$ for $\tau < t < \tau_e$). Moreover, there is a function $\phi = \phi(\delta) > 0$ satisfying $\phi(\delta) \to 0$ as $\delta \to 0$ such that $|dy/dx| < \phi(\delta)$ for $\tau < t < \tau_e$ as long as $0 < |x| < \varphi(\delta)$.*

This Theorem can be explained simply as, any trajectory which hits the line $f = 0$ close to the equilibrium value once it crosses this line proceeds almost horizontally until it escapes the vicinity of the equilibrium. Figure 4.1 presents a numerical solution of system

$$\begin{aligned} (Px)' &= x - y \\ y' &= x + y. \end{aligned}$$

This result agrees with the theoretical prediction of Theorem 4.1.

4.4.3 Systems with $f_x(0, 0) < 0$

Theorem 4.2. *Let $f_x(0, 0) < 0$, $j_0 < 0$ and $f_y(0, 0) \neq 0$. There is a function $\varphi = \varphi(\delta)$ satisfying $0 < \varphi(\delta) < \delta$ such that if, at some moment τ, a trajectory*

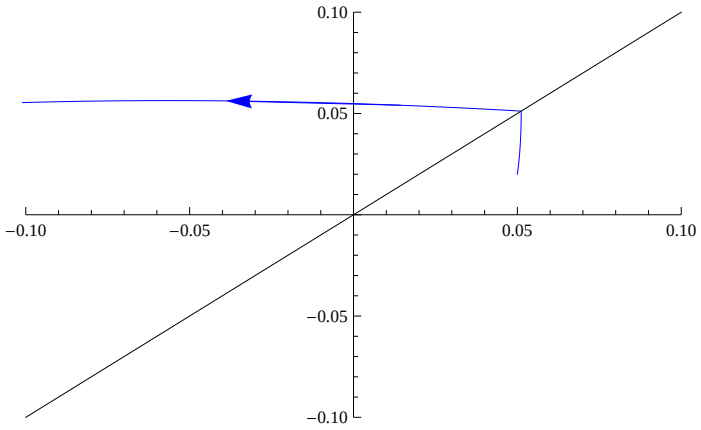

Figure 4.1: A numerical solution of system $(Px)' = x - y$, $y' = x + y$. The line with the arrow shows the trajectory of the solution, the arrow points in the direction of the trajectory. The other line is the line for $f(x, y) = 0$. The Preisach weight function used for the calculation is $\mu(\alpha, \beta) = 1$. The initial state of the Preisach operator is a single horizontal line connected to the edge of the bounding triangle T.

of system (4.8) *hits the line* $f = 0$ *at a point* (x, y) *with* $0 < |x| < \varphi(\delta)$ *for a sufficiently small* δ*, then the trajectory escapes the strip* $|x| < \delta$*. The* x*-component of the trajectory is strictly monotone between the moment* τ *and the moment* $\tau_e > \tau$ *when the trajectory first hits one of the lines* $x = \pm\delta$ *(hence, the trajectory does not intersect the line* $f = 0$ *for* $\tau < t < \tau_e$*). Moreover, there is a function* $\phi = \phi(\delta) > 0$ *satisfying* $\phi(\delta) \to 0$ *as* $\delta \to 0$ *such that a trajectory lies in the angle* $|f_x(0,0)x + f_y(0,0)y| < \phi(\delta)|x|$ *for* $\tau < t < \tau_e$ *whenever it hits the line* $f = 0$ *at a point* (x, y) *with* $0 < |x| < \varphi(\delta)$*.*

This Theorem can be explained simply as, when the trajectory hits the line $f = 0$ for this system it proceeds to follow the line $f = 0$ until it escapes from the equilibrium. Figure 4.2 presents the results for the system

$$\begin{aligned}(Px)' &= -2x + y\\ y' &= -x + y.\end{aligned}$$

This numerical verifies the Theorem 4.2 for the implementation of the triangular method.

Theorem 4.3. *Let* $f_x(0,0) < 0$*,* $j_0 > 0$ *and* $f_y(0,0) \neq 0$*. Then any trajectory of system* (4.8) *that hits the line* $f = 0$ *sufficiently close to the zero equilibrium at some moment* τ*, converges to the zero equilibrium, but never reaches it. The* x*-component of the trajectory is strictly monotone for* $t > \tau$ *(hence, the trajectory does not intersect the line* $f = 0$ *for* $t > \tau$*). Moreover, there is a function*

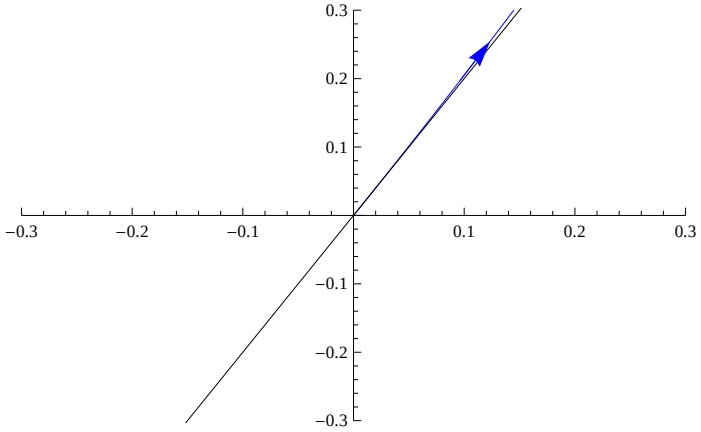

Figure 4.2: A numerical solution of system $(Px)' = -2x + y$, $y' = -x + y$. The line with the arrow shows the trajectory of the solution, the arrow points in the direction of the trajectory. The other line is the line for $f(x, y) = 0$. The Preisach weight function used for the calculation is $\mu(\alpha, \beta) = 1$. The initial state of the Preisach operator is an initial vertical line connected to a horizontal line which goes to the edge of the strip bounding triangle T. Here the trajectory starts from the point $(x_0, y_0) = (0.0001, 0.0001)$

$\phi = \phi(\delta) > 0$ *satisfying* $\phi(\delta) \to 0$ *as* $\delta \to 0$ *such that* $|f_x(0,0)x + f_y(0,0)y| < \phi(|x(\tau)|)|x|$ *for* $t > \tau$.

This Theorem is simplified as, when the trajectory hits the line $f = 0$ it follows the line $f = 0$ towards the zero equilibrium. Figure 4.3 shows numerical simulations for the system

$$\begin{aligned}(Px)' &= -x + y\\ y' &= -2x - y.\end{aligned}$$

Again this numerical result agrees with the theoretical result of Theorem 4.3.

4.5 Similarity with slow-fast systems

The behaviour of trajectories of system (4.8) described in Theorems 4.1 - 4.3 after a trajectory hits the line $f = 0$ near the zero equilibrium is similar to that of the slow-fast system

$$\begin{aligned}\varepsilon x' &= f(x, y),\\ y' &= g(x, y)\end{aligned} \tag{4.14}$$

with $0 < \varepsilon \ll 1$. The reason for this similarity is that the factor $L(x)$ in equation (4.12) equivalent to system (4.8) is small after the trajectory intersects the line

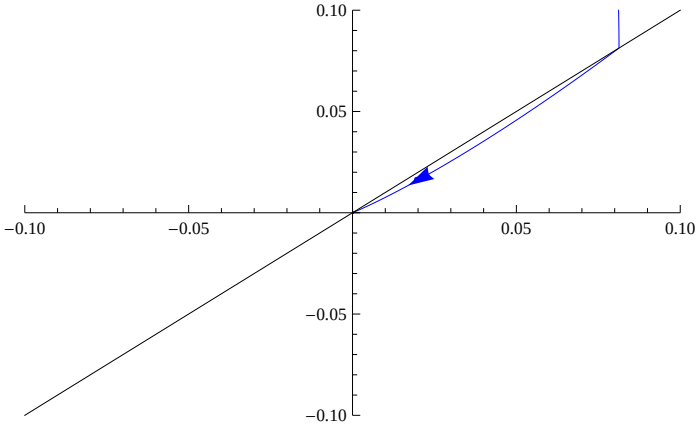

Figure 4.3: A numerical solution of system $(Px)' = -x + y$, $y' = -2x - y$. The line with the arrow shows the trajectory of the solution, the arrow points in the direction of the trajectory. The other line is the line for $f(x, y) = 0$. The Preisach weight function used for the calculation is $\mu(\alpha, \beta) = 1$. The initial state of the Preisach operator is a single horizontal line connected to the edge of the bounding triangle T.

$f = 0$. Some difference is due to the fact that, when a trajectory moves away from the line $f = 0$ after having hit this line, the value of $L(x)$ increases from zero to positive values, hence it is first smaller than any ε and later it becomes larger than a sufficiently small ε. For the three examples illustrating Theorems 4.1 – 4.3 in the previous Section, $(Px)'$ is replaced with $\varepsilon x'$ and Figure 4.4 presents trajectories of the resulting linear systems.

Note that if a trajectory of system (4.8) approaches a neighbourhood of the zero equilibrium from a distance without hitting the line $f = 0$, then $L(x)$ is not small and therefore this part of the trajectory is not similar to trajectories of system (4.14).

4.6 Conclusions

In this chapter consideration is given to autonomous systems where two scalar differential equations are coupled with the input-output relationship of the Preisach hysteresis operator, which has an infinite-dimensional memory. Examples of such systems include electric circuits and lumped hydrological models with a hysteretic constitutive law; they can also appear as components of the recently proposed models of population dynamics, epidemiology and economics. Here the systems were examined numerically to test a modification of the triangular method numerical scheme presented in Chapter 3 against known results about the behaviour

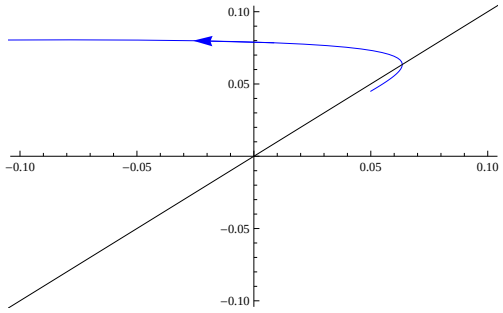

(a) A trajectory of the system $\varepsilon x' = x - y$, $y' = x + y$ is similar to the trajectory of system $(Px)' = x - y$, $y' = x + y$ shown in Figure 4.1 after the trajectories cross the line $x - y = 0$.

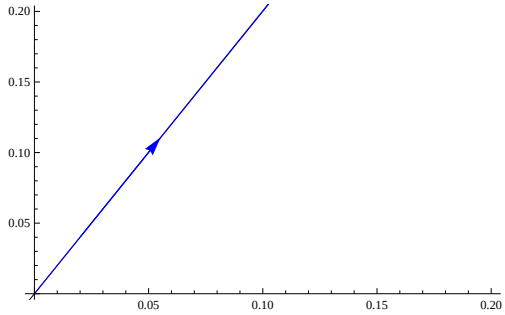

(b) A trajectory of the system $\varepsilon x' = -2x+y$, $y' = -x + y$ is similar to the trajectory of system $(Px)' = -2x + y$, $y' = -x + y$ shown in Figure 4.2 after the trajectories cross the line $-2x + y = 0$.

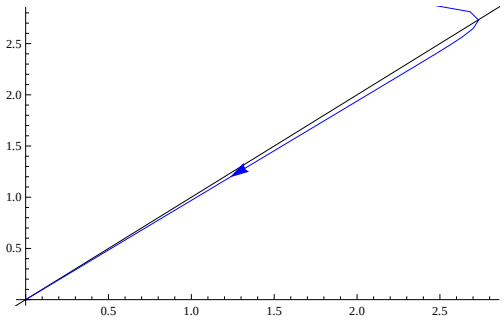

(c) Trajectory of the system $\varepsilon x' = -x + y$, $y' = -2x-y$ is similar to the trajectory of the system $(Px)' = -x + y$, $y' = -2x - y$ shown in Figure 4.3 after the trajectory crosses the line $-x + y = 0$.

Figure 4.4: Trajectories of the slow-fast ordinary differential systems corresponding to the Preisach systems shown in Figures 4.1-4.3. The initial conditions used for these solutions are the same as those used in the corresponding system with the Preisach operator.

of the system near equilibrium. The system has a singularity on the nullcline of the input variable x of the Preisach operator (which is, simultaneously, the nullcline of the output); the role of this nullcline is similar to that of a switching line (surface) in switching systems. In particular, a trajectory makes a corner when it crosses the nullcline. The theoretical results for this type of system state that after hitting the nullcline, a trajectory either converges to, or diverges from, the equilibrium along the nullcline, or escapes from a neighbourhood of the equilibrium along the axis of the Preisach operator input variable x. Implementation of the triangular method for three model systems corresponding to each of the possible outcomes following hitting the nullcline is shown in this chapter. There was good agreement between the numerical trajectories obtain from use of the triangular method and the theoretical behaviour. The results in this chapter fur-

ther validate the triangular method as a numerical scheme for solving differential equations containing the derivative of the Preisach operator. The behaviour of such trajectories is similar to that of trajectories of the slow-fast planar system with the fast variable x and the critical curve coinciding with the nullcline of the system with the Preisach operator.

Chapter 5

Model of a two-phenotype bacteria

Long-term memory underpins genetic inheritance mechanisms and functioning of the immune system in higher organisms. Many regulatory networks exhibit complex dynamics and multi-stable states, also linked to memory. There is mounting evidence that microorganisms such as bacteria which have experienced different environmental histories may respond differently to their current conditions and that an environmental memory can grant fitness to bacteria in the evolutionary game. For example, history dependent behaviour was shown experimentally, and quantified in the information theory framework, in *B. subtilis* [89]. Environmental memory has been shown in DNA methylation in chemotaxing bacteria [90], genetic and epigenetic phase variation mechanisms in pathogenic bacteria [91, 92] and switch-type bistable systems in regulatory networks [93–96]. Further work focuses on designing biological memory switches such as a heritable switch with multiple states which are encoded into the DNA sequence [97].

Simple bacterial systems are an attractive test bed for developing an understanding of adaptation mechanisms which help organisms to survive and improve fitness in a fluctuating environment. One example is bacteria capable of switching behaviour, phenotype, or state in response to fluctuations of external conditions if different phenotypes are well adapted to different conditions. In particular, *E. coli* generate multistability of gene expression states under different perturbations [98–101]. Evidence for the evolution of phenotypic switching both experimentally and theoretically is given in [102–105].

A number of conceptual, technically simple, mathematical models have been pro-

posed to understand how certain switching strategies can help bacteria to increase fitness, which is often measured by the net population growth rate. The hybrid linear differential model proposed in [106] shows that a dynamically heterogeneous bacterial population can sometimes achieve a higher growth rate than a homogeneous one provided that the rate of a transition between phenotypes is comparable to, or lower than, the rate of variations of the environment. In this case, bacteria can anticipate sudden fluctuations of the environment by having a subpopulation ready in an appropriate phenotype before the environment changes to a state favouring this phenotype. This effect is more pronounced for predictable environments, such as periodic, but was also shown to be present for stochastic environments in narrower parameter ranges [106]. The optimal heterogeneous distribution between phenotypes is achieved dynamically by allowing some positive rate of transitions from the currently most favoured phenotype to an unfavoured one.

If the rate of transitions between phenotypes is higher than the rate of environment variations, then, under the assumptions of the model studied in [106], the maximal fitness is achieved by the responsive switching strategy whereby all the bacteria switch to the currently most favoured phenotype. However, if the responsive strategy is penalised, then it can be not optimal. This penalty can be associated with the cost of sensing the environment as bacteria have to maintain some sensory machinery in order to respond to changes.

Another linear hybrid differential model, where the cost of sensing was implemented as an explicit reduction in the growth rates, shows that stochastic switching can confer more fitness to the population than the responsive switching in slowly varying environments [107]. This result, as well as the results in [106] for faster environments, support the idea that diversity (heterogeneity) can help improve fitness in varying conditions, which is the view well established in ecology.

Memory can also grant fitness to bacteria. For instance, past phosphate limitation was shown to lead to a faster response to successive periods of phosphate limitation in *E. coli*, and this faster response was suggested to be survival enhancing [108]. An advantage of using strategies with memory can be shown in the framework of the game theory [109–111] applied to models where bacteria are considered as players in an evolutionary game [95, 107, 112].

Differential models proposed in [106, 107] are memoryless in slowly varying environmental conditions. In the adiabatic limit when the ratio of environment variation rate and the switching rate between phenotypes tends to zero, the state

of the system is completely determined by the state of the environment. In this chapter, using a modification of the model proposed in [106], I show that a long-term bistability type memory can increase fitness of bacteria in a stochastically varying environment. The model includes a cost of switching in the form of a temporary inhibition of the reproductive activity in bacteria undergoing a transition to a different phenotype. It is shown that the memory confers fitness when the rates of the environment variation and switching are comparable. In this state, the system achieves dynamic heterogeneity, which is consistent with the results in [106]. However, a static memory in this model persists in the limit of slow environments. This memory is characterised by a responsiveness parameter α; the value $\alpha = 0$ corresponds to a memoryless system.

More specifically, considered is a linear model of a growing population of bacteria, which respond to variations of external conditions (environment) by switching between two phenotypes. A demonstration of a possible scenario where memory can help achieve better fitness is given. The effect of external conditions is modelled by varying the availability of nutrients and, by this, the growth rate of each phenotype; fitness is measured by the average growth rate of the total population. It is assumed that each phenotype consumes a different type of food, for example, one consumes lactose, the other consumes glucose. A mixture of the two nutrients is supplied at a constant rate, while the proportion of the two ingredients in the mixture, measured by a variable E, varies in time. Bacteria sense changes in E and thus, by changing to the phenotype for which more food is available, can potentially increase the growth rate of the population. In this way, the system is similar to the model studied in [106]. However, instead of the binary environment, a continuous input $E(t)$ is used and a threshold type response for the bacteria is assumed. Namely, bacteria decide to switch their phenotype after E passes a certain threshold value. Importantly, the threshold value E_1 for switching from phenotype one to phenotype two can be different from the threshold value E_2 for inverse switching. The equality $E_1 = E_2$ corresponds to memoryless bacteria, while the case $E_1 \neq E_2$ indicates the presence of memory as a bacterium has to know (remember) its phenotype in order to decide whether to switch or not at a certain value of E. This is the type of memory of a non-ideal relay (bistable switch), see Chapter 2.

Some *in vitro* experimental studies give evidence that the process of changing phenotype can be stressful for bacteria. In particular, bacteria may not reproduce within a period of time preceding, during, or following this process. In these experiments, a colony of bacteria grown in a Petri dish with one nutrient is

swapped to a Petri dish with another nutrient. After a period of inactivity, or a shock, following the swap, bacteria start a transition to the other phenotype which is better fit for consuming the new type of food. If this is the case, a delay in growth appears to be a natural cost associated with phenotype switching. Assuming such a cost in the model, it will be shown that having memory can be an advantage for bacteria living in a stochastically varying environment. The memory, by introducing the difference between the thresholds, prevents switching when E varies in the interval $E_1 < E < E_2$ around the value $E_T = 0.5$ with equally available nutrients. This somewhat conservative strategy may increase the population's growth rate as small random fluctuations of E near the point E_T can keep more sensitive (responsive) bacteria, such as memoryless bacteria with $E_1 = E_2 = E_T$, or bacteria with $E_1 \approx E_2 \approx E_T$, in a transition non-reproductive state forever, thus stopping the growth.

5.1 Mathematical model

The following model of two phenotype bacteria residing in a discretely switching binary environment was presented in [106]

$$\tilde{x}' = \gamma_1 \tilde{x} - \kappa_1 \tilde{x} + \kappa_2 \tilde{y} \tag{5.1a}$$

$$\tilde{y}' = \gamma_2 \tilde{y} - \kappa_2 \tilde{y} + \kappa_1 \tilde{x} \tag{5.1b}$$

Here the function $\tilde{x} = \tilde{x}(t)$ is the population of bacteria in one of the phenotypes and $\tilde{y} = \tilde{y}(t)$ is the population in the other phenotype. The parameters γ_1 and γ_2 describe the growth rate of the phenotypes $\tilde{x}$ and $\tilde{y}$, respectively, in the current environmental state. The parameters κ_1 and κ_2 give the transition rates between the two phenotypes based on the current environmental state. The values of the parameters γ_1, γ_2, κ_1 and κ_2 change whenever the environment changes state. In order to visualise the behaviour of these parameter see Figure 5.1 where the effect of switching from environmental state 2 to state 1 is represented.

In this work, examination is made of the case where the environment changes continuously within an interval of values, as opposed to discretely as in the case of [106]. I introduce the continuous variable E to denote which of the environmental states the system is currently in. The value E is a measure of the relative abundance of one saturated environmental state over the other saturated state in the current intermediate (mixed) state. For example, if the environmental

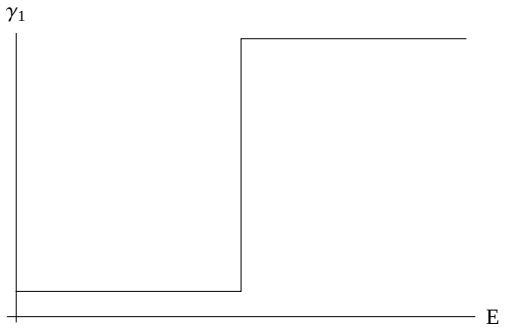

(a) The effect on the parameter γ_1 as the environment changes to the state preferred by population x.

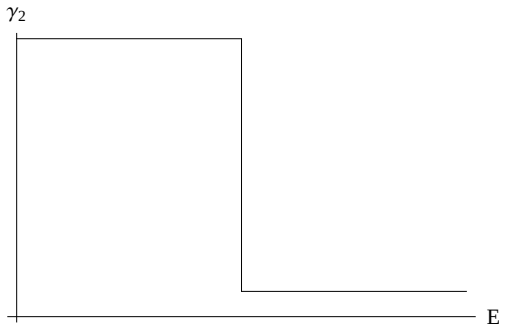

(b) The effect on the parameter γ_2 when the environment becomes the state unfavoured by population y.

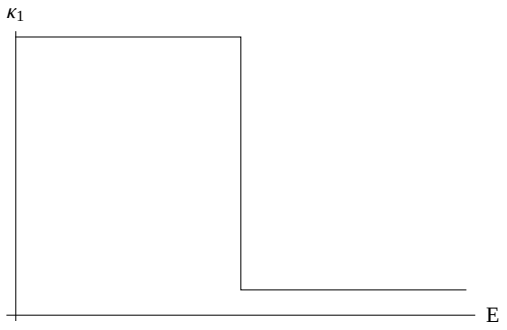

(c) The effect on the parameter κ_1 as the environment changes to the state preferred by population x.

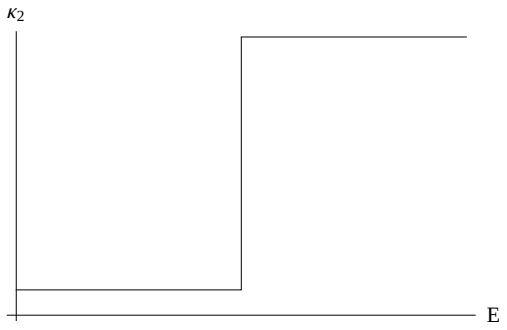

(d) The effect on the parameter κ_2 when the environment becomes the state unfavoured by population y.

Figure 5.1: Representation of the effect of a change in the environment from state 2 to state 1 on the parameters γ_1, γ_2, κ_1 and κ_2 of the model (5.1).

conditions that are being considered were a glucose/lactose mix, then E would tell us how much glucose there was compared to lactose. Some definitions about the value of the variable E are as follows; the case of $E \leq 0$ is chosen to be the case where the phenotype $\tilde{x}$ is fully favoured, that is the growth rate of $\tilde{x}$ is at its maximum and the growth rate of $\tilde{y}$ is at its minimum. Similarly, for $E \geq 1$ is the case that where the phenotype $\tilde{y}$ is fully favoured. Intermediate values of E give rise to partial favouring of one phenotype over the other. The value $E = 0.5$ is defined as the environmental threshold, E_T, the point at which both phenotypes are equally favoured, that is there is an equal mix of each environmental state and each phenotype grows at the same rate.

In the case of a discrete (binary) environment, like that considered in [106], it is realistic to assume that the growth rates of the two phenotypes are discrete as well and switch each time the environment switches state. Since in this work gradual changes of the environment between its continuous states are assumed and that there is only a partial favouring of one phenotype over the other, it

seems natural to use functions that change the growth rate gradually as the environment fluctuates. With this in mind, replace γ_1 and γ_2 in the model (5.1) with the functions $\Gamma_1(E)$ and $\Gamma_2(E)$ given by

$$\Gamma_1(E) = \begin{cases} \gamma_{unfit} + \sigma & E \leq 0 \\ \gamma_{unfit} + \sigma(1-E) & 0 < E < 1 \\ \gamma_{unfit} & E \geq 1 \end{cases} \tag{5.2}$$

$$\Gamma_2(E) = \begin{cases} \gamma_{unfit} & E \leq 0 \\ \gamma_{unfit} + \sigma E & 0 < E < 1 \\ \gamma_{unfit} + \sigma & E \geq 1 \end{cases} \tag{5.3}$$

where γ_{unfit} is the growth rate when the phenotype is unfavoured by the environment and σ is the benefit for the environment being in the state that is preferred by the phenotype, see Figure 5.2.

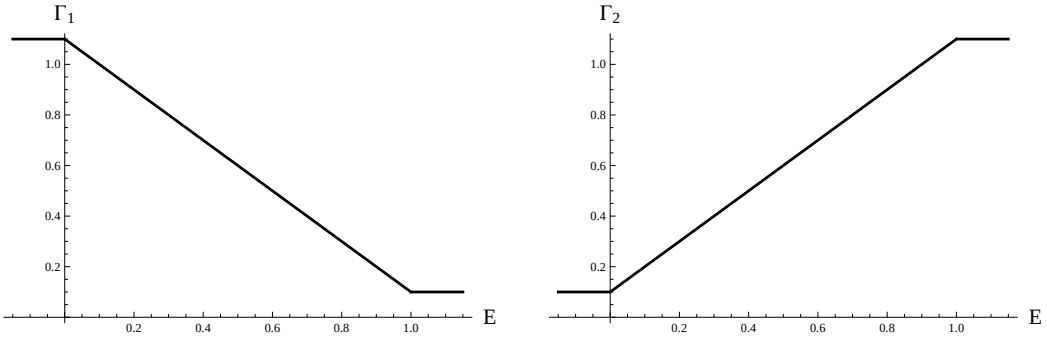

(a) How the function $\Gamma_1(E)$ varies as the value of E is changed from -0.15 to 1.15.

(b) How the function $\Gamma_2(E)$ varies as the value of E is changed from -0.15 to 1.15.

Figure 5.2: Representation of the functions $\Gamma_1(E)$ and $\Gamma_2(E)$ given by the equations (5.2) and (5.3).

A positive transition rate κ from the phenotype that is unfavoured by the environment to the favoured phenotype is assumed, and a zero transition rate from the favoured phenotype. The transition rate changes when the environmental state E reaches a threshold value. That is the parameters κ_1 and κ_2 in (5.1) are step functions of the variable E,

$$\kappa_1(E) = \begin{cases} 0 & E \leq E_T + \alpha \\ \kappa & E > E_T + \alpha \end{cases} \tag{5.4}$$

$$\kappa_2(E) = \begin{cases} \kappa & E \leq E_T - \alpha \\ 0 & E > E_T - \alpha \end{cases} \tag{5.5}$$

where α is a parameter which measures the bacteria's responsiveness to changes

in the environmental input, it behaves as a shift in the environment threshold at which the transition rates change. Note that if $\alpha > 0$ then no transitions occur as long as $E_T - \alpha < E(t) < E_T + \alpha$.

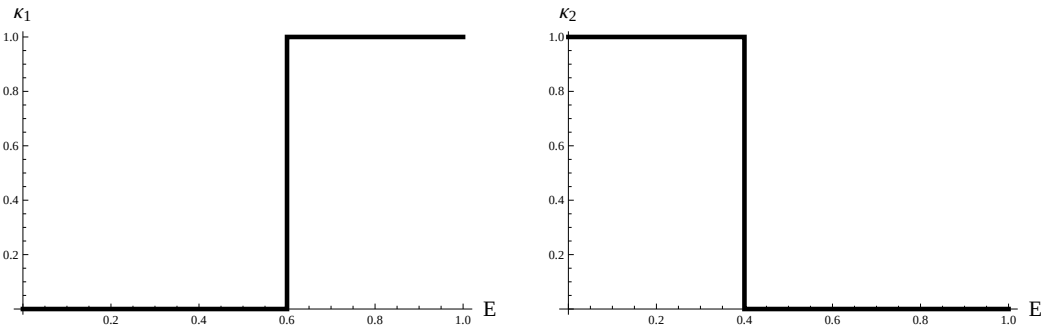

(a) $\kappa_1(E)$. (b) $\kappa_2(E)$

Figure 5.3: The behaviour of the functions $\kappa_1(E)$ and $\kappa_2(E)$ given by a equations (5.4) and (5.5) for a positive value of the parameter α.

These modifications give the model

$$\tilde{x}' = \Gamma_1(E)\tilde{x} - \kappa_1(E)\tilde{x} + \kappa_2(E)\tilde{y} \tag{5.6a}$$

$$\tilde{y}' = \Gamma_2(E)\tilde{y} - \kappa_2(E)\tilde{y} + \kappa_1(E)\tilde{x} \tag{5.6b}$$

This model is the starting point of the analysis and is presented as a frame of reference for an extended model considered below.

5.2 Analysis of the initial model

If the total population of bacteria as a function of time is $N(t)$ that is $N = \tilde{x} + \tilde{y}$ then for the model (5.6) the rate of change of the population is

$$N' = \Gamma_1(E)\tilde{x} + \Gamma_2(E)\tilde{y}$$

If this system was regarded as growing at an average growth rate λ then the population at a time t would be given by $N = N_0 e^{\lambda t}$. The average growth rate for system (5.6) is

$$\lambda = \lim_{t\to\infty} \frac{1}{t} \int_0^t (\Gamma_1(E)x + \Gamma_2(E)y)d\tau \tag{5.7}$$

where x and y are the fractional populations of the phenotypes $\tilde{x}$ and $\tilde{y}$ and $\Gamma_1(E)$ and $\Gamma_2(E)$ are the growth rates of these phenotypes.

In order to facilitate numerical simulation of the model a change of variables

is performed and instead consideration is given to the population of bacteria of a given phenotype in terms of its fraction of the total population. Define the population x as the fraction of total population currently in the phenotype $\tilde{x}$ that is

$$x = \frac{\tilde{x}}{N}$$

thus this change of variable gives that

$$\begin{aligned}
x' &= \left(\frac{\tilde{x}}{N}\right)' \\
&= \frac{1}{N}\tilde{x}' - \frac{\tilde{x}}{N^2}N' \\
&= \frac{1}{N}(\Gamma_1(E)\tilde{x} - \kappa_1(E)\tilde{x} + \kappa_2(E)\tilde{y}) - \frac{x}{N}(\Gamma_1(E)\tilde{x} + \Gamma_2(E)\tilde{y}) \\
&= \Gamma_1(E)x - \kappa_1(E)x + \kappa_2\frac{\tilde{y}}{N} - \Gamma_1(E)x^2 - \Gamma_2(E)x\frac{\tilde{y}}{N} \\
x' &= \Gamma_1(E)(1-x)x - \kappa_1(E)x + \kappa_2(E)\frac{\tilde{y}}{N} - \Gamma_2(E)x\frac{\tilde{y}}{N}.
\end{aligned}$$

Define the population y as the fraction of the total population in the phenotype $\tilde{y}$ that is

$$y = \frac{\tilde{y}}{N}$$

which gives the change of variables

$$\begin{aligned}
y' &= \left(\frac{\tilde{y}}{N}\right) \\
&= \frac{1}{N}\tilde{y}' - \frac{\tilde{y}}{N^2}N' \\
&= \frac{1}{N}(\Gamma_2(E)\tilde{y} - \kappa_2(E)\tilde{y} + \kappa_1(E)\tilde{x}) - \frac{y}{N}(\Gamma_1(E)\tilde{x} + \Gamma_2(E)\tilde{y}) \\
&= \Gamma_2(E)y - \kappa_2(E)y + \kappa_1(E)x - \Gamma_1(E)xy - \Gamma_2(E)y^2 \\
y' &= \Gamma_2(E)(1-y)y - \kappa_2(E)y + \kappa_1(E)x - \Gamma_1(E)xy.
\end{aligned}$$

This gives the model for numerical simulation as

$$x' = \gamma_1(E)(1-x)x - \kappa_1(E)x + \kappa_2(E)y - \gamma_2(E)xy \tag{5.8a}$$

$$y' = \gamma_2(E)(1-y)y - \kappa_2(E)y + \kappa_1(E)x - \gamma_1(E)xy \tag{5.8b}$$

What is of interest for this model is to examine what effect there is on the average growth rate of the system when changes to the responsiveness parameter α of the functions $\kappa_1(E)$ and $\kappa_2(E)$ are made. Only the case of symmetric shifts in the switching thresholds is taken for consideration, that is if the threshold is adjusted

by an amount α then the switching threshold of $\kappa_1(E)$ is $E_T+\alpha$ and the switching threshold of $\kappa_2(E)$ is $E_T-\alpha$, see equations (5.4) and (5.5) for reference.

The system will be considered for two different environmental inputs. The first environmental input consider will be the periodic input given by

$$E = \frac{1}{2}(\sin t + 1). \tag{5.9}$$

The second input that is being examined is chosen to vary as a stochastic single well potential centered at the value E_T. Thus this environmental input for the system (5.8) is given by

$$\mathrm{d}E = -a(E - E_T)\mathrm{d}t + \mathrm{d}W_t \tag{5.10}$$

where W_t is the Wiener process and a is a parameter determining the steepness of the well potential. As the mean value of E equals $E_T = 0.5$, in the absence of any stochastic fluctuations both phenotypes grow at the same rate. Numerical confirmation that the system (5.8) converges to an average growth for the two environmental inputs that are being considered is shown in Figure 5.4. Since the system converges to an average growth rate for both environmental inputs then the examination of the system in the proposed manner is justified.

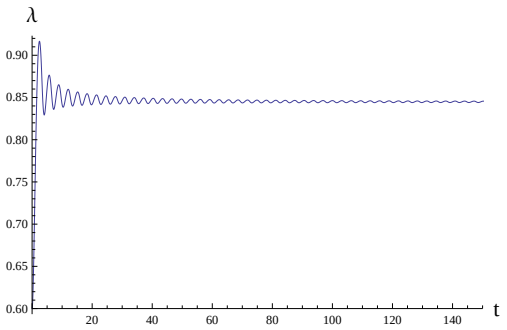

(a) Convergence to the average growth rate for the system (5.8) for the periodic environmental input given in (5.9).

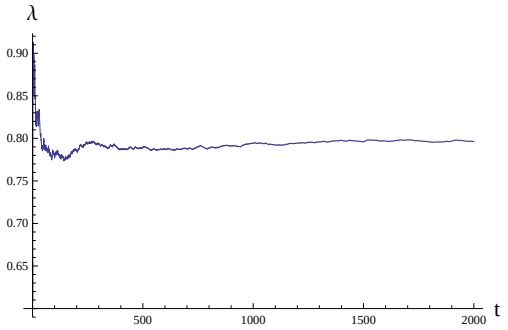

(b) Convergence to the average growth rate for the system (5.8) for the stochastic environmental input given in (5.10).

Figure 5.4: Convergence of the system (5.8) to an average growth rate for two different environmental inputs. The parameters used in the simulation were $x_0 = 0.5$, $y_0 = 0.5$, $\gamma_{unfit} = 0.1$, $\sigma = 1$, $\kappa = 1.5$, $a = 1$ and $\alpha = 0$.

The value of α is varied over the range $(-3, 3)$. A negative value of α means that the bacteria begin to change before the environment has stopped favouring their phenotype. Switching in this region will be referred to as *predictive* switching as the bacteria attempt to predict changes in the environment before they occur. A zero value of α means that the bacteria switch phenotype when the environment

starts to favour the other phenotype marginally stronger. Switching at this value will be called *environmental* switching, or *memoryless* switching, as the bacteria switch each time the environment passes the point $E = E_T$. A positive value of α means that the bacteria do not switch until a sufficient bias for the other phenotype has been created in the environment. This switching scheme is called *delayed* switching as the bacteria delay changing phenotypes until there is a strong favouring of the other phenotype. A positive value of α introduces memory into the system as the response of the bacteria to variations of the environment depends on their state (phenotype).

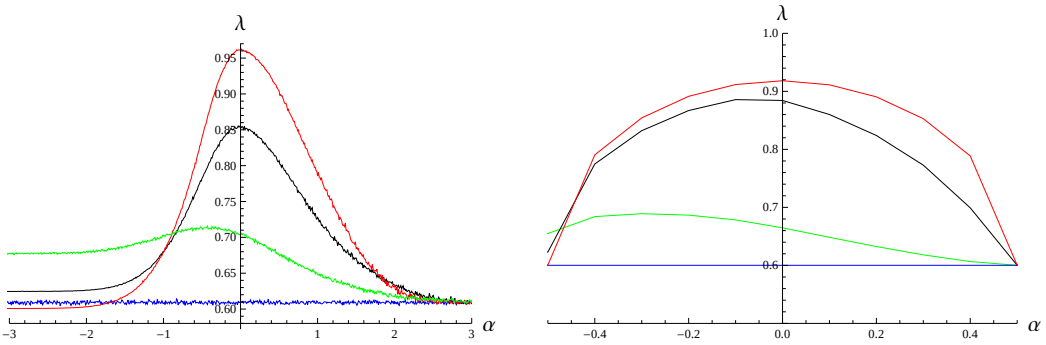

(a) Results for the stochastic environmental input given by (5.10)

(b) Results for the periodic environmental input given by (5.9)

Figure 5.5: Plots of the average growth rate obtained by averaging 20 simulations of the system of equations given in equation (5.8) for different α values. The blue line corresponds to $\kappa = 0$ when there are no transitions between phenotypes. The green, black and red lines are for $\kappa = 0.3, 2.6, 100$ respectively. The other parameters used in the simulations are $\gamma_{unfit} = 0.1$, $\sigma = 1$ and $a = 1$. The initial populations were $x_0 = 0.5$ and $y_0 = 0.5$.

The results obtained for this system are shown in Figure 5.5. In this figure the blue line represents the results obtained for $\kappa = 0$, the case of no flow between phenotypes. In this situation the system has a steady average growth rate close to the arithmetic mean 0.6 of the values used for Γ_1 and Γ_2. The other three curves correspond to $\kappa = 0.3$, $\kappa = 2.6$ and $\kappa = 100$.

In the case of the stochastic input given by (5.10) there is a distinct peak in the average growth rate when transitions between the two phenotypes are allowed (that is for $\kappa > 0$), see Figure 5.5a. It is of note that the peak in the curves for low transition rates occurs for $\alpha < 0$, that is the system begins the switching of phenotypes before the environment changes which phenotype it favours. As the transition rate increases there is a shift in the location of the peak to $\alpha = 0$, that is the system undergoes switching at the same moment as the environment starts to favour one phenotype over the other. This behaviour suggests that the best

strategy for bacteria which switch slowly is to attempt to predict the environment by use of the *predictive* switching since it will take them a long time change the full population to the new phenotype, while the bacteria who can change phenotype faster will grow better if they use the *environmental* switching.

In Figure 5.5a the curves for $\kappa = 0.3$, $\kappa = 2.6$ and $\kappa = 100$ converge to the blue curve as $\alpha \to +\infty$. This occurs because the value of α is sufficient so that the environmental input rarely alters the value of the functions κ_1 and κ_2. Since in this region α is positive, both κ_1 and κ_2 are nearly always zero and the majority of bacteria never transition phenotype. In this region the plots of λ for non-zero values of κ tend to that obtained for $\kappa = 0$ as α increases.

In the case of $\alpha \to -\infty$ there is a different result, here the threshold values are sufficient so that the environmental input is also rarely able to alter the functions κ_1 and κ_2. Since α is negative and the thresholds of κ_1 and κ_2 are rarely crossed the majority of bacteria are nearly always transitioning phenotype. This is similar to introducing a back flow to the model as was considered in [106]. Here for a low transition rate the average growth rate is higher than that obtained for no transitions between states. As the transition rate is increased the average growth rate is less than that obtained for no transitions. This result for the model with a continuous environmental input is the equivalent of the result obtained in [106] for the model with a binary environmental input which showed that for certain value of the transition rate the average growth rate could be maximised by having a transition into the unfavoured phenotype.

In the case of the periodic environmental input given by (5.9), see Figure 5.5b, the *predictive* switching strategy is nearly always the optimal strategy. However when the bacteria can transition extremely fast so that the population in one phenotype nearly instantly transitions to the other phenotype then the *environmental* switching strategy becomes the more favourable strategy.

5.3 Extension of the model

The model described by equation (5.8) does not include any form of a penalty for bacteria changing from one phenotype to the other. This would be a justifiable assumption in particular for the case where the time taken for the bacteria to change phenotype is shorter than the time between the occurrence of these transitions as is the case studied in [106]. Considered here is the alternative case

where a cost for the transition is incorporated into the model. This cost is assumed to be that when a bacterium begins to change phenotype it undergoes a period of shock during which it does not reproduce.

In order to encapsulate this idea I introduce two additional groups for the bacteria population, $\tilde{z}$ and $\tilde{w}$, which represent intermediate states in the transition from phenotype $\tilde{x}$ to the phenotype $\tilde{y}$ and vice versa, respectively. That is when a bacterium in the phenotype $\tilde{x}$ undergoes a transition to the phenotype $\tilde{y}$, it first enters the population $\tilde{z}$ and spends a period of time in this group where it does not reproduce. The bacterium then moves from the group $\tilde{z}$ to the phenotype $\tilde{y}$. The group $\tilde{w}$ works in a similar manner for transitions from the phenotype $\tilde{y}$ to the phenotype $\tilde{x}$ this gives the new model

$$\tilde{x}' = \Gamma_1(E)\tilde{x} - \kappa_1(E)\tilde{x} + \delta_2\tilde{w} \tag{5.11a}$$

$$\tilde{y}' = \Gamma_2(E)\tilde{y} - \kappa_2(E)\tilde{y} + \delta_1\tilde{z} \tag{5.11b}$$

$$\tilde{z}' = \kappa_1(E)\tilde{x} - \delta_1\tilde{z} \tag{5.11c}$$

$$\tilde{w}' = \kappa_2(E)\tilde{y} - \delta_2\tilde{w} \tag{5.11d}$$

where $\Gamma_1(E)$ and $\Gamma_2(E)$ are given by equations (5.2) and (5.3); $\kappa_1(E)$ and $\kappa_2(E)$ are the step functions given by equations (5.4) and (5.5) with the jumps occurring at $E = E_T + \alpha$ and $E = E_T - \alpha$, respectively; and the parameters δ_1 and δ_2 represent the inverse of the average shock period that the bacteria undergo for changing phenotypes.

5.4 Examination of the extended model

The same analysis carried out before is applied to the extended model. Initially only consideration is given to the stochastic environmental input given by (5.10). For numerical implementation of the system (5.11) a change of variables needs to be performed in order to consider the fraction of the total population in each population group. To that end introduce the variables x, y, w and z which are defined as

$$x = \frac{\tilde{x}}{N}, \quad y = \frac{\tilde{y}}{N}, \quad w = \frac{\tilde{w}}{N}, \quad z = \frac{\tilde{z}}{N}$$

where N is the total population given by $N = \tilde{x} + \tilde{y} + \tilde{w} + \tilde{z}$. Note that changing the definition of N in this manner does not change the value of N' since the populations $\tilde{z}$ and $\tilde{w}$ do not add to the bacteria's growth rate and as a result the

value of the average growth rate λ is still given by (5.7). This change of variables gives for the phenotype $\tilde{x}$ that

$$\begin{aligned} x' &= \left(\frac{\tilde{x}}{N}\right)' \\ &= \frac{1}{N}\tilde{x}' - \frac{\tilde{x}}{N^2}N' \\ &= \Gamma_1(E)x - \kappa_1(E)x + \delta_2 w - \Gamma_1(E)x^2 - \Gamma_2(E)xy \\ x' &= \Gamma_1(E)(1-x)x - \kappa_1(E)x + \delta_2 w - \Gamma_2(E)xy \end{aligned}$$

and for the phenotype $\tilde{y}$

$$\begin{aligned} y' &= \left(\frac{\tilde{y}}{N}\right)' \\ &= \frac{1}{N}\tilde{y}' - \frac{\tilde{y}}{N^2}N' \\ &= \Gamma_2(E)y - \kappa_2(E)y + \delta_1 z - \Gamma_2(E)y^2 - \Gamma_1(E)xy \\ y' &= \Gamma_2(E)(1-y)y - \kappa_1(E)x + \delta_1 z - \Gamma_1(E)xy. \end{aligned}$$

The population group $\tilde{w}$ becomes

$$\begin{aligned} w' &= \left(\frac{\tilde{w}}{N}\right)' \\ &= \frac{1}{N}\tilde{w}' - \frac{\tilde{w}}{N^2}N' \\ w' &= \kappa_2(E)y + \delta_2 w - \Gamma_1(E)wx - \Gamma_2(E)wy. \end{aligned}$$

Finally the population $\tilde{z}$ is

$$\begin{aligned} z' &= \left(\frac{\tilde{z}}{N}\right)' \\ &= \frac{1}{N}\tilde{z}' - \frac{\tilde{z}}{N^2}N' \\ z' &= \kappa_1(E)x + \delta_1 z - \Gamma_1(E)zx - \Gamma_2(E)zy. \end{aligned}$$

These give the model for simulation as

$$x' = \Gamma_1(E)(1-x)x - \kappa_1(E)x + \delta_2 w - \Gamma_2(E)xy \tag{5.12a}$$

$$y' = \Gamma_2(E)(1-y)y - \kappa_1(E)x + \delta_1 z - \Gamma_1(E)xy \tag{5.12b}$$

$$w' = \kappa_2(E)y + \delta_2 w - \Gamma_1(E)wx - \Gamma_2(E)wy \tag{5.12c}$$

$$z' = \kappa_1(E)x + \delta_1 z - \Gamma_1(E)zx - \Gamma_2(E)zy \tag{5.12d}$$

For simplicity the average shock period undergone by bacteria is assumed to be the same in each direction that is $\delta_1 = \delta_2 = \delta$.

A comparison of Figures 5.5a and 5.6 shows that there is a big effect on the model by the introduction of the switching cost in this form. In order to explain the effects present; the plot is divided into 3 regions. Take $\alpha \leq -1$ as region 1 and $\alpha \geq 2$ as region 2 and $-1 < \alpha < 2$ as region 3. As in the case of the Figure 5.5a the blue line represents the results for $\kappa = 0$, the case where no transitions between the phenotypes occur. As before the average growth rate in this case is close to the arithmetic mean of Γ_1 and Γ_2 for the chosen parameter values. Any variabilities in the lines in the plot are a result of the stochastic nature of the input to the system and should be eliminated by the inclusion of more simulations and by increasing the time length of the simulations.

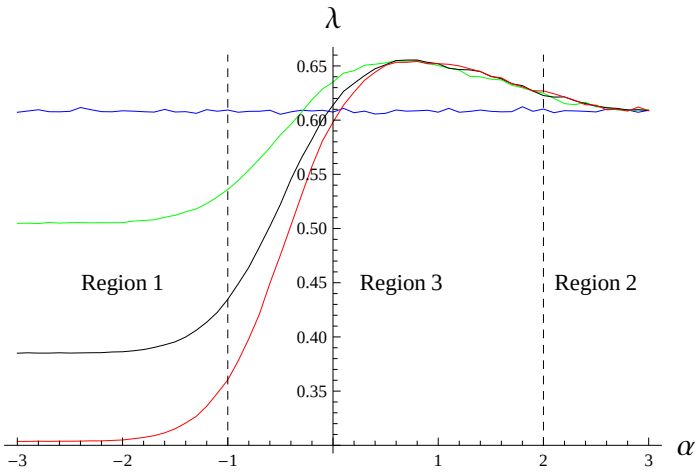

Figure 5.6: Plots of the average growth rate (5.7) obtained by averaging 20 simulations of the system (5.12) for different α values. The blue line corresponds to $\kappa = 0$ when there is no flow between phenotypes. The green, black and red lines are for $\kappa = 0.5, 1, 1.5$, respectively. Parameters $\sigma = 1$, $a = 1$, $\gamma_{unfit} = 0.1$ are the same as in Figure 5.5; $\delta = 1$. The initial population values were $x_0 = 0.5$, $y_0 = 0.5$, $w_0 = 0$ and $z_0 = 0$. The environmental input had the initial condition $E_0 = 0$.

In region 1 it can be seen that increasing the value of κ causes the average growth rate of the system to tend to zero rapidly. For the green, black and red lines the absolute value of α is sufficiently large so that the environmental input E rarely reaches the thresholds of κ_1 and κ_2. Since α is negative and the thresholds of the functions κ_1 and κ_2 are rarely reached the majority of the bacteria are nearly always in a transition state. The higher the transition rate κ becomes the greater the percentage of the total population that gets stuck in the intermediate groups z and w which do not add to the growth of the system resulting in the average

growth rate, λ, tending to zero. While not shown in Figure 5.6 for low transition rates it is possible to have the growth rate maximised by having a back flow into the unfavoured phenotype present as was found for the system (5.8).

In region 2 the value of α is also sufficient so that the environment rarely alters the value of the functions κ_1 and κ_2. Since in this region the value of α is positive the functions κ_1 and κ_2 are nearly always zero valued and thus the majority of bacteria remain in the non-transition states x and y. As the value of α is increased in this region the plots of λ for non-zero values of κ tend to that obtained for $\kappa = 0$.

The results obtained in region 3 are the most interesting. In this region each of the lines corresponding to a non-zero value of κ has a distinct peak average growth rate for some $\alpha > 0$. This means that the population achieves the maximum average growth rate by adopting the *delayed* switching strategy. That is bacteria delay from switching their current phenotypes until the environment has a higher preference for the other phenotype than that given by just crossing the environmental threshold E_T. The benefit of this delayed switching arises from the elimination of any unnecessary switching that may occur as the environment stochastically varies. This unnecessary switching would be the result of the environmental input crossing the threshold E_T and then quickly switching back.

5.4.1 Effects of altering the parameters of the model

Now examination is performed on the response of the system (5.12) to variations of the model parameters δ, which controls how long bacteria stay in the non-reproductive delay groups; the difference of the growth rates of a favoured and unfavored phenotypes σ; and, the steepness of the potential well a, which controls fluctuations of the environment. The results are presented in Figures 5.7 and 5.8.

Examining the plots showing the dependence $\lambda(\alpha)$ in Figure 5.7a for several values of the steepness of the potential well of the environmental input, a, it can be seen that as the well becomes steeper and the environmental input is forced to spend more time around the environmental threshold E_T, the value of the peak in the average growth rate λ decreases. When the well becomes sufficiently steep, the peak is lost and the average growth rate maximum converges to the value $\gamma_{unfit} + 0.5\sigma$ of the average growth rate of the system with no transitions between phenotypes.

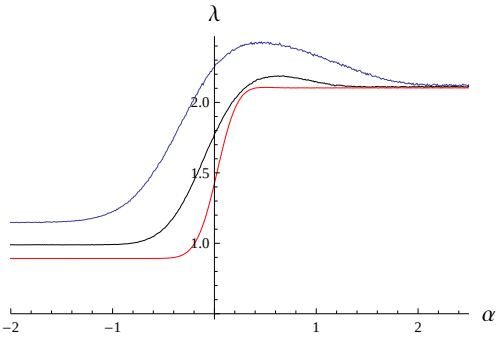

(a) The effect of changing the steepness of the potential well, a. The blue, back, and red lines are for $a = 2, 5, 21$, respectively. Other parameters are $\sigma = 4$, $\kappa = 2.6$, $\delta = 1$ and $\gamma_{unfit} = 0.1$.

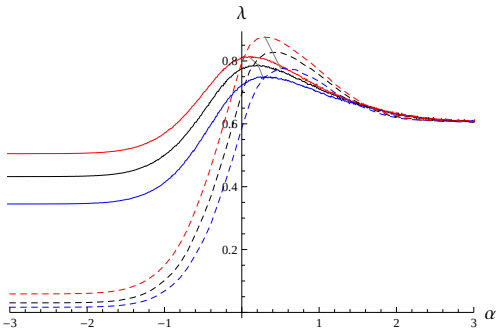

(b) The effect of altering the average delay time, $1/\delta$. The blue, black, and red lines are for $\delta = 2.8, 5.3, 10.3$, respectively. The solid coloured lines are for $\kappa = 2.6$, the dashed lines are for $\kappa = 100$. The gray lines connect the maxima of the curves for different values of the parameter δ. Other parameters are $\sigma = 1$, $a = 1$ and $\gamma_{unfit} = 0.1$.

Figure 5.7: The effect of changes in the parameters a and δ of model (5.12) on the average growth rate of the population, λ, and the optimal value of the threshold parameter α, which maximizes λ.

Figure 5.7b shows the effect that variations in the length of the delay characteristic times, $1/\delta$, have on the graphs $\lambda(\alpha)$. Increasing the value of δ is equivalent to shortening the time a bacterium in transition spends in the non-reproductive state (groups z and w). For increasing values of δ the peak of the average growth rate moves left towards $\alpha = 0$. This result is to be expected as shortening the delay period is equivalent to returning to model (5.8) without delay.

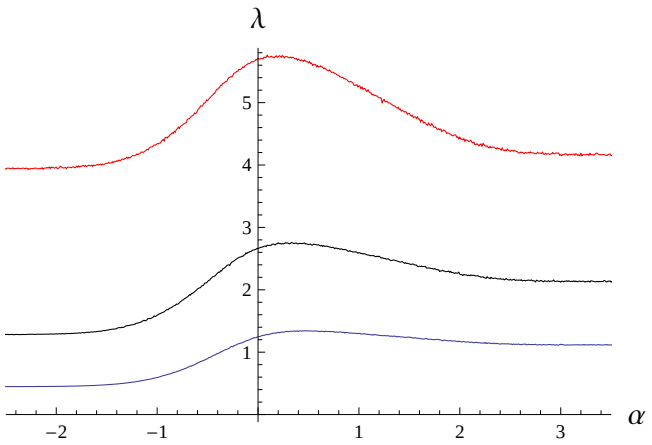

Figure 5.8: Results of modifying the benefit to the growth rate for being the favoured phenotype, σ, for model (5.12). The blue, black, and red lines correspond to $\sigma = 2, 4, 8$, respectively. Other parameters are $\kappa = 2.6$, $\delta = 1$, $a = 1$ and $\gamma_{unfit} = 0.1$.

Finally, in Figure 5.8, the parameter σ is varied, which controls the benefit to

the growth rate that bacteria in a favoured phenotype gain over bacteria in the unfavoured phenotype. Increasing the value of σ has an effect similar to that of shortening the delay period by increasing δ. This result can be understood if σ is viewed as a penalty for being in the wrong phenotype when the environment changes. When the penalty becomes sufficiently high it is no longer worth delaying changing phenotype and becomes better to change with the environment using the *memoryless* responsive strategy.

Alterations to the parameter γ_{unfit}, the growth rate of the unfavoured phenotype, simply causes a translation of the plots up the λ axis; that is, γ_{unfit} is an additive constant to the average growth rate.

5.4.2 Other environmental inputs

In this Section, the response of the model (5.12) to environmental inputs different from (5.10) is explored. Two alternative inputs are presented here: a stochastic motion in a double well potential defined by the stochastic differential equation

$$dE = \left(2(E - E_T) - 8(E - E_T)^3\right) dt + dW_t; \tag{5.13}$$

and the periodic input given by (5.9).

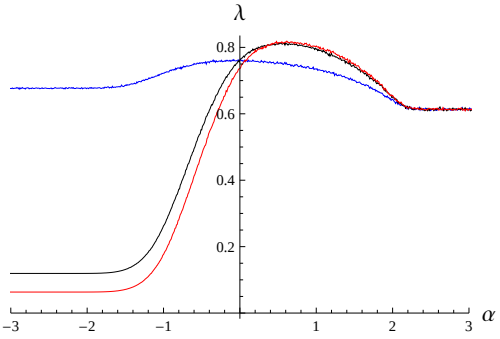

(a) Results for the stochastic input (5.13). The blue, black, and red lines correspond to $\kappa = 0.2, 4.7, 9.2$, respectively.

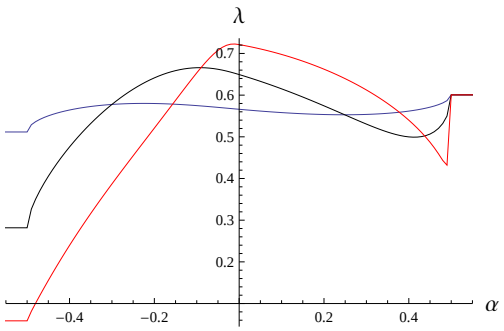

(b) Results for the periodic environmental input. The blue, black, and red lines are for $\kappa = 0.45, 0.7, 1.7$, respectively.

Figure 5.9: Dependence of the average growth rate λ on the parameter α for alternative environmental inputs to model (5.12). Parameters $\sigma = 1$, $\gamma_{unfit} = 0.1$ and $\delta = 1$ are the same as in Figure 5.6. The initial population values were $x_0 = 0.5$, $y_0 = 0.5$, $w_0 = 0$ and $z_0 = 0$.

Figure 5.9a presents data obtained for the stochastic input (5.13). This figure shows that if the transitions rate κ is low, then the average growth rate is maximized by $\alpha = 0$. As the transition rate increases, the peak in the average growth

rate shifts to the region of positive α, that is the delayed strategy based on memory of the state grants more fitness than the memoryless strategy. The result is similar to that obtained for the stochastic environmental input (5.10) generated the single well potential, see Figure 5.6.

The plot in Figure 5.9b was obtained for the periodic input given by equation (5.9), which represents a fully predictable deterministic pattern of environment variations. The blue curve corresponds to a low transition rate κ. From Figure 5.9b it is clear that the graph $\lambda(\alpha)$ follows a complex profile as α is varied from the region $\alpha < -0.5$, where the transition rates $\kappa_{1,2}(E)$ are always equal to κ, to the region $\alpha > 0.5$, where there are no transitions between the phenotypes ($\kappa_{1,2}(E) = 0$). The average growth rate λ has a local peak for an $\alpha < 0$. However, the value of λ at the peak is less than the growth rate $\gamma_{unfit} + 0.5\sigma$, which is achieved for $\alpha > 0.5$ by the regime without transitions. The local peak value of λ increases with increasing κ. At $\kappa \approx 0.7$, the peak is the same height as the average growth rate for the region $\alpha > 0.5$ (the black line in Figure 5.9b). For larger κ, the maximum average growth rate is achieved for $\alpha < 0$. As κ increases further, the peak in the region $\alpha < 0$ is shifted towards $\alpha = 0$. The peak at a negative value of α means that the growth rate is maximized by the *predictive* switching strategy. This result is in line with findings in [106]. However, for this model the value of κ should be large enough to favour the *predictive* strategy; otherwise, the negative effect of the switching cost dominates and the strategy forbidding transitions between the phenotypes becomes optimal.

5.5 Introduction of transitions to the favoured phenotype

This section considers the effect of allowing transitions into the unfavoured phenotype to occur, that is equations (5.4) and (5.5) are modified to instead be

$$\kappa_1(E) = \begin{cases} \phi & E \leq E_T + \alpha \\ \kappa & E > E_T + \alpha \end{cases} \tag{5.14}$$

$$\kappa_2(E) = \begin{cases} \kappa & E \leq E_T - \alpha \\ \phi & E > E_T - \alpha \end{cases} \tag{5.15}$$

where κ remains as before the transition rate to the favoured phenotype and ϕ is the rate of transitions from the phenotype favoured by the environment to the

phenotype unfavoured by the current environmental condition.

In [106] it was shown that in a discrete periodic environment the model (5.1) the average growth rate of the bacteria for a range of values of κ was maximised by a value of $\phi > 0$, that is the average growth rate was maximised by allowing transitions into the unfavoured phenotype.

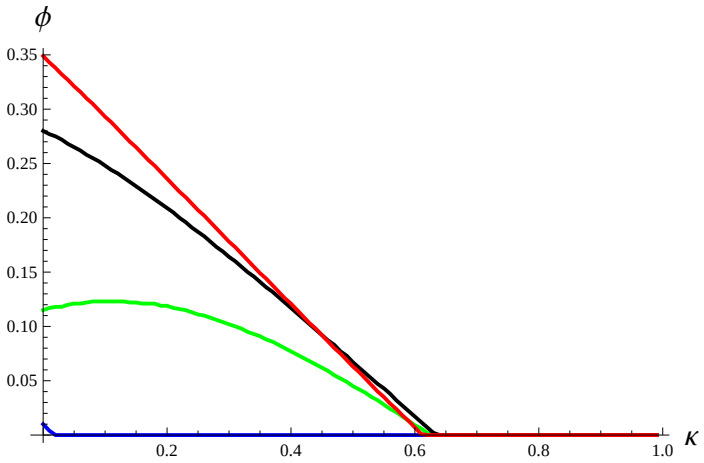

Figure 5.10: Plot of the value of transition rate to the unfit phenotype that maximises the average growth rate for a given value of κ for the model (5.11). The blue line corresponds to $\sigma = 1$. The green line to $\sigma = 2$, the black line to $\sigma = 3$ and the red line to $\sigma = 4$. The other parameters used in the simulation were $\gamma_{unfit} = 0.1$, $\delta = 1$, $\alpha = 0$.

Figure 5.10 shows the value of ϕ as a function of κ which maximises the average growth rate for the system (5.12) with the periodic environmental input given by (5.9) for the memoryless system ($\alpha = 0$) for different values of σ. This figure shows that for values of $\sigma \geq 1$ then there is a value of κ below which the average growth rate is maximised by a value of $\phi > 0$ (the range of κ values depends on the value of σ, for example $\sigma = 1$ the range is $0 \leq \kappa \leq 0.01$). This means that the result of [106] still hold when the environmental input is considered as a continuous variation and a penalty for transitioning bacteria is applied, although the range of κ values that benefit from a non-zero value of ϕ is significantly reduced.

Figure 5.11 shows the dependence of the average of growth rate λ on α for different values of the parameter ϕ for the system (5.12) with the stochastic input given by equation (5.10). The blue line shows the case for $\phi = 0$, that is it is the result obtained when only transitions are allowed from the unfavoured phenotype to the favoured phenotype, this is the same as the system previously studied and is presented as a frame of reference for the rest of Figure 5.11. The green and

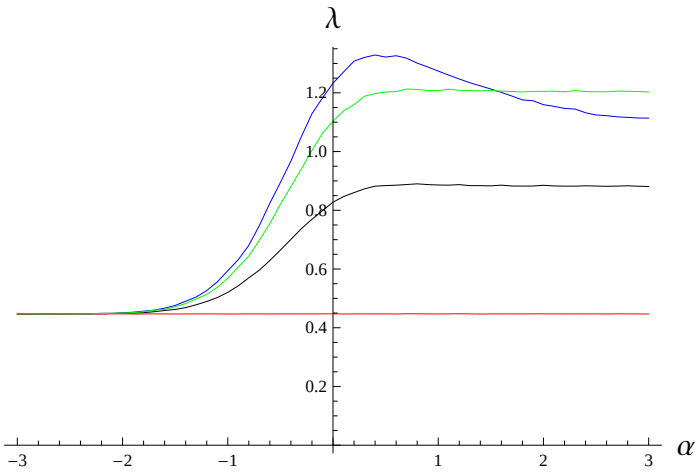

Figure 5.11: Plots of the average growth rate (5.7) obtained by averaging 20 simulations of the system (5.12) for different α values. The blue line corresponds to $\phi = 0$ when there is only flow from the unfavoured to the favoured phenotype. The green, black and red lines are for $\phi = 0.3, 1, 2.6$, respectively. Parameters $\sigma = 2$, $a = 1$, $\gamma_{unfit} = 0.1$, $\kappa = 2.6$ and $\delta = 1$. The initial population values were $x_0 = 0.5$, $y_0 = 0.5$, $w_0 = 0$ and $z_0 = 0$. The environmental input had the initial condition $E_0 = 0$.

black lines correspond to the cases $\phi = 0.3, 1$ respectively. Examination of Figure 5.11 shows that for the chosen parameter values the introduction of a flow into the unfavoured phenotype alters the observed dynamics. For $\phi > 0$ the distinct peak value of α which maximises the average growth rate is lost, instead there is a value of $\alpha_1 > 0$ where the average growth rate λ remains constant for $\alpha \geq \alpha 1$. With the chosen parameter set the average growth rate decreases as the value of ϕ is increased, for the chosen parameter values the average growth is maximised by $\phi = 0$. The red line for $\phi = 2.6$ is almost perfectly horizontal across the range of α values, this is because for this line $\phi = \kappa$ so for all values of α the transition rates are the same.

5.6 Multi-species model

5.6.1 Model equations

In the previous sections of this chapter it was shown that if bacteria delay switching between phenotypes it can help them to achieve a higher average growth rate in a stochastic environment in model (5.12). If bacteria maximise the average growth rate by having a delay of α on the environmental threshold, then in the

case of a transition rate κ which is sufficiently high enough so that the whole population in a given phenotype transitions instantaneously to the other phenotype and a brief shock period, that is a high value of δ, the dynamics of the state that bacteria are in can be modelled by the non-ideal relay, R_α, with thresholds $-\alpha$, α, output values ± 1, and input E; for a discussion of the dynamics of the non-ideal relay, see Chapter 2. When $R_\alpha = 1$, the bacteria is in the state (phenotype) which favours the nutrient F_1; if $R_\alpha = -1$, then the bacteria favours the nutrient F_2. Adopting this model for the states of the bacteria, now consider a collection of populations of bacteria with different thresholds α sharing the same food supply. The density of bacteria with the threshold α at a moment t is denoted by $n(t, \alpha)$. The assumption is made that a bacterium can sporadically change its threshold α. The resulting variability in α is modelled by a diffusion process. Additional diffusion of the thresholds can occur in the birth process under the assumption that a bacterium with a threshold α can produce offspring with different thresholds, for example, according to the Gaussian distribution centered at α. With these assumptions, consider the following model of evolution of bacteria and food,

$$\frac{\partial n}{\partial t} = k\Delta n + \frac{1}{2}(1 + R_\alpha(p; R_\alpha^0))nF_1 + \frac{1}{2}(1 - R_\alpha(p; R_\alpha^0))nF_2, \tag{5.16a}$$

$$\frac{\mathrm{d}F_1}{\mathrm{d}t} = -\frac{1}{2}F_1 \int_{\underline{\alpha}}^{\overline{\alpha}} (1 + R_\alpha(p; R_\alpha^0))n \,\mathrm{d}\alpha, \tag{5.16b}$$

$$\frac{\mathrm{d}F_2}{\mathrm{d}t} = -\frac{1}{2}F_2 \int_{\underline{\alpha}}^{\overline{\alpha}} (1 - R_\alpha(p; R_\alpha^0))n \,\mathrm{d}\alpha. \tag{5.16c}$$

Here all the non-ideal relays have the same input $p = E - E_T$ where $E = F_1/(F_1 + F_2)$ which is the current proportion of the nutrient F_1 in the total supply of nutrients, $E_T = 0.5$ as before; the state $R_\alpha(p; R_\alpha^0)$ of the non-ideal relay R_α is a binary function of time; R_α^0 denotes the initial state of this relay; k is the rate at which the diffusion of the thresholds in the birth process occurs; $\frac{1}{2}(1 + R_\alpha)F_1 n$ is the growth rate for bacteria in the state 1; and, $\frac{1}{2}(1 - R_\alpha)F_2 n$ is the growth rate for bacteria in the state -1. Both growth rates are proportional to the population density with the coefficient of proportionality scaled to unity. The rate of consumption of food in the equation for $F_i = F_i(t)$ is proportional to the total number of bacteria in the phenotype eating this type of food, hence the integral (the coefficient of proportionality is also set to unity for simplicity); $\underline{\alpha}$ and $\overline{\alpha}$ are the lower and upper bounds on available threshold values, respectively. A certain amount of food is available at the initial moment; the food is not supplied after that moment. The assumption is made that bacteria do not die but stop

growing when all the food has been consumed.

In model (5.16), it is assumed that for a given α all the bacteria with this α value are in the same state at a particular time moment. That is, $n(t, \alpha)$ is the total population of bacteria with the threshold α at the moment t and they are all in the same state. It means that when a bacterium with a threshold α' sporadically changes its threshold to a different value α, it simultaneously copies the state from other bacteria which have the threshold α. In particular, this may require a bacterium to change the state when its threshold changes.

To complete the model, the α values of bacteria are restricted to a selected region $\underline{\alpha} \leq \alpha \leq \overline{\alpha}$ and so apply the Neumann boundary conditions

$$\frac{\partial n}{\partial \alpha} = 0, \quad \alpha = \underline{\alpha}, \overline{\alpha}$$

to system (5.16). Replacing the variables F_1, F_2 with the new variables $F = F_1 + F_2$, the total food, and $p = E - E_T = F_1/(F_1 + F_2) - 0.5$, the deviation of the fraction of the food F_1 from 0.5,

$$\begin{aligned}
\frac{\mathrm{d}F}{\mathrm{d}t} &= \frac{\mathrm{d}F_1}{\mathrm{d}t} + \frac{\mathrm{d}F_2}{\mathrm{d}t} \\
&= -\frac{1}{2}F_1 \int_{\underline{\alpha}}^{\overline{\alpha}} (1 + R_\alpha(p; R_\alpha^0)) n \mathrm{d}\alpha - \frac{1}{2}F_2 \int_{\underline{\alpha}}^{\overline{\alpha}} (1 - R_\alpha(p; R_\alpha^0)) n \mathrm{d}\alpha \\
&= -\frac{1}{2}(F_1 + F_2) \int_{\underline{\alpha}}^{\overline{\alpha}} n \mathrm{d}\alpha - \frac{1}{2}(F_1 - F_2) \int_{\underline{\alpha}}^{\overline{\alpha}} n R_\alpha(p; R_\alpha^0) \mathrm{d}\alpha \\
\frac{\mathrm{d}F}{\mathrm{d}t} &= -\frac{1}{2}F \int_{\underline{\alpha}}^{\overline{\alpha}} n \mathrm{d}\alpha - pF \int_{\underline{\alpha}}^{\overline{\alpha}} n R_\alpha(p; R_\alpha^0) \mathrm{d}\alpha
\end{aligned}$$

$$\begin{aligned}
\frac{\mathrm{d}p}{\mathrm{d}t} &= \frac{1}{F_1 + F_2}\frac{\mathrm{d}F_1}{\mathrm{d}t} - \frac{F_1}{(F_1 + F_2)^2}\left(\frac{\mathrm{d}F_1}{\mathrm{d}t} + \frac{\mathrm{d}F_2}{\mathrm{d}t}\right) \\
&= -\frac{F_1}{2F} \int_{\underline{\alpha}}^{\overline{\alpha}} n(1 + R_\alpha(p; R_\alpha^0)) \mathrm{d}\alpha + \frac{F_1}{2F} \int_{\underline{\alpha}}^{\overline{\alpha}} n \mathrm{d}\alpha + \frac{pF_1}{F} \int_{\underline{\alpha}}^{\overline{\alpha}} n R_\alpha(p; R_\alpha^0) \mathrm{d}\alpha \\
&= \frac{F_1}{F}\left(p - \frac{1}{2}\right) \int_{\underline{\alpha}}^{\overline{\alpha}} n R_\alpha(p; R_\alpha^0) \mathrm{d}\alpha \\
&= \left(p + \frac{1}{2}\right)\left(p - \frac{1}{2}\right) \int_{\underline{\alpha}}^{\overline{\alpha}} n R_\alpha(p; R_\alpha^0) \mathrm{d}\alpha \\
\frac{\mathrm{d}p}{\mathrm{d}t} &= \left(p^2 - \frac{1}{4}\right) \int_{\underline{\alpha}}^{\overline{\alpha}} n R_\alpha(p; R_\alpha^0) \mathrm{d}\alpha
\end{aligned}$$

Which gives the following system which is equivalent to the system (5.16)

$$\frac{\partial n}{\partial t} = k\Delta n + \frac{1}{2}Fn + pFnR_\alpha(p; R^0_\alpha), \tag{5.17a}$$

$$\frac{\mathrm{d}F}{\mathrm{d}t} = -\frac{1}{2}F\int_{\underline{\alpha}}^{\overline{\alpha}} n\,\mathrm{d}\alpha - pF\int_{\underline{\alpha}}^{\overline{\alpha}} nR_\alpha(p; R^0_\alpha)\,\mathrm{d}\alpha, \tag{5.17b}$$

$$\frac{\mathrm{d}p}{\mathrm{d}t} = (p^2 - \frac{1}{4})\int_{\underline{\alpha}}^{\overline{\alpha}} nR_\alpha(p; R^0_\alpha)\,\mathrm{d}\alpha. \tag{5.17c}$$

The last integral in the second equation and the integral term in the last equation are the Preisach operator with the input $p = p(t)$ and the time dependent density function $n(t, \alpha)$ concentrated on the bisector $\beta = -\alpha$ of the Preisach half-plane, Chapter 2.

5.6.2 Results for the multi-species model

The distribution of phenotypes for different threshold values after long time simulation of system (5.17) is shown in Figures 5.12 and 5.13. In each simulation, the distribution, which at any point in time is a binary function of α, stabilises to some stationary limit profile. Initially, all the non-ideal relays were set to be in the state $R^0_\alpha = 1$, $\underline{\alpha} \le \alpha \le \overline{\alpha}$. The initial population density $n(0, \alpha)$ was set to a non-zero value at the point $\alpha = \overline{\alpha}$ and to zero in all the other nodes of the α-mesh; that is, all the population initially consisted of bacteria with the largest threshold. The food supply was equally distributed between the food types F_1 and F_2, that is the initial value of p was $p(0) = 0$.

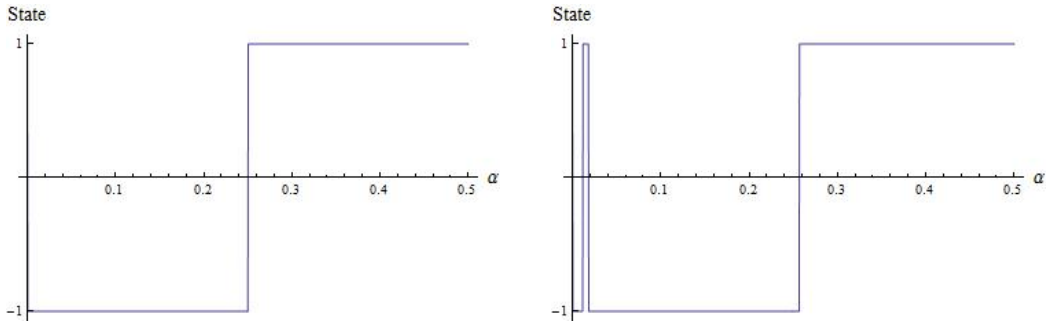

(a) The initial food supply $F(0) = 10$ and the diffusion rate $k = 0.1$.

(b) The initial food supply $F(0) = 100$ and the diffusion rate $k = 0.1$.

Figure 5.12: Stationary limit distribution of the states of the relays after long time simulation of the system (5.17) in case of faster diffusion. The range of available thresholds is $[\underline{\alpha}, \overline{\alpha}] = [0, 0.5]$.

By comparing Figures 5.12a and 5.13a, it is shown that with the decrease of the

diffusion rate, k, the limit distribution takes on a different form. In the case of faster diffusion between populations with different α, the phenotypes split equally into two regions, those in the region $0 \leq \alpha \leq 0.25$ are in the state -1 and those in the region $0.25 < \alpha \leq 0.5$ are in the state 1. In the case of slower diffusion, observation is made of a more oscillatory pattern in the limit distribution. In both cases, the density n converges to the same constant value.

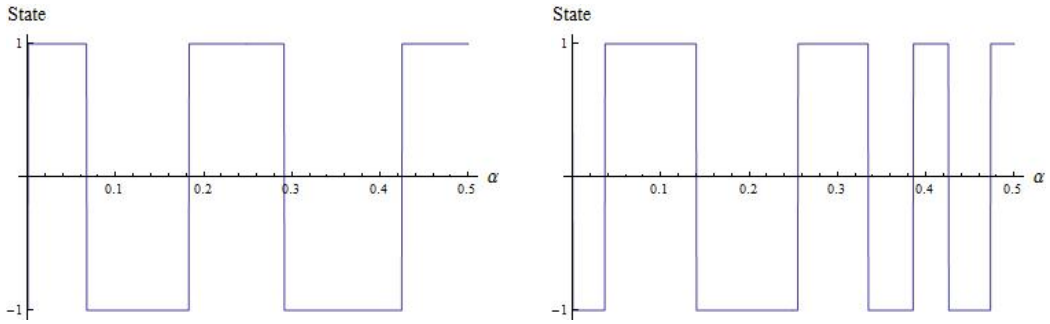

(a) The initial food supply $F(0) = 10$ and the diffusion rate $k = 0.001$.

(b) The initial food supply $F(0) = 100$ and the diffusion rate $k = 0.001$.

Figure 5.13: Stationary limit distribution of the states of the relays after long time simulation of the system (5.17) in case of slower diffusion. The range of available thresholds is $[\underline{\alpha}, \overline{\alpha}] = [0, 0.5]$.

Figures 5.12b and 5.13b show the changes in the distribution caused by increasing the initial food supply. Increasing the initial food supply increases the number of oscillations in the distribution of the relays. Decreasing the diffusion rate has a greater effect on causing the distribution to take on an oscillatory pattern.

5.7 Conclusions

In this chapter a model for two phenotype bacteria with a cost for transitioning between phenotypes was developed and the model shows that, in an environment that varies stochastically, the average growth rate of the system could be maximised by the bacteria delaying the phenotype switching until there was a stronger favouring of the other phenotype. Dynamics of the optimal system can be interpreted as a kind of a probabilistic memory switch, or relay, driven by a varying input (environment). The standard deterministic non-ideal relay R_α switches from state -1 to state 1 when the input reaches the threshold value α, and switches back when the input achieves the value $-\alpha$; transitions in both directions are instantaneous. Define the switching rules for the probabilistic relay as follows: The relay does not switch from state -1 to state 1 as long as the input

satisfies $p < \alpha$. When $p \geq \alpha$, assume a positive transition probability rate κ for transitioning from -1 to 1 (that is, the exponential distribution of the resident time in state -1 before switching, as in the Poisson process). Similarly, there is no switching from state 1 to -1 as long as $p > -\alpha$; and, the transition probability rate $\kappa > 0$ when $p \leq -\alpha$.

Model (5.12), also has intermediate states, so that when the relay departs from state -1 (or, 1), it spends a period of time in the intermediate state before arriving in state 1 (state -1, respectively). A similar behaviour of the probabilistic relay can be achieved by adding two intermediate states A and B; assuming the transition probability rate $\kappa > 0$ from state -1 to A when $p \geq \alpha$ and zero probability rate from -1 to A for $p < \alpha$; assuming a positive probability rate δ_1 from A to 1 (independent of the value of p); and, similarly, assuming the transition probability rate κ from state 1 to B when $p \leq -\alpha$, zero probability rate from 1 to B for $p > -\alpha$, and a positive probability rate δ_2 from B to -1 independent of p. With this modification, the evolution of the probabilities to find the probabilistic non-ideal relay in states $-1, 1, A, B$ is described by deterministic equations similar to (5.12).

The above dynamics, which are achieved in model (5.12) for positive α, can maximise the growth rate of the population of bacteria in a stochastic environment if the typical time that bacteria spend in the intermediate states is comparable to the characteristic time of the input variation. A positive delay α prevents transitions from the less favoured phenotype to the more favoured phenotype when the favouring is not strong. A slight decrease in the growth rate due to small fluctuations of the environment from the point E_T can be less dramatic than a drop in the growth rate due to passing through the intermediate states where bacteria do not reproduce. This trade off between large responsiveness (small α), with the associated cost of often transitions between phenotypes, and large inertia (large α), which leaves too many bacteria in unfavoured states, shifts α_{opt} to the positive range provided that the time bacteria have to spend in the intermediate states is significant.

If transitions between the states are fast compared to the time scale of input variations (large κ and δ), then dynamics of system (5.12) can be approximated by the deterministic non-ideal relay R_α. For example, this is the case for a population of bacteria which are best fit to some stochastic environmental input with $\alpha \approx \alpha_{opt}$ in model (5.12), and then change the input to a much slower, less variable, or more predictable environment (such as, for instance, in a lab).

In the new environment E_{slow}, nearly all the population, at almost any given instant on the slow time scale, will have the same phenotype; transitions between the phenotypes will be almost instantaneous; and, switching between the two phenotypes will be described by the deterministic non-ideal relay R_α with the input E_{slow}; that is, the system will demonstrate persistent bistable (hysteretic) memory.

Assuming this simpler switching regime, consideration was given to a reaction-diffusion model of multiple populations of bacteria competing for food. The switching rules for each population were modelled by the deterministic relay R_α; the populations were parameterised by the thresholds α varying over an interval of values. In the model, a finite amount of food is available, bacteria stop growing but do not die when all the food has been consumed, and the population density $n(t, \alpha)$ tends to a positive constant as t increases. It was shown numerically that a binary function describing the distribution of two phenotypes among bacteria with different α also converges to a stationary pattern. However, this sign changing pattern is different for different initial data. The limit stationary pattern becomes more oscillatory with the increase of the initial food supply. The limit pattern is sensitive to the diffusion rate between species with different thresholds. Lowering the diffusion rate leads to more patterns with a greater number of oscillations.

It would be interesting to consider variations of the multi-species model (5.17) and their effect on the attractor and the pattern formation. Possible modifications might account for the death process and constant or variable food supply; testing the model with no diffusion process; the inclusion of relays $R_{\alpha,\beta}$ with asymmetric thresholds α, β, $\beta \neq -\alpha$; variations of the boundary conditions; replacing each deterministic relay with the differential model (5.12); or, modelling populations by a collection of probabilistic memory switches using stochastic differential equations. Systems of reaction-diffusion equations coupled to ordinary differential equations with bistable dynamics have been used in [113,114] to model the formation of spatial patterns observed experimentally in a culture of bacteria grown in a Petri dish. An important assumption made in multi-species model (5.17) was that bacteria, when sporadically changing their threshold α' to a new value α, simultaneously copy the state from their peers who have the same threshold α. It would be natural to explore a model where the state remains unchanged when the threshold changes. Such a model should have simultaneous nonzero populations of bacteria with the same threshold in two phenotypes. This is a subject of future work.

The nonlocal terms introduced by the integral $\int_{\underline{\alpha}}^{\overline{\alpha}} nR_\alpha(p; R^0_\alpha)\,\mathrm{d}\alpha$ in equations (5.17) is the Preisach operator with the input p and the time dependent density function $n(t, \alpha)$. The evolution of the Preisach density function is coupled to the evolution of other variables in the system. This contrasts to all the variety of known applications of the Preisach operator model, where one needs to know the Preisach density function *a priori* in order to parameterise the model [68]. Identification of the Preisach density function is a daunting task requiring multiple experiments in applied physics and engineering [11]; measurements of the density function in applications to economics and finance are even less accessible. In model (5.17) and its modifications, the profile of the density function at any moment is defined by its initial profile $n(0, \alpha)$. However, if one is interested in long term behaviour, then no (or, little) information about the initial profile is needed provided that the attractor has a simple structure. That is, in this case, one does not need to solve the problem of identification of the Preisach operator density function.

Chapter 6

Conclusion

In the areas of economics and terrestrial hydrology many deterministic models containing a hysteresis operator have been developed. The drawback of these models is that they do not include any of the stochastic nature present in these areas. The first focus of the work in this thesis was to develop tools in order to have a means of examining numerically possible stochastic counterparts to the deterministic models in these areas. The intention of this work was to develop a numerical scheme for a class of stochastic differential equations where the time derivative of the output of the Preisach operator is included.

This class of stochastic differential equations was proposed as a prototype model for these areas in order to act as a stochastic counterpart to deterministic models which have been previously proposed for the areas of economics, finance, terrestrial hydrology and biology. The initial aim was to develop numerical schemes which were similar to the numerical schemes that have been developed for dealing with ordinary differential equations where the time derivative of the Preisach operator appears.

Towards that goal Chapter 3 presented work where two Euler based numerical schemes were developed for solving stochastic differential equations which contain the time derivative of the Preisach operator. A price dynamics model was presented as a motivation for the development of numerical schemes of this type. This model considers a group of traders, who have two different thresholds for buying and selling an asset. That is each trader behaves as a non-ideal relay. Each trader has a different level of effect on the opinion towards the market, so the overall effect of the traders on the market can be modelled by the Preisach operator. In this model the Preisach operator term introduces a negative feedback

loop on the price dynamics.

The two numerical schemes presented in Chapter 3 differ in the way that they calculate the change in the output of the Preisach operator between two consecutive time steps. The first scheme, called the rectangular method, uses a rectangular approximation of the change in the output of the Preisach operator in a manner similar to the numerical scheme for deterministic differential equations presented in [48]. The other numerical scheme, called the triangular method, uses an exact measure of the change in the output for its calculations.

These schemes were shown numerically to converge as the time step used for the calculations was decreased and the same realisation of the Wiener process was used. Comparison between numerical simulations of the developed price dynamics model and a similar stochastic differential equation where the Preisach term had been excluded (where both simulations used the same realisation of the Wiener process) showed that the Preisach term acted as dampening effect on the price trajectory by limiting the size of jumps and crashes in the price. This effect was the expected outcome as the Preisach term added a source of negative feedback into the price which acts as a stabilising agent.

The triangular method was believed to be the more accurate of the two schemes when compared with the implementation of the rectangular method, as the rectangular method occasionally had larger jumps in response to turning points than the triangular method. As a result the triangular method was also subjected to other validation methods, the output of the scheme for a simple deterministic hydrology model was compared to the output for the same system given by the implementation of the numerical scheme from [48] used in [51]. There was good agreement between the two schemes for this model which suggests that the triangular method could also be useful in the solution of deterministic equations. The probability distribution of the first link of the Preisach staircase greater than a given ϵ for the inverse Preisach operator after long-time input by the Wiener process was compared to the results obtained by numerical implementation of the triangular method, a reasonable agreement between the analytic expectation and the numerical results was obtained. These tests of the scheme showed it to be an effective means of generating numerical solutions of stochastic differential equations which contain the Preisach operator.

In Chapter 3 a second price dynamics model was also formulated. The difference between the two models was that the traders in the second model would continue to purchase the asset as long as they had the means to, i.e. the money or resources

necessary to buy the asset. The sum of all the traders influence on the market was modelled by the Prandtl-Ishlinskii operator. It was shown in Chapter 2 that the Preisach operator can be represented by the Prandtl-Ishlinskii operator, which means that both models contain the Preisach operator.

The main difference between the two models for asset price dynamics presented in Chapter 3 was that in the second model the hysteresis term introduces a positive feedback loop on the price instead of a negative feedback. This positive feedback loop should cause strong upward or downward trends in the price to have large jumps, similar to avalanche switching presented in [115]. This avalanche behaviour would require a significant modification of the presented numerical schemes in order to account for the correct size of the avalanches and presents an interesting area for future study.

In Chapter 4 an implementation of the triangular method numerical scheme developed in Chapter 3 is used to solve a system which consists of a deterministic differential equation where the time derivative of the Preisach operator appears coupled with an ordinary differential equation. This modification of the numerical scheme was made in order to test the scheme on higher order deterministic equations. The behaviour of numerical generated trajectories of this type of system were compared to known theoretical results relating to the behaviour of this type of system near an equilibrium of the system.

The theoretical results state that the trajectory of the system should behave in one of three ways when crossing the line $f = 0$, where $f = 0$ is the switching line where the input of the Preisach operator makes turning points, depending on certain parameters of the system. The numerical results produced by the implementation of the triangular method gave a good match to the theoretical result for each condition on the system. This result further confirms the accuracy of the triangular method for solving differential equations containing the time derivative of the Preisach operator. These coupled systems containing the Preisach operator were found to behave in a similar manner to systems where the Preisach operator was replaced by a singular perturbation. This similarity is due to the Preisach term near the line $f = 0$ being smaller than a given ϵ and growing as the trajectory moves away.

In recent years much work has been done on considering simple models of two phenotype bacteria. These models have been used to give some understanding as to how bi-stable states have developed in certain bacteria. Also of interest in bacteria of this type is what simple changes to the way or conditions by which

the bacteria switch between phenotypes would give an overall improvement to the growth of the colony as a whole. Thus the work in Chapter 5 addresses this question. In Chapter 5 a simple linear model for two phenotype bacteria was examined. This model was subjected to both stochastic and deterministic inputs.

In an expansion of work carried out in the literature this model was considered with a continuous input as opposed to a discrete input. A direct cost for transitions between the phenotypes was introduced into the model. The inclusion of this switching cost resulted in a change to the switching patterns of the bacteria that maximises the average growth rate of the system in a stochastically varying environment. This change was for the bacteria to delay switching phenotypes until the environment had a strong favouring of the other phenotype. If the bacteria switch phenotypes in this delayed manner then they behave in a similar manner to a non-ideal relay. This result shows for the first time that a hysteretic type behaviour in living organisms may appear and that it could provide a better fitness (measured by the average growth rate). This improved fitness for bacteria with hysteresis type memory could grant them an evolutionary advantage over memoryless bacteria in certain environmental conditions.

This concept was used to develop a model of a colony of bacteria which had a spread of different switching thresholds where all the bacteria behaved as symmetric non-ideal relays, that is the α threshold of the non-ideal relay is $\alpha = -\beta$. In this setting a reaction-diffusion element was used to model the spread of the bacteria between the different threshold values due to variability of the bacteria as part of the birth process. The system was found to have a limit distribution of the states of the relays after long-time simulation, this distribution was found to be sensitive to many parameters of the system, such as the initial availability of the food supply and rate of the diffusion between the switching thresholds.

This area has many possibilities for further work. In the single switching threshold setting of interest would be the effect of non-symmetric switching thresholds as well as a more detailed study of the implications of the introduction of a switching rate into the unfavoured phenotype. There is a large scope of study that could be taken on the multi-threshold model as this work is only an initial examination of the subject.

Some of the content of this thesis has been presented at both the 5th International Workshop on Multi-Rate Processes and Hysteresis (MURPHYS 2010) in Pécs, Hungary and the 6th International Workshop on Multi-Rate Processes and Hysteresis (MURPHYS 2012) in Suceava, Romania. Appendix B contains a list

of the papers published in relation to the work carried out in this thesis.

Bibliography

[1] M. Brokate and J. Sprekels, *Hysteresis and phase transitions*, vol. 121 of *Applied Mathematical Sciences*. New York: Springer-Verlag, 1996.

[2] A. Visintin, *Differential models of hysteresis*, vol. 111 of *Applied Mathematical Sciences*. Berlin: Springer-Verlag, 1994.

[3] A. Pimenov, T. Kelly, A. Korobeinikov, M. O'Callaghan, A. Pokrovskii, and D. Rachinskii, "Memory effects in population dynamics: Spread of infectious disease as a case study," *Mathematical Modelling of Natural Phenomena*, vol. 7, pp. 204–226, 2012.

[4] M. Brokate, S. MacCarthy, A. Pimenov, A. Pokrovskii, and D. Rachinskii, "Modelling energy dissipation due to soil-moisture hysteresis," *Environmental Modeling & Assessment*, vol. 16, pp. 313–333, 2011.

[5] I. Mayergoyz, "Stochastic aspects of hysteresis," in *The Science of Hysteresis vol I* (I. Mayergoyz and G. Bertotti, eds.), pp. 529–604, Elsevier, Academic Press, 2006.

[6] M. Dimian and I. Mayergoyz, "Spectral noise density of the preisach model," *Magnetics, IEEE Transactions on*, vol. 40, pp. 2134–2136, July 2004.

[7] I. Mayergoyz, "Mathematical models of hysteresis," *Magnetics, IEEE Transactions on*, vol. 22, pp. 603 – 608, Sep 1986.

[8] R. Cross, "Mach, methodology, hysteresis and economics," *Journal of Physics: Conference Series*, vol. 138, no. 1, p. 012004, 2008.

[9] J. A. Ewing, "On the production of transient electric currents in iron and steel conductors by twisting them when magnetised or by magnetising them when twisted," *Proceedings of the Royal Society of London*, vol. 33, pp. 21–23, 1881.

[10] M. A. Krasnosel′skiĭ and A. V. Pokrovskiĭ, *Systems with hysteresis*. Berlin: Springer-Verlag, 1989. Translated from the Russian by Marek Niezgódka.

[11] I. D. Mayergoyz, *Mathematical models of hysteresis*. San Diego, CA: Elsevier, 2 ed., 2003.

[12] J. A. Ewing, "Experimental research in magnetism," *Philosophical Transactions of the Royal Society of London*, vol. 176, no. II, 1895.

[13] F. Preisach, "Über die magnetische nachwirkung," *Zeitschrift für Physik*, vol. 94, pp. 277–302, 1938.

[14] H. Cramer, "A moving preisach vector hysteresis model for magnetic recording media," *Journal of Magnetism and Magnetic Materials*, vol. 88, no. 1–2, pp. 194–204, 1990.

[15] S. Hui and J. Zhu, "Numerical modelling and simulation of hysteresis effects in magnetic cores using transmission-line modelling and the preisach theory," *Electric Power Applications, IEEE Proceedings* -, vol. 142, pp. 57–62, Jan 1995.

[16] A. Bergqvist and G. Engdahl, "A stress-dependent magnetic preisach hysteresis model," *Magnetics, IEEE Transactions on*, vol. 27, pp. 4796–4798, Nov 1991.

[17] D. Šumarac, B. Medjo, and N. Trišović, "Hysteretic behaviour modeling of elastoplastic materials," *Theoretical and Applied Mechanics*, vol. 35, no. 1-3, pp. 287–304, 2008.

[18] M. Brokate, K. Dreßler, and P. Krejčí, "Rainflow counting and energy dissipation for hysteresis models in elastoplasticity," *European Journal of Mechanics*, vol. 15, pp. 705–737, 1996.

[19] D. Sumarac and S. Stosic, "The preisach model for the cyclic bending of elato-plastic beams," *European Journal of Mechanics. A/Solids*, vol. 15, no. 1, pp. 155–172, 1996.

[20] P. Kordulová, "Hysteresis in flow through porous media," *Journal of Physics: Conference Series*, vol. 268, no. 1, p. 012014, 2011.

[21] J. P. O'Kane, "The fest model–a test bed for hysteresis in hydrology and soil physics," *Journal of Physics Conference Series*, vol. 22, pp. 148–163, 2005.

[22] B. Appelbe, D. Flynn, H. McNamara, P. O'Kane, A. Pimenov, A. Pokrovskii, D. Rachinskii, and A. Zhezherun, "Rate-independent hysteresis in terrestrial hydrology," *Control Systems,IEEE*, vol. 29, pp. 44–69, Feb. 2009.

[23] R. Cross, M. Grinfeld, and H. Lamba, "Hystersis and economics," *Control Systems,IEEE*, vol. 29, February 2009.

[24] H. A. McNamara and A. V. Pokrovskii, "Hysteresis in the trade cycle," *Physica B: Condensed Matter*, vol. 372, no. 1–2, pp. 202–206, 2006.

[25] R. Cross, H. McNamara, and A. Pokrovskii, "Modelling macroeconomic flows related to large ensembles of elementary exchange operations," *Physica B: Condensed Matter*, vol. 403, no. 2–3, pp. 451–455, 2008.

[26] D. Hughes and J. T. Wen, "Preisach modeling of piezoceramic and shape memory alloys," *Smart Mater. Struct.*, vol. 6, pp. 287–300, 1997.

[27] S. Doraiswamy, A. Rao, and A. R. Srinivasa, "Combining thermodynamic principles with preisach models for superelastic shape memory allo wires," *Smart Materials and Structures*, vol. 20, no. 8, p. 085032, 2011.

[28] K. K. Ahn and N. B. Kha, "Internal model control for shape memory alloy actuators using fuzzy based preisach model," *Sensors and Actuators A: Physical*, vol. 136, no. 2, pp. 730–741, 2007.

[29] M. Al Janaideh, S. Rakheja, and C.-Y. Su, "An analytical generalized Prandtl-Ishlinskii model inversion for hysteresis compensation in micropositioning control," *Mechatronics, IEEE/ASME Transactions on*, vol. 16, pp. 734 –744, Aug. 2011.

[30] A. El-Shaer, M. Janaideh, P. Krejci, and M. Tomizuka, "Robust performance enhancement using disturbance observers for hysteresis compensation based on generalized prandtl-ishlinskii model," in *American Control Conference (ACC), 2012*, pp. 1664 –1669, June 2012.

[31] P. Krejčí, "On maxwell equations with the preisach hysteresis operator: The one-dimensional time-periodic case," *Aplikace matematiky*, vol. 34, no. 5, pp. 364 –374, 1989.

[32] M. Eleuteri, J. Kopfová, and P. Krejčí, "Magnetohydrodynamic flow with hysteresis," *SIAM J. Math. Anal.*, vol. 41, no. 2, pp. 435–464, 2009.

[33] D. Flynn, *Modelling the flow of water through multiphase porous media with the Preisach operator*. PhD thesis, Dept. Civil & Environmental Engineering & Dept. Applied Mathematics, University College Cork, Ireland, 2010.

[34] D. Flynn, H. McNamara, P. O'Kane, and A. Pokrovskii, "Application of the preisach model to soil-moisture hysteresis," in *The Science of Hysteresis vol III* (I. Mayergoyz and G. Bertotti, eds.), pp. 689–744, Elsevier, Academic Press, 2006.

[35] I. D. Mayergoyz and C. E. Korman, "Preisach model with stochastic input as a model for viscosity," *Journal of Applied Physics*, vol. 69, no. 4, pp. 2128–2134, 1991.

[36] P. Rugkwamsook, C. E. Korman, G. Bertotti, and M. Pasquale, "Dependence of aftereffect on magnetization history," *Journal of Applied Physics*, vol. 85, no. 8, pp. 4361–4363, 1999.

[37] I. Mayergoyz, A. Adly, M. Huang, and C. Krafft, "Scaling and data collapse in magnetic viscosity (creep) of superconductors," *Magnetics, IEEE Transactions on*, vol. 36, pp. 3208 –3210, Sep 2000.

[38] M. Dimian, E. Coca, and V. Popa, "Analytical and experimental analysis of noise passage through hysteretic systems," *Journal of Applied Physics*, vol. 105, no. 7, p. 07D515, 2009.

[39] M. Dimian, A. Adedoyin, A. Gindulescu, and P. Andrei, "Modeling and simulation of noise induced phenomena in complex hysteretic systems," *Magnetics, IEEE Transactions on*, vol. 45, pp. 5231 –5234, Nov. 2009.

[40] P. D. Spanos, P. Cacciola, and J. Redhorse, "Random vibration of sma systems via preisach formalism," *Nonlinear Dynamics*, vol. 36, pp. 405–419, 2004.

[41] I. Rychlik and S. Gupta, "Rain-flow fatigue damage for transformed gaussian loads," *International Journal of Fatigue*, vol. 29, no. 3, pp. 406 – 420, 2007.

[42] H. Lamba and T. Seaman, "Market statistics of a psychology-based heterogeneous agent model," *International Journal of Theoretical & Applied Finance*, vol. 11, no. 7, pp. 717–737, 2008.

[43] R. Cross, M. Grinfeld, H. Lamba, and T. Seaman, "Stylized facts from a threshold-based heterogeneous agent model," *The European Physical Journal B - Condensed Matter and Complex Systems*, vol. 57, pp. 213–218, 2007.

[44] R. Cross, M. Grinfeld, H. Lamba, and T. Seaman, "A threshold model of investor psychology," *Physica A: Statistical Mechanics and its Applications*, vol. 354, pp. 463 – 478, 2005.

[45] H. Lamba and T. Seaman, "Rational expectations, psychology and inductive learning via moving thresholds," *Physica A: Statistical Mechanics and its Applications*, vol. 387, no. 15, pp. 3904 – 3909, 2008.

[46] H. Lamba, "A queueing theory description of fat-tailed price returns in imperfect financial markets," *The European Physical Journal B - Condensed Matter and Complex Systems*, vol. 77, pp. 297–304, 2010.

[47] J. A. D. Appleby and H. Wu, "Exponential growth and gaussian—like fluctuations of solutions of stochastic differential equations with maximum functionals," *Journal of Physics: Conference Series*, vol. 138, no. 1, p. 012002, 2008.

[48] D. Flynn and O. Rasskazov, "On the integration of an ode involving the derivative of a preisach nonlinearity," *Journal of Physics: Conference Series*, vol. 22, no. 1, p. 43, 2005.

[49] D. Flynn, J. P. O'Kane, and A. Zhezherun, "Numerical solution of odes involving the derivative of a preisach operator and with discontinuous rhs," *Journal of Physics: Conference Series*, vol. 55, no. 1, p. 63, 2006.

[50] D. Flynn, A. Zhezherun, A. Pokrovskii, and J. O'Kane, "Modeling discontinuous flow through porous media using odes with preisach operator," *Physica B: Condensed Matter*, vol. 403, no. 2–3, pp. 440–442, 2008.

[51] H. McNamara, *Development and analysis of macroeconomic models incorporating Preisach hysteresis*. PhD thesis, Dept. Applied Mathematics, University College Cork, Ireland, 2008.

[52] A. Amann, M. Brokate, D. Rachinskii, and G. Temnov, "Distribution of return point memory states for systems with stochastic inputs," *Journal of Physics: Conference Series*, vol. 268, no. 1, p. 012001, 2011.

[53] M. Göcke, "Various concepts of hysteresis applied in economics," *Journal of Economic Surveys*, vol. 16, no. 2, pp. 167–188, 2002.

[54] S. McCarthy and D. Rachinskii, "Dynamics of systems with preisach memory near equilibria," *Mathematica Bohemica*, accepted.

[55] A. Rezaei-Zare, M. Sanaye-Pasand, H. Mohseni, S. Farhangi, and R. Iravani, "Analysis of ferroresonance modes in power transformers using preisach-type hysteretic magnetizing inductance," *Power Delivery, IEEE Transactions on*, vol. 22, pp. 919 –929, April 2007.

[56] K. Kuhnen and P. Krejci, "Compensation of complex hysteresis and creep effects in piezoelectrically actuated systems—a new Preisach modeling approach," *IEEE Trans. Automat. Control*, vol. 54, no. 3, pp. 537–550, 2009.

[57] C. Visone, "Hysteresis modelling and compensation for smart sensors and actuators," *Journal of Physics: Conference Series*, vol. 138, no. 1, p. 012028, 2008.

[58] D. Davino, A. Giustiniani, and C. Visone, "Compensation and control of two-inputs systems with hysteresis," *Journal of Physics: Conference Series*, vol. 268, no. 1, p. 012005, 2011.

[59] R. V. Iyer, X. Tan, and P. S. Krishnaprasad, "Approximate inversion of the Preisach hysteresis operator with application to control of smart actuators," *IEEE Trans. Automat. Control*, vol. 50, no. 6, pp. 798–810, 2005.

[60] J. Cagnol, B. Miara, A. Mielke, and G. Stavroulakis, "State of the art, trends, and directions in smart systems 1," *http://www.wias-berlin.de/people/mielke/papers/stateoftheart.pdf*.

[61] A.-L. Bessoud and U. Stefanelli, "Magnetic shape memory alloys: three-dimensional modeling and analysis," *Math. Models Methods Appl. Sci.*, vol. 21, no. 5, pp. 1043–1069, 2011.

[62] M. Eleuteri, L. Lussardi, and U. Stefanelli, "A rate-independent model for permanent inelastic effects in shape memory materials," *Netw. Heterog. Media*, vol. 6, no. 1, pp. 145–165, 2011.

[63] K. A. Dahmen and Y. Ben-Zion, "Jerky motion in slowly driven magnetic and earthquake fault systems, physics of," in *Encyclopedia of Complexity and Systems Science* (R. A. Meyers, ed.), pp. 5021–5037, Springer, 2009.

[64] J. P. Sethna, K. A. Dahmen, and O. Perković, "Random-field Ising models of hysteresis.." Bertotti, Giorgio (ed.) et al., The science of hysteresis. Vol. II. Physical modeling, micromagnetics, and magnetization dynamics. Amsterdam: Elsevier/Academic Press. 107-179 (2006)., 2006.

[65] J. P. Gleeson, "High-accuracy approximation of binary-state dynamics on networks," *Phys. Rev. Lett.*, vol. 107, p. 068701, Aug 2011.

[66] D. Cellai, A. Lawlor, K. A. Dawson, and J. P. Gleeson, "Tricritical point in heterogeneous k-core percolation," *Phys. Rev. Lett.*, vol. 107, p. 175703, Oct 2011.

[67] A. Ivanyi, *Preisach Memorial Book*. Akademiai Kiado, 2005.

[68] G. Bertotti and I. D. Mayergoyz, eds., *The science of hysteresis.* Elsevier/Academic Press, Amsterdam, 2006.

[69] P. Krejčí, "Resonance in Preisach systems," *Appl. Math.*, vol. 45, no. 6, pp. 439–468, 2000.

[70] D. Ekanayake and R. Iyer, "Asymptotic behavior of a low-dimensional model for magnetostriction for periodic input," *Physica B: Condensed Matter*, vol. 403, no. 2–3, pp. 257–260, 2008.

[71] M. Brokate, A. Pokrovskii, D. Rachinskii, and O. Rasskazov, "Differential equations with hysteresis via a canonical example." Bertotti, Giorgio (ed.) et al., The science of hysteresis. Vol. I. Amsterdam: Elsevier/Academic Press. 125-291 (2006)., 2006.

[72] H. Lamba, M. Grinfeld, S. McKee, and R. Simpson, "Subharmonic ferroresonance in an lcr circuit with hysteresis," *Magnetics, IEEE Transactions on*, vol. 33, pp. 2495 –2500, Jul 1997.

[73] H. Lamba, S. McKee, and R. Simpson, "The effect of circuit parameters on ferroresonant solutions in an lcr circuit," *Journal of Physics A: Mathematical and General*, vol. 31, no. 34, p. 7065, 1998.

[74] B. Jayawardhana, H. Logemann, and E. P. Ryan, "Infinite-dimensional feedback systems: the circle criterion and input-to-state stability," *Commun. Inf. Syst.*, vol. 8, no. 4, pp. 413–414, 2008.

[75] P. Spanos, P. Cacciola, and G. Muscolino, "Stochastic averaging of preisach hysteretic systems," *Journal of Engineering Mechanics*, vol. 130, no. 11, pp. 1257–1267, 2004.

[76] Y. Wang, Z. Ying, and W. Zhu, "Nonlinear stochastic optimal control of preisach hysteretic systems," *Probabilistic Engineering Mechanics*, vol. 24, no. 3, pp. 255 – 264, 2009.

[77] D. Rachinskii, "Asymptotic stability of large-amplitude oscillations in systems with hysteresis," *NoDEA Nonlinear Differential Equations Appl.*, vol. 6, no. 3, pp. 267–288, 1999.

[78] M. Brokate, A. Pokrovskii, and D. Rachinskii, "Asymptotic stability of continuum sets of periodic solutions to systems with hysteresis," *J. Math. Anal. Appl.*, vol. 319, no. 1, pp. 94–109, 2006.

[79] B. Appelbe, D. Rachinskii, and A. Zhezherun, "Hopf bifurcation in a van der pol type oscillator with magnetic hysteresis," *Physica B: Condensed Matter*, vol. 403, no. 2–3, pp. 301–304, 2008.

[80] Z. Balanov, W. Krawcewicz, D. Rachinskii, and A. Zhezherun, "Hopf bifurcation in symmetric networks of coupled oscillators with hysteresis," *Journal of Dynamics and Differential Equations*, vol. 24, pp. 713–759, 2012.

[81] A. Krasnosel'skii and D. Rachinskii, "On a bifurcation governed by hystersis nonlinearity," *NoDEA. Nonlinear Differential Equations and Applications*, vol. 9, no. 1, pp. 93–115, 2002.

[82] J. O'Kane, "Hysteresis in hydrology," *Acta Geophys. Pol.*, vol. 53, no. 4, pp. 373–383, 2005.

[83] J. O'Kane, "The fest model - a test bed for hysteresis in hydrology and soil physics," *Journal of Physics: Conference Series*, vol. 22, no. 1, pp. 148–163, 2005.

[84] P. Krejci, J. O'Kane, A. Pokrovskii, and D. Rachinskii, "Properties of solutions to a class of differential models incorporating preisach hysteresis operator," *Physica D: Nonlinear Phenomena*, vol. 241, no. 22, pp. 2010–2028, 2012.

[85] P. Krejci, J. O'Kane, A. Pokrovskii, and D. Rachinskii, "Stability results for a soil model with singluar hysteretic hydrology," *Journal of Physics: Conference Series*, vol. 268, no. 1, p. 012016, 2011.

[86] J. O'Kane, "The hysteretic linear reservoir - a new preisach model," *Physica B: Condensed Matter*, vol. 372, no. 1-2, pp. 388–392, 2006.

[87] G. C. Sander, O. J. Glidewell, and J. Norbury, "Dynamic capillary pressure, hysteresis and gravity-driven fingering in porous media," *Journal of Physics: Conference Series*, vol. 138, no. 1, p. 012023, 2008.

[88] P. O'Kane, A. Pokrovskii, P. Krejci, and R. Haverkamp, "Hysteresis and terrestrial hydrology," *Geophysical Research Abstracts*, vol. 5, p. 6154, 2003.

[89] D. M. Wolf, L. Fontaine-Bodin, I. Bischofs, G. Price, J. Keasling, and A. P. Arkin, "Memory in microbes: Quantifying history-dependent behavior in a bacterium," *PLoS ONE*, vol. 3, p. e1700, 02 2008.

[90] D. Koshland, "A response regulator model in a simple sensory system," *Science*, vol. 196, no. 4294, pp. 1055–1063, 1977.

[91] B. Hallet, "Playing dr jekyll and mr hyde: combined mechanisms of phase variation in bacteria," *Current Opinion in Microbiology*, vol. 4, no. 5, pp. 570 – 581, 2001.

[92] N. J. Holden and D. L. Gally, "Switches, cross-talk and memory in escherichia coli adherence," *Journal of Medical Microbiology*, vol. 53, no. 7, pp. 585–593, 2004.

[93] D. Dubnau and R. Losick, "Bistability in bacteria," *Molecular Microbiology*, vol. 61, no. 3, pp. 564–572, 2006.

[94] O. A. Igoshin, C. W. Price, and M. A. Savageau, "Signalling network with a bistable hysteretic switch controls developmental activation of the σ^F transcription factor in bacillus subtilis," *Molecular Microbiology*, vol. 61, no. 1, pp. 165–184, 2006.

[95] D. M. Wolf and A. P. Arkin, "Motifs, modules and games in bacteria," *Current Opinion in Microbiology*, vol. 6, no. 2, pp. 125 – 134, 2003.

[96] A. Arkin, J. Ross, and H. H. McAdams, "Stochastic kinetic analysis of developmental pathway bifurcation in phage λ-infected escherichia coli cells," *Genetics*, vol. 149, no. 4, pp. 1633–1648, 1998.

[97] T. S. Ham, S. K. Lee, J. D. Keasling, and A. P. Arkin, "Design and construction of a double inversion recombination switch for heritable sequential genetic memory," *PLoS ONE*, vol. 3, p. e2815, 07 2008.

[98] A. Novick and M. Weiner, "Enzyme induction as an all-or-none phenomenon," *Proceedings of the National Academy of Sciences*, vol. 43, no. 7, pp. 553–566, 1957.

[99] J. E. F. Jr, "Self-perpetuating states in signal transduction: positive feedback, double-negative feedback and bistability," *Current Opinion in Cell Biology*, vol. 14, no. 2, pp. 140 – 148, 2002.

[100] S. R. Biggar and G. R. Crabtree, "Cell signaling can direct either binary or graded transcriptional responses.," *EMBO J*, vol. 20, no. 12, pp. 3167–76, 2001.

[101] M. Thattai and B. I. Shraiman, "Metabolic switching in the sugar phosphotransferase system of escherichia coli.," *Biophys J*, vol. 85, no. 2, pp. 744–54, 2003.

[102] H. Beaumont, J. Gallie, C. Kost, G. Ferguson, and P. Rainey, "Experimental evolution of bet hedging," *Nature*, vol. 462, pp. 90 – 93, 2009.

[103] M. Salathe, J. Van Cleve, and M. Feldman, "Evolution of stochastic rates in asymmetric fitness landscapes," *Genetics*, vol. 182, pp. 1159 – 1164, August 2009.

[104] P. Rainey, H. Beaumont, G. Ferguson, J. Gallie, C. Kost, E. Libby, and X. Zhang, "The evolutionary emergence of stochastic phenotype switching in bacteria," *Microbial Cell Factories*, vol. 10, no. Suppl 1, p. S14, 2011.

[105] B. Gaal, J. Pitchford, and A. Wood, "Exact results for the evolution of stochastic switching in variable asymmetric environments," *Genetics*, vol. 184, pp. 1113 – 1119, April 2010.

[106] M. Thattai and A. van Oudenaarden, "Stochastic gene expression in fluctuating environments," *Genetics*, vol. 167, no. 1, pp. 523–530, 2004.

[107] E. Kussell and S. Leibler, "Phenotypic diversity, population growth, and information in fluctuating environments," *Science*, vol. 309, no. 5743, pp. 2075–2078, 2005.

[108] S. M. Hoffer, H. V. Westerhoff, K. J. Hellingwerf, P. W. Postma, and J. Tommassen, "Autoamplification of a two-component regulatory system results in "learning" behavior.," *J Bacteriol*, vol. 183, no. 16, pp. 4914–7, 2001.

[109] R. J. Aumann and M. B. Maschler, *Repeated games with incomplete information*. Cambridge, MA: MIT Press, 1995. With the collaboration of Richard E. Stearns.

[110] M. Nowak and K. Sigmund, "A strategy of win-stay, lose-shift that outperforms tit-for-tat in the prisoner's dilemma game.," *Nature*, vol. 364, no. 6432, pp. 56–8, 1993.

[111] R. Axelrod and W. Hamilton, "The evolution of cooperation," *Science*, vol. 211, no. 4489, pp. 1390–1396, 1981.

[112] D. M. Wolf, V. V. Vazirani, and A. P. Arkin, "Diversity in times of adversity: probabilistic strategies in microbial survival games.," *J Theor Biol*, vol. 234, no. 2, pp. 227–53, 2005.

[113] C. Chiu, F. C. Hoppensteadt, and W. Jäger, "Analysis and computer simulation of accretion patterns in bacterial cultures," *Journal of Mathematical Biology*, vol. 32, pp. 841–855, 1994. 10.1007/BF00168801.

[114] C. Chiu and N. Walkington, "Analysis of hysteretic reaction-diffusion systems," *Quart. Appl. Math.*, vol. 56, no. 1, pp. 89–106, 1998.

[115] K. Dahmen and J. P. Sethna, "Hysteresis, avalanches, and disorder-induced critical scaling: A renormalization-group approach," *Phys. Rev. B*, vol. 53, pp. 14872–14905, Jun 1996.

Appendix A

Proofs of theorems used in Chapter 4

Presented here are the proofs of the Theorems 4.1-4.3 used in Chapter 4 for validating the triangular method numerical scheme developed in Chapter 3. In this appendix each Theorem is presented again followed by the proof of the Theorem. An additional Theorem relating to the behaviour of the derivative of $x(t)$ when crossing the line $f = 0$, the result of this Theorem is used in the proof the remaining Theorems.

A.1 Theorem A.1

Theorem A.1. *Assume that $f_y(0,0) \neq 0$. The set of the moments t_k when a trajectory of a solution $(x(t), y(t))$ of system (4.8) intersects the line $f = 0$ away from the origin consists (if non-empty) of isolated points. Each point t_k is a local extremum point of the component $x(t)$, which is strictly monotone to the left and right of t_k. The derivative of $x(t)$ has a jump at each point t_k: the left derivative $D_-x(t_k)$ is zero, while the right derivative is defined by the formula*

$$D_+x(t_k) = \frac{\operatorname{sign}(f_y g)}{2\mu_0}\left(f_x + \sqrt{(f_x)^2 + 4\mu_0|f_y g|}\right) \tag{A.1}$$

where f_x, f_y, g are evaluated at the point $(x(t_k), y(t_k))$ and $\mu_0 = \mu(x(t_k), x(t_k))$.

According to this theorem, any trajectory has a corner point when it crosses the line $f = 0$ away from the origin. It approaches and leaves the line $f = 0$

transversally passing to the other side of the line and changing the direction at the crossing point. A trajectory always approaches the line $f = 0$ vertically; for the intersections near the origin, it leaves the line $f = 0$ almost horizontally in case $f_x(0,0) > 0$, and almost parallel to the line $f = 0$ in case $f_x(0,0) < 0$.

Theorem A.1 implies that a trajectory of equation (4.8) either has at most finite number of intersections with the line $f = 0$ on any finite time interval and never reaches the origin or a trajectory reaches the zero equilibrium in finite time making infinitely many intersections with the line $f = 0$. In the latter case, the intersection moments $t_1 < t_2 < t_3 < \cdots < \infty$ converge to the moment when the trajectory reaches the origin.

A.1.1 Proof of Theorem A.1

Suppose a trajectory $(x(t), y(t))$ hits the line $f = 0$ at a moment $t = \tau$ at a point $(x_0, y_0) \neq 0$ close to the origin. Assume

$$f_y(x_0, y_0)g(x_0, y_0) > 0 \tag{A.2}$$

(the other case $f_y(x_0, y_0)g(x_0, y_0) < 0$ can be considered similarly). Consider

$$\frac{df(x(t), y(t))}{dt} = f_x(x(t), y(t))x'(t) + f_y(x(t), y(t))g(x(t), y(t)). \tag{A.3}$$

As on some time interval $\tau - \delta < t < \tau$ the component $x(t)$ is strictly monotone, x' is defined and satisfies $|x'(t)| < k|f(x(t), y(t))|$ with some $k > 0$ almost everywhere on $\tau - \delta/2 < t < \tau$. This inequality combined with (A.2), (A.3) and $f(x_0, y_0) = 0$ implies that $f(x(t), y(t))$ strictly increases on a sufficiently small time interval $(\tau - \varepsilon, \tau]$, hence $f(x_0, y_0) = 0$ implies $f(x(t), y(t)) < 0$ for $t \in (\tau - \varepsilon, \tau)$. If we assume that $f(x(t), y(t)) \leq 0$ also on some time interval $(\tau, \tau + \delta_1)$ after the moment τ, then, similarly, $df(x(t), y(t))/dt > 0$ almost everywhere on a sufficiently small time interval $(\tau - \varepsilon, \tau + \varepsilon)$, hence $f(x(t), y(t)) > 0$ for $t > \tau$, i.e., we arrive at a contradiction. Therefore, there are moments $\theta > \tau$ arbitrarily close to τ such that $f(x(\theta), y(\theta)) > 0$. Moreover, if θ is such a moment and if we assume that $f(x(t), y(t)) > 0$ on a time interval $[\theta, \theta_1)$ with $f(x(\theta_1), y(\theta_1)) = 0$, while the trajectory does not leave some sufficiently small neighbourhood of the point (x_0, y_0) during this time interval, then (A.3) implies that $df(x(t), y(t))/dt > 0$ almost everywhere on some interval $t \in (\theta_1 - \delta, \theta_1) \subset (\theta, \theta_1)$, which implies $f(x(t), y(t)) < f(x(\theta_1), y(\theta_1)) = 0$ on

$(\theta_1 - \delta, \theta_1)$ and thus makes a contradiction with the assumption $f(x(t), y(t)) > 0$ on the whole interval $[\theta, \theta_1)$. This contradiction shows that if $f(x(\theta), y(\theta)) > 0$ for a $\theta > \tau$ sufficiently close to τ, then $f(x(t), y(t)) > 0$ for $t > \theta$ as long as the trajectory is sufficiently close to (x_0, y_0). As such θ exist arbitrarily close to τ, we conclude that $f(x(t), y(t)) > 0$ on some time interval $(\tau, \tau + \varepsilon)$.

The relations $f(x(t), y(t)) < 0$ on $t \in (\tau - \varepsilon, \tau)$ and $f(x(t), y(t)) > 0$ on $(\tau, \tau + \varepsilon)$ imply that the intersection point τ of the trajectory with the line $f = 0$ is isolated and that τ is a minimum point of the component $x(t)$, which strictly decreases to the left of τ and strictly increases to the right of τ.

It remains to prove formulas $D_- x(\tau) = 0$ and (A.1) at $t_k = \tau$. The first one follows from the relations $f(x_0, y_0) = 0$, $L(x(t)) > 0$ where $L(x)$ is the coefficient (4.13) in the ordinary differential system (4.12) which is equivalent to system (4.8) on the time interval $\tau - \varepsilon < t < \tau$. To prove the second formula, note that $x(t)$ is absolutely continuous for $t \geq \tau$. (Indeed, consider the function $z(x) = \int_{x(\tau)}^{x} L(s)\, ds$; the first equation of system (4.12) implies $z' = f(x(z), y)$, hence $z(t)$ is continuously differentiable for $t \geq \tau$ and $x(t) = x(z)(t)$ is continuously differentiable for $t > \tau$ and absolutely continuous for $t \geq \tau$). Therefore, $x(t) - x(\tau) = \int_\tau^t x'(\theta)\, d\theta$. Set $\Delta x = x(t) - x(\tau)$, $\Delta y = y(t) - y(\tau)$, $\Delta t = t - \tau$. Assume $\Delta x \geq k \Delta t$ with $k > 0$, then relations

$$x' = \frac{1}{\mu_0 + o(1)} \left(f_x + \frac{f_y \Delta y}{\Delta x} + o(1) \frac{|\Delta y| + \Delta x}{\Delta x} \right) \quad \text{as} \quad \Delta t \to 0+$$

and $\Delta y = g \Delta t + o(\Delta t)$ with $f_x = f_x(x_0, y_0)$, $f_y = f_y(x_0, y_0)$, $g = g(x_0, y_0)$ imply

$$x' = \frac{1}{\mu_0} \left(f_x + \frac{f_y g}{k} + o(1) \right);$$

here $o(1)$ is a small quantity which vanishes at the point (x_0, y_0). The expression in the right hand side is less than k for sufficiently small Δt provided that $k > k_+$, where k_+ is the positive root of the quadratic equation $\mu_0 k^2 - f_x k - f_y g = 0$. Hence,

$$\Delta x(t) \geq k \Delta t > k_+ \Delta t \quad \Rightarrow \quad x'(t) < k \tag{A.4}$$

for small enough $\Delta t > 0$. Similarly,

$$\Delta x(t) \leq k \Delta t < k_+ \Delta t \quad \Rightarrow \quad x'(t) > k. \tag{A.5}$$

If $\Delta x(t) > k \Delta t > k_+ \Delta t$ and $t_1 \in [\tau, t]$ is the latest moment such that $\Delta x(t_1) =$

$k\Delta t_1$, then integrating the inequality $x'(t) < k$ over the segment $[t_1, t]$, we obtain $x(t) - x(t_1) < k(t - t_1)$ which contradicts $x(t) - x(t_1) = \Delta x(t) - \Delta x(t_1) > k\Delta t - k\Delta t_1 = k(t - t_1)$. Hence, given any $k > k_+$, (A.4) implies $\Delta x(t) \leq k\Delta t$ for all sufficiently small $\Delta t > 0$. Similarly, given a $k < k_+$, (A.5) implies $\Delta x(t) \geq k\Delta t$. Hence, $D_+x(\tau) = k_+$ and the proof is complete.

A.2 Theorem 4.1

Theorem 4.1. *Let $f_x(0,0) > 0$. There is a function $\varphi = \varphi(\delta)$ satisfying $0 < \varphi(\delta) < \delta$ such that if, at some moment τ, a trajectory of system (4.8) hits the line $f = 0$ at a point (x, y) with $0 < |x| < \varphi(\delta)$ for a sufficiently small δ, then the trajectory escapes the strip $|x| < \delta$. The x-component of the trajectory is strictly monotone between the moment τ and the moment $\tau_e > \tau$ when the trajectory first hits one of the lines $x = \pm\delta$ (hence, the trajectory does not intersect the line $f = 0$ for $\tau < t < \tau_e$). Moreover, there is a function $\phi = \phi(\delta) > 0$ satisfying $\phi(\delta) \to 0$ as $\delta \to 0$ such that $|dy/dx| < \phi(\delta)$ for $\tau < t < \tau_e$ as long as $0 < |x| < \varphi(\delta)$.*

A.2.1 Proof of Theorem 4.1

The notation of Subsection A.1.1 will be used here. Given any small $\varepsilon, \nu > 0$, we can choose a $\delta > 0$ such that $|g(x, y)| < \varepsilon$ in rectangle $K = \{|x| \leq \delta, |y| \leq \delta + 2\delta\nu\}$. Assume that a trajectory $(x(t), y(t))$ hits the line $f = 0$ at a moment $t = \tau$ at a point $(x_0, y_0) \neq 0$ inside the rectangle $|x| < \delta, |y| < \delta$. To be definite, assume $x(t)$ strictly increases on an interval $[\tau, \tau_1)$ (the case when $x(t)$ strictly decreases after the moment τ is similar). According to (A.1),

$$D_+x(\tau) = f_x(0,0)/\mu_0 + o(1) > 0 \quad \text{as} \quad \delta \to 0,$$

while $|y'(\tau)| = |g(x_0, y_0)| < \varepsilon$, hence choosing $\nu = 2\varepsilon\mu_0/f_x(0,0)$ and making $\delta > 0$ sufficiently small ensures that the trajectory enters the angle $A = \{|y - y_0| < \nu(x - x_0)\}$. Also, the smallness of ν ensures that the set $A \cap K$, which is at the same time the intersection of the angle A with the vertical strip $|x| \leq \delta$, does not intersect the line $f = 0$. Hence, as long as the trajectory belongs to $A \cap K$, the function x increases and satisfies

$$\Delta x \mu x' = L(x)x' = f(x(t), y(t)) = f_x\Delta x + f_y\Delta y \tag{A.6}$$

where f_x, f_y are evaluated at some intermediate points in A and $\mu(x,\xi)$ is evaluated at an intermediate point of the segment $|\xi| \le \delta$. Therefore, taking into account that $|\Delta y/\Delta x| < \nu$ due to $(x,y) \in A$,

$$x' = \frac{f_x(0,0)}{\mu_0} + \frac{f_y(0,0)\Delta y}{\mu_0 \Delta x} + o(1) > \frac{f_x(0,0)}{\mu_0} - \frac{\nu |f_y(0,0)|}{\mu_0} + o(1) \qquad \text{(A.7)}$$

with the small term vanishing as $\delta \to 0$. As $\nu > \varepsilon\mu_0/(f_x(0,0) - \nu|f_y(0,0)|)$ for small ε, relation (A.7) combined with $|y'| < \varepsilon$ for $(x,y) \in K$ implies $|dy/dx| < \nu$. Thus, $|dy/dx| < \nu$ as long as the trajectory is inside the intersection of A with the vertical strip $|x| \le \delta$ and conclude that the trajectory is included in A until it hits the line $x = \delta$, which proves the Theorem.

A.3 Theorem 4.2

Theorem 4.2. *Let $f_x(0,0) < 0$, $j_0 < 0$ and $f_y(0,0) \neq 0$. There is a function $\varphi = \varphi(\delta)$ satisfying $0 < \varphi(\delta) < \delta$ such that if, at some moment τ, a trajectory of system (4.8) hits the line $f = 0$ at a point (x,y) with $0 < |x| < \varphi(\delta)$ for a sufficiently small δ, then the trajectory escapes the strip $|x| < \delta$. The x-component of the trajectory is strictly monotone between the moment τ and the moment $\tau_e > \tau$ when the trajectory first hits one of the lines $x = \pm\delta$ (hence, the trajectory does not intersect the line $f = 0$ for $\tau < t < \tau_e$). Moreover, there is a function $\phi = \phi(\delta) > 0$ satisfying $\phi(\delta) \to 0$ as $\delta \to 0$ such that a trajectory lies in the angle $|f_x(0,0)x + f_y(0,0)y| < \phi(\delta)|x|$ for $\tau < t < \tau_e$ whenever it hits the line $f = 0$ at a point (x,y) with $0 < |x| < \varphi(\delta)$.*

A.3.1 Proof of Theorem 4.2

Again use the notation of Subsection A.1.1, but assume that $f_x(0,0) < 0$, $j_0 < 0$. To be definite, assume again that $x(t)$ strictly increases on some interval $[\tau, \tau_1)$ after the trajectory $(x(t), y(t))$ hits the line $f = 0$ at a point (x_0, y_0) at the moment τ, *i.e.* $f_y(x_0,y_0)g(x_0,y_0) > 0$ in formula (A.1) and, by continuity, $f_y(0,0)g(x_0,y_0) > 0$. Relations $f(x_0,y_0) = f(0,0) = g(0,0) = 0$ imply $f_x(0,0)x_0 + f_y(0,0)y_0 = o(x_0)$ and

$$g(x_0,y_0) = g_x(0,0)x_0 + g_y(0,0)y_0 + o(x_0) = -\frac{j_0 x_0}{f_y(0,0)} + o(x_0), \qquad \text{(A.8)}$$

hence from $f_y(0,0)g(x_0,y_0) > 0$, $j_0 < 0$ it follows that $x_0 > 0$. Thus, the component $x(t)$ of the trajectory is positive and increasing on a time interval $[\tau, \tau_1)$ after the moment τ. According to Theorem A.1, $x(t)$ will be increasing and positive as long as the trajectory does not intersect the line $f = 0$ and does not leave some fixed neighbourhood U_0 of the origin. Furthermore, Theorem A.1 implies that any trajectory crossing the line $f = 0$ in the half-plane $x > 0$ close to the origin must approach this line vertically and from the same direction (from below if $-j_0/f_y(0,0) > 0$ and hence relations $x > 0$, $f(x,y) = 0$ imply $y' = g(x,y) > 0$ for small x, and from above if $-j_0/f_y(0,0) < 0$ and hence the relations $x > 0$, $f(x,y) = 0$ imply $g(x,y) < 0$). Since the trajectory we consider has crossed the line $f = 0$ at the moment τ, we conclude that it will not cross this line again in U_0 after the moment τ. Hence $x(t)$ is positive and increasing for $t \in [\tau, \tau_u]$ where τ_u is the first moment when the trajectory reaches the boundary of U_0. As $x(t)$ increases, the pair $(x(t), y(t))$ for $\tau + \varepsilon \le t \le \tau_u$ is a solution of ordinary differential system (4.12) with an equilibrium at the origin, which is unique in U_0, hence the trajectory leaves U_0 in finite time, *i.e.*, $\tau_u < \infty$.

It remains to prove the relation $|f_x(0,0)x(t) + f_y(0,0)y(t)| = o(1)|x(t)|$ for $t \in [\tau, \tau_e]$ as $\delta \to 0$, which also implies $\tau_e < \tau_u$, *i.e.*, the trajectory hits the line $x = \delta$ before it leaves U_0. In order to do this, given a sufficiently small $\nu > 0$, consider the domain

$$\bar{A}_\delta = \left\{(x,y):\ f(x,y) \ge 0,\ \sigma\left(\Delta y + \frac{f_x(x_0,y_0)}{f_y(x_0,y_0)}\Delta x\right) \le \nu \Delta x,\ x_0 \le x \le \delta\right\}$$

where $x_0 < \delta$, $\Delta x = x - x_0$, $\Delta y = y - y_0$, and $\sigma = \operatorname{sign} f_y(0,0)$. Relations (A.1) and $f_x(x_0,y_0) < 0$ imply $D_+x(\tau) = -f_y(x_0,y_0)g(x_0,y_0)/f_x(x_0,y_0) + o(g(x_0,y_0))$, while $y'(\tau) = g(x_0,y_0)$, hence the right derivative $(dy/dx)_+$ at the point (x_0,y_0) equals

$$\left(\frac{dy}{dx}\right)_+ = -\frac{f_x(x_0,y_0)}{f_y(x_0,y_0)} + o(1)$$

with $o(1)$ vanishing at the origin. Combining this relation with the fact that $\sigma y(t)$ increases in a neighbourhood of the point τ, we see that the trajectory $(x(t), y(t))$ enters the domain $\bar{A}_\delta$ through its vertex (x_0,y_0) at the moment τ and remains in the interior of $\bar{A}_\delta$ for all $t > \tau$ sufficiently close to τ. Note that $(x(t), y(t))$ is continuously differentiable for $\tau < t < \tau_u$, since it is a solution of ordinary differential system (4.12) on each time interval $\tau < \tau + \varepsilon \le t < \tau_u$.

As we have seen, the trajectory $(x(t), y(t))$ can not leave $\bar{A}_\delta$ through the line

$f = 0$. Relations (A.6) imply

$$\frac{dy}{dx} = \frac{y'}{x'} = \frac{\mu(x_1, y_1)g(x, y)}{f_x(x_2, y_2) + f_y(x_3, y_3)\Delta y/\Delta x}$$

with some $(x_i, y_i) \in U_0$. Hence, on the line ℓ which is a part of the boundary of $\bar{A}_\delta$ and which is defined by $\sigma(\Delta y + f_x(x_0, y_0)\Delta x/f_y(x_0, y_0)) = \nu\Delta x$,

$$\frac{dy}{dx} = \frac{\mu(x_1, y_1)g(x, y)}{f_x(x_2, y_2) + f_y(x_3, y_3)(-f_x(x_0, y_0)/f_y(x_0, y_0) + \sigma\nu)} = o(1)$$

where $o(1)$ vanishes as the diameter of U_0 tends to zero for a constant $\nu > 0$. Noting that for $\sigma > 0$ the line ℓ has a positive slope and bounds the domain $\bar{A}_\delta$ from above, while for $\sigma < 0$ the line ℓ has a negative slope and bounds $\bar{A}_\delta$ from below, we see that the trajectory can not leave the domain $\bar{A}_\delta$ through the line ℓ if $\delta > 0$ is sufficiently small due to the relation $dy/dx = o(1)$, $\delta \to 0$ on ℓ. Hence, the trajectory leaves $\bar{A}_\delta$ through the line $x = \delta$. Finally, $\bar{A}_\delta \subset \{(x, y) : |y + f_x(0, 0)x/f_y(0, 0)| \le 2\nu|x|,\ x \ge 0\}$ for small $\delta > 0$, which completes the proof.

A.4 Theorem 4.3

Theorem 4.3. *Let $f_x(0, 0) < 0$, $j_0 > 0$ and $f_y(0, 0) \neq 0$. Then any trajectory of system (4.8) that hits the line $f = 0$ sufficiently close to the zero equilibrium at some moment τ, converges to the zero equilibrium, but never reaches it. The x-component of the trajectory is strictly monotone for $t > \tau$ (hence, the trajectory does not intersect the line $f = 0$ for $t > \tau$). Moreover, there is a function $\phi = \phi(\delta) > 0$ satisfying $\phi(\delta) \to 0$ as $\delta \to 0$ such that $|f_x(0, 0)x + f_y(0, 0)y| < \phi(|x(\tau)|)|x|$ for $t > \tau$.*

A.4.1 Proof of Theorem 4.3

To be definite, assume again that the component $x(t)$ strictly increases on some interval $[\tau, \tau_1]$ after a trajectory $(x(t), y(t))$ hits the line $f = 0$ at a point (x_0, y_0) at the moment τ, *i.e.* $f_y(x_0, y_0)g(x_0, y_0) > 0$. Under the conditions of Theorem 4.3, $j_0 > 0$, hence relations (A.8) imply $x_0 < 0$. Using the same argument as in the proof of Theorem 4.2, we see from formula (A.8) that any trajectory crossing the line $f = 0$ in the half-plane $x < 0$ close to the origin must approach

this line vertically and from the same direction (from below if $-j_0/f_y(0,0) < 0$ and from above if $-j_0/f_y(0,0) > 0$). Therefore the trajectory we consider does not cross the line $f = 0$ after the moment τ as long as the trajectory does not leave the open left half-plane $x < 0$ and, furthermore, $x(t)$ increases all the time the trajectory is in this half-plane. To complete the proof, let us show that, given any small $\delta > 0$, the trajectory does not cross the line $\ell_\delta = \{(x, y) : y = ((-f_x(0,0) - \delta)/f_y(0,0))x,\ x < 0\}$ if $|x_0|$ is sufficiently small, and hence the trajectory converges to the zero equilibrium in the angle $\mathcal{A}_\delta$ between the lines $f = 0$ and ℓ_δ. Indeed, the derivative dy/dx on the line ℓ_δ for $t > \tau$ is

$$\frac{dy}{dx} = L(x)\frac{g_x(0,0)x + g_y(0,0)((-f_x(0,0) - \delta)/f_y(0,0))x + o(x)}{f_x(0,0)x + f_y(0,0)((-f_x(0,0) - \delta)/f_y(0,0))x + o(x)}$$

with $x_0 < x < 0$ and $L(x) = \mu(0,0)x_0 + o(x_0)$, hence

$$\frac{dy}{dx} = \frac{\mu(0,0)(-j_0 - g_y(0,0)\delta)}{-f_y(0,0)\delta}\, x_0 + o(x_0).$$

If $|x_0|$ is sufficiently small, then the absolute value of the slope dy/dx is less than the absolute value of the slope of the line ℓ_δ and hence the trajectory can not leave the angle $\mathcal{A}_\delta$ through this line. Finally, the fact that $x(t)$ increases implies that $(x(t), y(t))$ for $t \geq \tau_1$ is a solution of ordinary differential system (4.12) with a smooth right-hand side, which has an isolated equilibrium at the origin, therefore the trajectory converges to the zero equilibrium but never reaches it.

Appendix B

Publications pertaining to the work presented in this thesis

B.1 Publications related to Chapter 3

B.1.1 Peer reviewed conference proceedings

S. McCarthy and D. Rachinskii, "Attempts at a numerical realisation of stochastic differential equations containing Preisach operator," *Journal of Physics: Conference Series*, vol. 268, no. 1, p. 012019, 2011.

B.2 Publications related to Chapter 4

B.2.1 Peer reviewed journal papers

S. McCarthy and D. Rachinskii, "Dynamics of systems with Preisach memory near equilibria," *Mathematica Bohemica*, accepted.

B.3 Publications related to Chapter 5

B.3.1 Peer reviewed conference proceedings

G. Friedman, P. Gurevich, S. McCarthy and D. Rachinskii, "Switching behaviour of two-phenotype bacteria in varying environment," *Journal of Physics: Conference Series*, accepted.

Appendix C

List of publications by the author not pertaining to this thesis

C.1 Peer reviewed journal papers

M. Burke, M. Chapwanya, K. Doherty, I. Hewitt, A. Korobeinikov, M. Meere, S. McCarthy, M. O'Brien, T. N. Tuoi Vo, J. Rojas, H. Winstanley and T. Zhelev, "Modeling, simulation and optimization of Autothermal Thermophylic Aerobic Digestion," *Mathematics-in-Industry Case Studies*, vol. 2, 2010.

M. Brokate, S. MacCarthy, A. Pimenov, A. Pokrovskii, and D. Rachinskii, "Modelling energy dissipation due to soil-moisture hysteresis," *Environmental Modeling & Assessment*, vol. 16, pp. 313–333, 2011.

C.2 Peer reviewed conference proceedings

A. Amann, M. Brokate, S. McCarthy, D. Rachinskii and G. Temnov, "Characterization of memory states of the Preisach operator with stochastic inputs," *Physica B: Condensed Matter*, vol. 407, no. 9, pp. 1404-1411, 2012.

D. Rachinskii, A. Amann, S. McCarthy and M. Brokate, "Cascading Effects in the Moving Preisach Model," *American Control Conference*, accepted.